Design of a Control Strategy for Optimal Operation of an Autonomous Distributed Generation System for Electricity and Heat

MASTER OF SCIENCE THESIS

submitted in partial fulfillment of the
requirements for the degree of

MASTER OF SCIENCE

in

SUSTAINABLE ENERGY TECHNOLOGY

by

Víctor Vélez
born in Quito, Ecuador

August 2010

Faculty of Electrical Engineering, Mathematics and Computer Sciences
Faculty of Applied Sciences
Delft University of Technology

TU Delft
Delft University of Technology

Delft University of Technology
Department of
Electrical Sustainable Energy

The undersigned hereby certify that they have read and recommend to the Faculty of Applied Sciences for acceptance a thesis entitled **"Design of a control strategy for optimal operation of an autonomous distributed generation system for electricity and heat"** by **Víctor Vélez** in partial fulfillment of the requirements for the degree of Master of Science.

Dated: August 12th, 2010

Head of department:

Prof. ir. L. van der Sluis

Supervisors:

Dr. ir. G.C. Paap

Ir. L. Ramírez Elizondo

Committee Member:

Ir. Theo Woudstra

Contents

List of Figures

List of Tables

Nomenclature

Acronyms

ACE	Area Control Error
AFR	Air-Fuel Ratio
AGC	Automatic Generation Control
CHP	Combined Heat and Power generator
DEMS	Distributed Energy Management System
DG	Distributed Generation
DGS	Distributed Generation System
DHS	District Heating System
EMS	Energy Management System
HAWT	Horizontal Axis Wind Turbine
HEx	Heat Exchanger
HR	Heat Rate
LHV	Lower Heat Value
LMTD	Logarithmic Mean Temperature Difference
PID	Proportional-Integrate-Derivative controller

General Symbols

A	Area
C	Coefficient
c_p	specific heat capacity
d	thickness
E	Energy
f	Frequency
h	Heat transfer coefficient
K	gain
L	Load
M	Mass
P	Power
pf	Participation Factor
T	Temperature
T_e	Electromagnetic Torque
T_m	Mechanical Torque
U	wind speed; overall heat transfer coefficient
V	Voltage
w	status binary variable

Greek Symbols

η, e	efficiency
θ	pitch angle; dimensionless temperature
λ	thermal conductivity; tip speed ratio
ν	dispatch factor
ϕ	flow
ω	speed

Subscripts

A	actuator
act	actual
Amb	ambient
batt	battery
CD	compressor discharge
ch	charging
cmd	command
CR	combustion reaction
D	derivative
dch	desired characteristic
DH	district heating
disch	discharging
e, ele	electrical
exh	exhaust gases
ER	Exhaust Recuperator
f	fuel
g	natural gas
h	heat
HEx	heat exchanger
hl	hot line
I	integral
m	mass; mechanical
n, nom	nominal
opt	optimal
P	proportional
P1	side 1, chamber P
P2	side 2, chamber P
pw	power
q	heat
r	rotor
rad	radiator
ref	reference
ret	return
S1	side 1, chamber S
S2	side 2, chamber S
sh	space heating
st	storage
sw	service water
TD	transport delay
th	thermal
V	valve
w	water
wnd	wind
wnds	windows

INTRODUCTION

The new forces acting over the current energy infrastructures will certainly lead to deep structural and technological changes. Indeed, the traditional specialized, dedicated and separated energy supply industry is changing to accommodate the new challenges imposed by the society, aiming a sustainable utilization of energy. Foreseeing of a rapid depletion of conventional fossil fuels, growing social-political concerns about energy security, continuous enlarging of energy demand and increasing attention to the mitigation of global climate change are some of the drivers for the changes towards a sustainable energy industry.

The emerging distributed generation technologies like Combined Heat and Power units or micro-CHP and in the last years, the strong development of alternative energy sources such as wind energy, solar energy, biofuels and others have created opportunities for new energy generation setups. Furthermore, the current trend towards systems that integrate generation of different forms of energy has created options for improving systems efficiency. Improvements gave through synergies among the transportation, conversion and storage capabilities of multiple energy carriers.

Hence, it is obvious that innovative approaches in the energy generation field and its management are currently in research. One of this is the “Intelligent energy supply at district level” research which is carried out at the Electrical Power Systems group. This research deals with the integration of renewable sources, storage devices and decentralized systems at district level. Moreover it includes multiple energy carriers.

As part of that research, this thesis manuscript reports the work done in the MSc thesis project “Design of a control strategy for optimal operation of an autonomous distributed generation system for electricity and heat”.

The operation of distributed generation units is performed by a dedicated system named Distributed Energy Management System. This is configured as a modular system made of Forecast and Prognosis module, Optimization module, and Controlling module. This MSc project slightly dealt with the Optimization module but its main work falls in the Controlling module.

An innovative approach for the optimization of multiple energy carries, called Energy Hub, has been selected for the Optimization module. The Controlling module is studied for an autonomous distributed generation system of electricity and district heating. This system comprises combined heat and power generators, a horizontal axis wind turbine, a hot water heating boiler, and electricity and heat storage devices.

This MSc thesis project aims to design a control strategy for the autonomous distributed generation system that should perform according to the optimal operation points determined by the Optimization module. Besides it should maintain the energy demand of electricity and heat properly satisfied every time and under any sudden change of it.

This MSc thesis report is structured as follow: Chapter 1 introduced the basic concepts used in the Optimization module and presents a description of what a district heating system is. Chapter 2 first makes a review of the traditional energy management system for power generation and later goes through the current research on concepts for distributed energy management systems. Chapter 3 states the thesis problem in detail and presents the work done into the Optimization module as part of the solution to the thesis problem. Chapter 4 describes the models implemented to characterize each of the components of the studied distributed generation system. Chapter 5 presents the designed control strategy and the results of the simulations carried out. Finally, conclusions and recommendations end this reports.

CHAPTER 1

General Concepts

Energy Hub Concept

Traditionally, energy demand has been supplied by specialized, dedicated and separated energy industries such as energy companies dedicated to electricity generation or gas companies providing fuel for heating needs. The current trend, however, is an integrated view for the generation of different energy forms. As an example, electricity and heat produced at the same time by a combined heat and power generator. This trend seeks synergies among multiple energy carriers in order to create opportunities for system improvement in their transportation, conversion and storage levels among others [1].

The integration of multiple energy carriers represents a challenge in combining their infrastructures such as electricity generators, transformers, wind turbines, micro-turbines, PV-panels, fuel cells, power-electronic converters, boilers and furnaces, heat exchangers, storage devices and so on in order to find optimal power exchange and coupling among them. Hence, a novel conceptual approach able to cope with this multiple energy carriers integration is introduced in [2] with the name of energy hub and defined as "an interface between different energy producers, consumers and transportation infrastructure".

An energy hub provides the inputs, outputs, conversion, and storage for multiple energy carriers. Figure 1 shows an example of energy hub, it exchanges energy through the input and output ports. The input ports demand energy that is converted and/or conditioned within the energy hub, whereas the output ports supply different forms of energy to the load. In an energy hub three kinds of elements could be found: direct connections, converters and conditioners, and storage devices. Direct connections convey an input energy carrier to an output without change; in Figure 1 these are the cables for grid electricity (P_e *to* L_e) and the pipelines for hydrogen (P_H *to* L_H). Converter element is the PEM fuel cell, while conditioners are the step-down transformer and the power-electronic inverter. Finally, storage devices are the electricity storage (battery stack) and the heat storage in the simple energy hub representation of Figure 1.

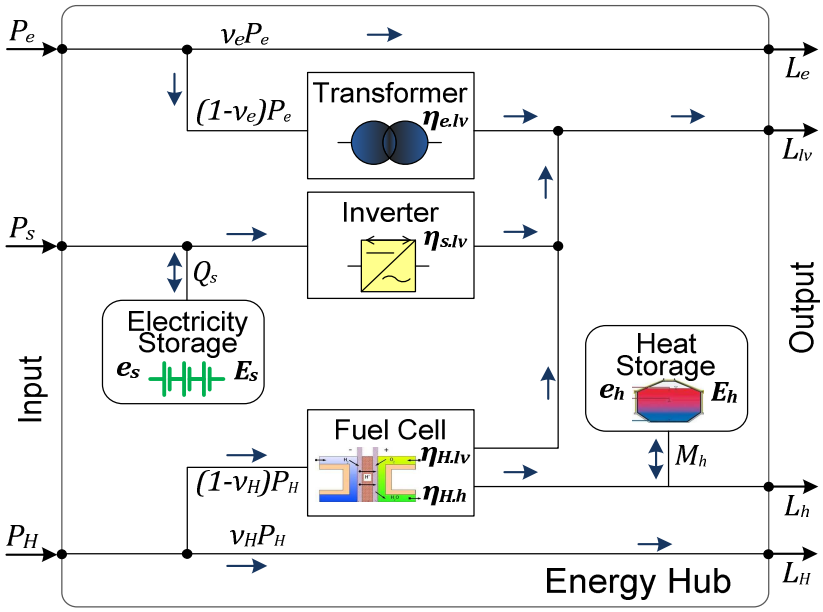

Figure 1 Energy Hub

The energy hub concept allows the modeling of interactions among multiple energy carriers through the hub's elements. Therefore, different analyses about their integrated features can be carried out such as power flow, reliability and system optimization. From Figure 1 some advantages can be directly drawn when comparing energy hubs with traditional energy supply systems. First, redundancy in supply of electricity at low voltage (L_{lv}) is achieved by the coupling of the outputs of the transformer, fuel cell and PV inverter. It increases the degree of freedom in reliability design of the infrastructures and brings about the issue of multiple energy carriers optimal supply. Second, the specific traits of each energy carriers can be used synergistically to enhance the system performance. For example electricity can be transmitted with relative fewer losses than other energies carriers, while fuels can be stored in a cheaper manner than electricity.

Modeling

The description of steady-state power flows of multiple energy carriers within an energy hub considers the following assumption for its modeling [3-4]:

- The system is believed in steady-state, where transients are not presents and quantities may fluctuate uniformly.
- Power flow through hub elements is characterized by power levels and efficiencies only.
- Unidirectional power flow from inputs to outputs is considered if not mentioned otherwise.
- Losses are just considered in converters and storage devices.

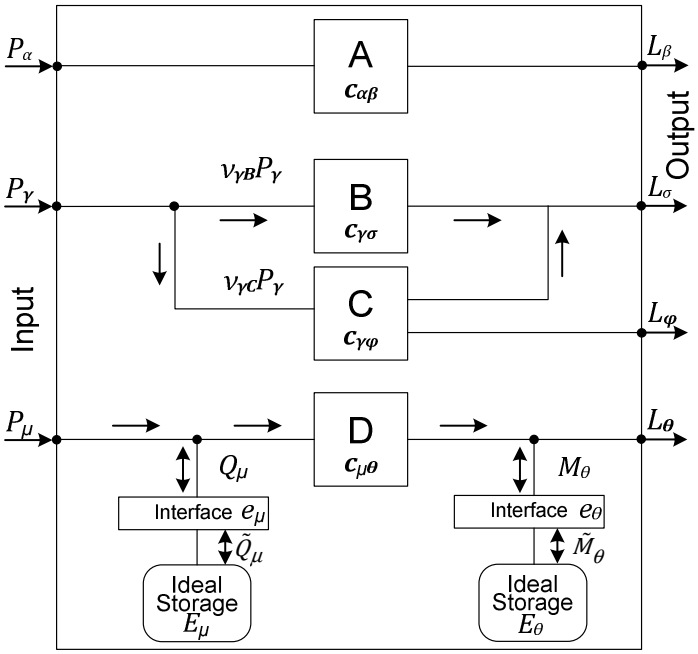

Figure 2 Schematic of Energy Hub elements

Consider the schematic of a basic energy hub in Figure 2. The input energy carrier α is transformed to β by action of the converter A. Its input and output power flows are coupled through:

$$\boldsymbol{L_\beta = c_{\alpha\beta} P_\alpha} \qquad \textbf{Eq. 1}$$

where P_α and L_β are the input and output powers, respectively, and $c_{\alpha\beta}$ is the coupling factor between energy carriers. This factor can vary between zero and one.

When multiple inputs are converted to multiple outputs, equation Eq. 1 becomes in a matrix equation, where vectors **P** and **L** state for multiple energy carriers inputs and outputs, respectively. **C** is the converter coupling matrix that stores the coupling factors that relate a particular input with a certain output. As it is possible to split the power of an input energy carrier to feed several converters, such as in converters B and C of Figure 2, a dispatch factor (*v*) is introduced to serve for this purpose. This factor specifies the amount of input power that flows towards each converter *k* by:

$$\boldsymbol{P_{\gamma k} = \nu_{\gamma k} P_{\gamma}} \quad \textbf{Eq. 2}$$

Further, the dispatch factors are subjects to: $0 \leq \nu_{\gamma k} \leq 1 \;\; and \;\; \sum_{k \in Converters} \nu_{\gamma k} = 1.$

In Figure 2 a general model of an energy storage device is depicted, it is formed by an interface and an internal ideal storage. The interface represents the conversion or condition of the energy carrier into another, for example DC electricity into chemical energy in a battery. However, when a storage device exchanges an energy carrier μ, it is not wrong to consider that it stores μ and not β even though β is internally stored [5].

Considering Q_{μ} as the input power to the interface and $\tilde{Q}_{\mu}$ as its output power towards the ideal storage, a relation between them is established through the storage factor (e_{μ}). As a storage device is intrinsically a bidirectional flow element, the storage coefficient's value will depend on the storage's operation mode, either charging or discharging. In the ideal storage element, energy is stored or delivered throughout a period of operation, thus introducing dependability on time in the energy exchanged. In accordance, the internal power $\widetilde{Q}_{\mu}$ corresponds to the time derivative of the storage energy (E_{μ}). These relations are formulated below, according to [3].

$$\boldsymbol{Q_{\mu} = \frac{1}{e_{\mu}} \frac{dE_{\mu}}{dt}} \quad \textbf{Eq. 3}$$

$$\boldsymbol{e_{\mu} = \begin{cases} e_{\mu}^{+} & if \;\; Q_{\mu} \geq 0 \;\; (charging/standby) \\ \dfrac{1}{e_{\mu}^{-}} & else \quad\quad (discharging) \end{cases}} \quad \textbf{Eq. 4}$$

During steady-state the change of stored energy can be approximated by $\frac{\Delta E_{\mu}}{\Delta t}$.

Within an energy hub, storage elements can be placed in either the input or output sides, influencing the hub's power flow. Figure 2 shows power flow Q_{μ} at the input side, it interacts with P_{μ} to form the power flow at the input of converter D. In the same way, but in the output side, M_{θ} forms together with the power flow output of converter D the hub energy carrier output L_{θ}. Generalizing to multiple storage devices, a matrix representation for the energy hub inputs-outputs relation follows, where **M** and **Q** are storage power flow vectors, for specific details view reference [3] .

$$\mathbf{L + M = C[P - Q]} \;\; \text{then}$$
$$\mathbf{L = CP - [CQ + M]} \quad \textbf{Eq. 5}$$

The term **[CQ + M]** represents the influence of the storage devices over the energy hub outputs. In general this term can take the following form:

$$[\mathrm{CQ} + \mathrm{M}]_{\theta} = \mathrm{c}_{\mu\theta} Q_{\mu} + M_{\theta} = \frac{\mathrm{c}_{\mu\theta}}{\mathrm{e}_{\mu}} \frac{\mathrm{dE}_{\mu}}{dt} + \frac{1}{\mathrm{e}_{\theta}} \frac{\mathrm{dE}_{\theta}}{dt}$$

Eq. 6

being the expression at the right side of the equation Eq. 6 suitable to be written in a matrix form, where the coefficients of the storage energy derivatives form a matrix **S** that multiples a vector **Ė** of storage energy derivatives.

Lastly, a general formulation for the input-output relation of energy carriers flow within the energy hub that considers converters, conditioners and storage elements is given by:

$$\mathbf{L} = \mathbf{C}\,\mathbf{P} - \mathbf{S}\,\dot{\mathbf{E}}$$

Eq. 7

Equation Eq. 7 models the energy hub and enables the analysis of its features in order to seek, for instance, operational or system optimization.

Optimal Dispatch of multiple energy carriers

In the power generation industry the economic dispatch of thermal units is a well-know problem. It consists in allocate the required load demand among the available generation units in such a way that the operation cost is minimized. Therefore, it is an optimization problem that looks for an optimum operation policy for the generation units [6].

In an energy hub, the same optimization problem can be stated for optimal system operation. The solution to this problem will reveal how much of which energy carriers the hub should consume. As an energy hub tries to take advantage of the synergy among energy carriers, the optimization objective may be not only cost minimization of energy carriers input to the hub, as similar to the classical economic dispatch, but also other current societal concerns such as emissions minimization. Composite objectives are possible too, for example an economic-environmental dispatch. This optimization of the power flows through a single energy hub under a defined objective is named as Optimal Dispatch [3].

Unit Commitment of multiple energy carriers

The commitment (turn on, synchronization and connection to deliver power) of a power generation unit has a specific economic cost, therefore it is possible cost optimization of a generation system by determining which and when its units should commit. The unit commitment problem in the power generation industry states that given a set of N generation units and a load demand forecast, there would be a subset of committed units that copes with the demand at the minimum operation cost in a determined period of time. The solution of this complex problem involves finding when each unit should be started, stopped and solving the economic dispatch problem for each of the possible subsets [6].

This optimization problem can be directly transferred to the case of an energy hub. In this case, a subset of hub elements commits during a period of time in order to achieve the optimal operation in processing multiple energy carriers, while obtaining optimal dispatch and power balance of the system [7].

District Heating

District heating is a thermal energy system that distributes from a central source heat to residential, commercial, and/or industrial consumers [8]. This energy system concept is more than one hundred years old but it was in the 1980s that a modern concept was introduced, incorporating automatic control and remote monitoring features. In this system, unlike conventional heating systems that produce thermal energy at the users' place, heat is supplied to the users by means of either steam or hot water external lines. District heating is applicable in locations where both the thermal load density and the annual load factor are high. This is due to the fact that the whole system is quite capital intensive [8].

District heating has several economic and environmental benefits, among them: reduction of local air pollution, increase of fuel flexibility, better energy security, maximize the energy efficiency of the electricity generation process through facilitating a means to use its waste heat, share of heat loads, thereby using heat plants more effectively and efficiently, and provision of opportunities for the introduction of industrial waste heat and renewable sources of energy [9].

Three primary components form the district heating system. The central energy source component can be any type of boiler, a refuse incinerator, a geothermal source, thermal solar energy, or any source that produces heat as a by-product such as an electricity generator that in its combined version is called CHP (Combined Heat and Power generator). The central energy source produces either steam or hot water as the heating medium. Being steam used mainly for industrial customers and for hospitals loads, while hot water is more appropriate for commercial and residential buildings. It is because hot water can cover a greater geographical area than steam by means of simple booster pumps [8].

The distribution network component transports the heating medium. Insulated pipelines in concrete tunnels or buried make up this network. The piping is often the most expensive portion of district heating system for that its use should be optimized. The final component is the consumer system. The consumer system can use the supplied heat through a direct connection or indirectly via a heat exchanger. In a direct connection the steam or hot water passes to the user heating system, thus, it may need reduction in pressure to be compatible with the user's system. Although direct connection is more economical, it carries the risk of incurring in contamination of water. On the other hand, indirect connection uses a heat exchanger so different water qualities between district heating and final user's system are not a problem. The rate of heat exchange, in both types of connections, is governed by a control valve that modulates to maintain a temperature set point on either side of the heat exchanger. Figure 3 shows a simplified sketch of a district heating system for a residential load. In residential application the district heating provides domestic hot water and space heating basically.

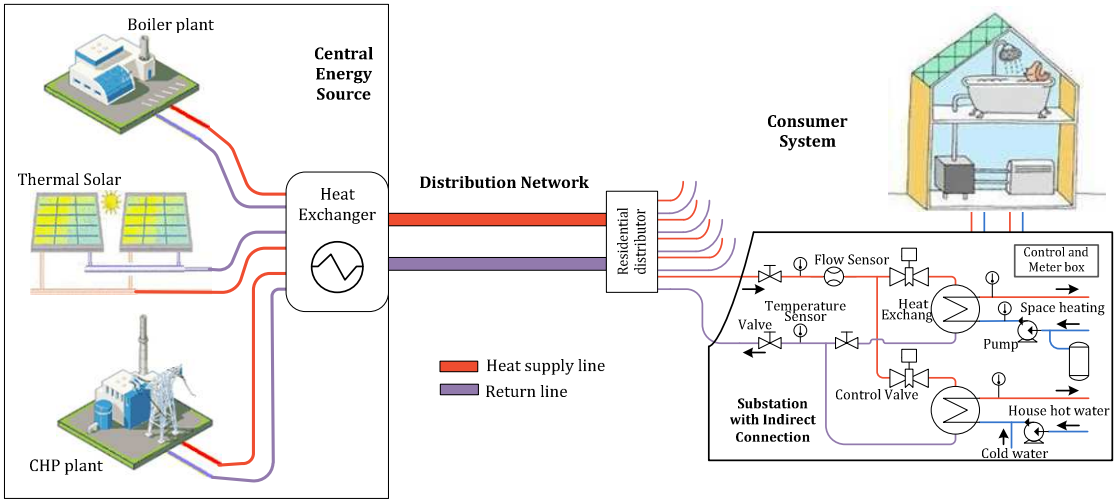

Figure 3 District heating system with residential load indirectly connected

CHAPTER 2

Review of Distributed Energy Management

This chapter presents the energy management system concept used in the power industry and the up to date concepts of energy management for distributed generation. On the latter, either proprietary concepts or outcomes from current scholar research that cope with the new demands in the energy industry are described. Thereby, this chapter briefly explores the field of energy management solutions, energy optimization approaches and control strategies for the optimal operation of energy systems.

Energy Management System

The operation of a traditional power system is based on technical and economic objectives driven by national-societal policies. In considering the constantly changing state of a power system, due to normal load fluctuations or unexpected contingencies, the main technical objective of a real-time power system operation can be drawn as providing power to the varying loads, while maintaining frequency and voltages within limits. Meanwhile the primary economic objective can be seen as minimization of operative costs, leading to an optimization problem of power generation. Thus, the task to fulfill these objectives requires a process guided by control and decisions based on constant monitoring of the power system condition [10].

The current centralized operation of a large power system is performed in a control center that uses communication technologies, advanced software, computer hardware and other support hardware in order to carry out the decision-control process. Ilic and Zaborszky describe this process consisting of a decision phase and a control phase. In the decision phase a continuous surveillance and monitoring is performed next to the decision on the system condition (normal or abnormal operation) and decisions of selecting the best control regime of actions (preventive, corrective, and/or control) in order to maintain normal operation condition or return the system to this condition. In the control phase, algorithms and control actions (commanded by the former) comprising the selected control regime are executed.

A normal operation condition occurs when the monitored power system conditions are stationary and as expected within their ranges, having only major changes as the result of load dynamics. Therefore, normal operation is suitable for online control through well-established analytic tools, allowing full automation of some actions. The normal operation control of a power system aims to solve the dispatch of generation to cover consumer demand under defined objectives. The decision phase on this condition uses algorithms such as: monitoring and estimation of load and generation, static state estimation, and monitoring of the system loading conditions and security. Whereas the control phase runs algorithms such as: unit commitment, economic dispatch, optimal power flow, automatic generation control, automatic voltage control, and load management [10].

Considering normal operation, the structure of the decision and control phase for generation-dispatch in order to satisfy consumer demand under defined objectives is depicted in Figure 4. Where elements in blue and green belong to control and decision phase respectively. The description of these elements is based on reference [10].

- ***Block 1*** sets the objectives and operative rules that govern the power system dispatch based on the policies and ideologies present in a society at the time. For example government regulated operation or deregulated operation of the power industry.

- ***Blocks 2, 3 and 4*** assure that the solutions to the problem of dispatch comply with the objectives and operating rules. Naturally this involves economic and power quality considerations. Block 2 and 4 perform an estimation of daily required generation based on historical load data and forecasts. Particularly block 4 determines the most economical set of generators to be committed, and block 2 distributes the generation economically to the committed units. Finally block 3 combines the generation estimations with the online generation corrections and translates this generation dispatch into control commands going towards the physical system.

- ***Block 5*** represents the physical system, comprising the model for dynamic and static behavior of the generation equipment, transmission network and control devices. Commands set the operation points of the physical system in order to achieve the aimed outcome in terms of powers, voltage and frequency (P_G, Q_G, V_G, ω_G).

- ***Block 6*** deals with the mismatch between estimated dispatch and current actual load through a closed-loop hierarchical generation control. This hierarchical control makes the appropriate dispatch corrections in order to balance the system and comply with power quality regulations. The hierarchical control comprises:
    a. The fast *Primary Control* of the individual machines (governors, exciters, etc). It assures that machines' output stabilizes the local output variables (frequency and voltage) as near as possible to the assigned setpoint.
    b. *Secondary Control* generates the corrective adjustments in a medium speed range adjusting the load forecasting results and the system frequency target in order to maintain synchronous frequency and eliminate voltage deviations. Considering Automatic Generation Control (AGC) this task is fully decentralized by driving an area control error (ACE) to zero. ACE is a linear combination of deviations frequency and area generation from the schedules. If all connected areas succeed in driving their ACEs to zero then both the system frequency and the sum of their tie-line exchange powers contracts maintain their assigned setpoints.
    c. Tertiary control is slow and covers the entire power system. It generates time error correction to compensate for the effects of interactions on the quasistatic changes of the interconnected system over the long-term time horizon.

- **Block 7 and 8** are part of the decision phase. They monitor the system composition and its state and send suitable information for the operation of the control algorithms.

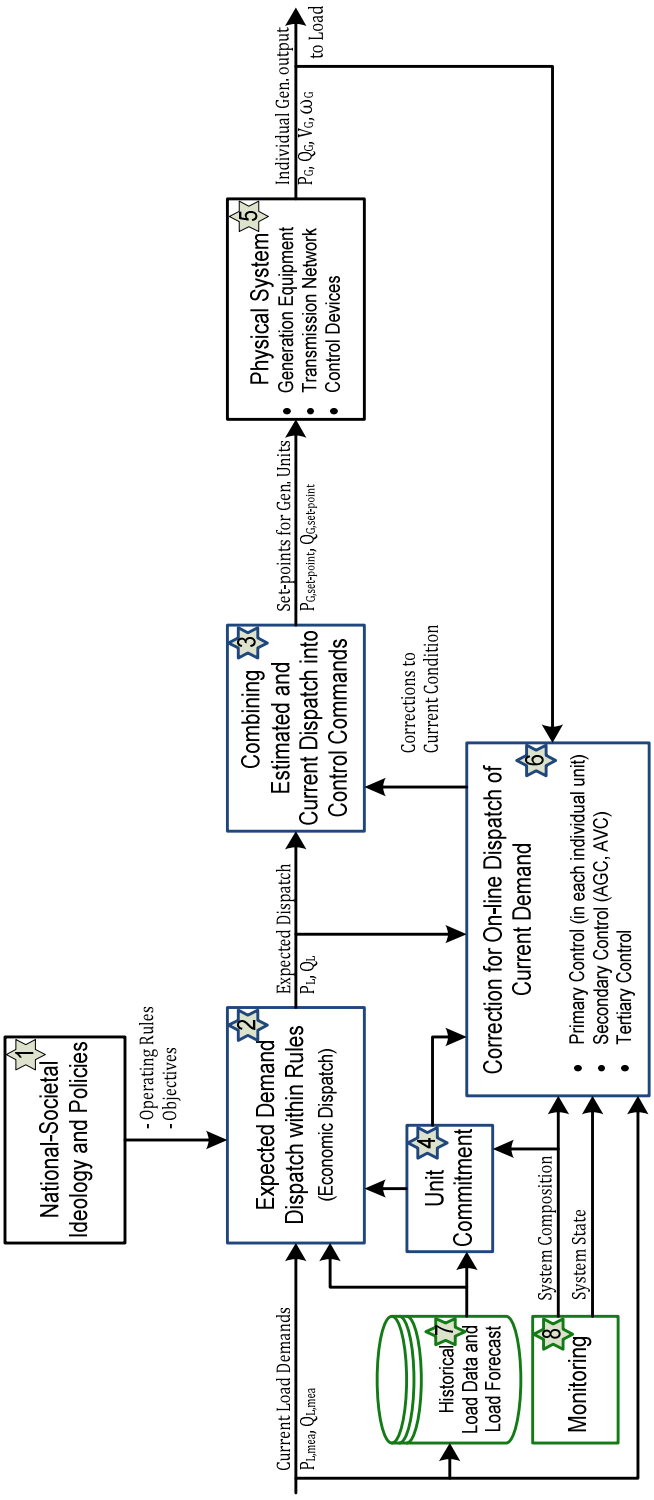

Figure 4 Decision and Control phase structure for generation dispatch in normal operation, adapted from reference [10].

The process for generation control described above can be organized in a system of computer-aided tools. The marketable suit of these computer-aided tools in the power industry has taken the name of Energy Management System (EMS). As defined per references [11] and [12] an EMS is a complex hardware and software system designed to assist in the monitoring and control of power generation and transmission systems. It provides real-time grid information to dispatchers and makes decisions about dispatch, control and network management in a way that it minimizes operating expenses, ensures a continuous supply of high quality power to customers and maintains safety operating margins. The EMS is made of a Supervisor Control And Data Acquisition system (SCADA), Power Advanced Software packages (PAS) which are used for energy analysis and management of the grid (software such as load forecast, economic dispatch, unit commitment, etc) and also commonly the EMS is supplied with a Dispatcher Training Simulator.

Figure 5 shows a generic graphical structure of the Energy Management System consisting in three modules [13]. Behind these modules the process for decision and control of generation dispatch is carried out.

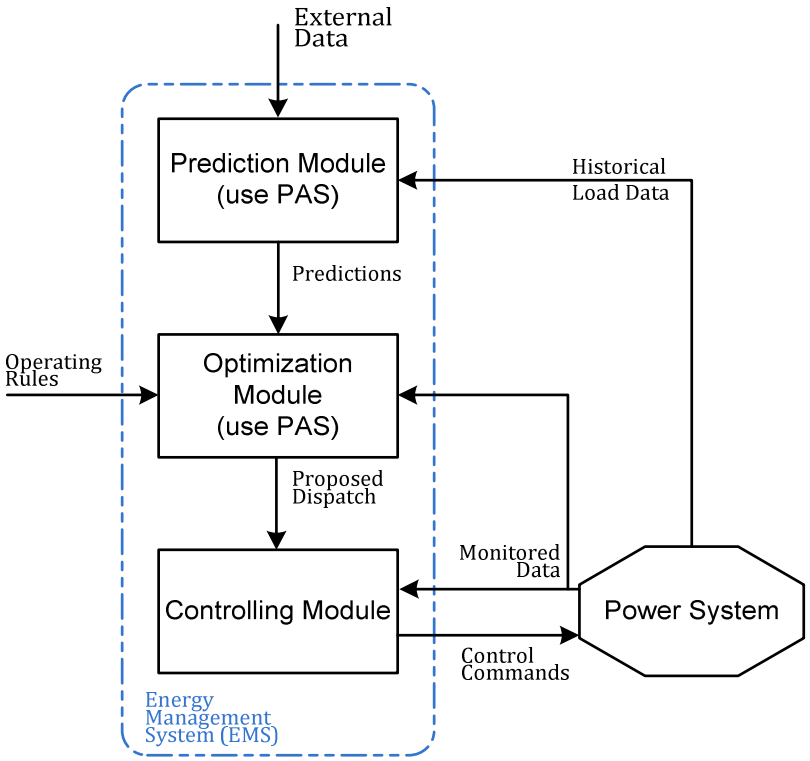

Figure 5 Generic description of an Energy Management System, adapted from reference [13]

This generic modular conception of EMS allows tailoring the modules to incorporate additional management traits such as the required for distributed generation sources or when dispatch of multi-energy carriers is intended.

Distributed Energy Management System

Currently the energy industry is changing its paradigms owing to the complex challenges that the world is facing. Predictions for rapid depletion of conventional fossil fuels, increasing demand of energy, global climate change, energy supply security concerns and liberalization of energy markets sum up these challenges. Thereby the introduction of distributed generation sources in the power system has taken an important role in recent years as a means to at least in part meet these challenges.

Distributed generation (DG) sources comprise several technologies going from diesel engines, micro turbines, combined heat and power (CHP) and fuel cells to wind turbines, photovoltaic energy systems, etc. These technologies together with controlling hardware and storages units for electricity, hydrogen, heat, etc make up the component level of a Distributed Generation System (DGS). The main benefits of DGSs are that they supply power locally; reduce grid investment, operation costs and losses in transmission and distribution lines; provide voltage support; complement the grid reciprocally, shorten the gap between peak and valley load and reduce environmental pollution [12, 14].

The introduction of DGS into a power system has led to a change in its operational characteristic, causing for example power flow reversals. Moreover the generation mix in a power system with DGS includes highly random power production from renewable sources. Both of these new grid traits stress the need of an energy management system that can integrate DG to the classical concept of generation dispatch. This envisioned system is termed Distributed Energy Management System (DEMS).

The discussion that follows examines up to date research on management of distributed generation. First, aspects that are believed a DEMS should have are summarized next to proposed DEMS concepts that somehow modify the modular structure described by Figure 5. Later, specific approaches that fall within the context of each module are presented.

Aspects to consider for DEMS

Yingyuan et al., based on existing achievements, summarize in nine points the aspects that a distributed energy management system should have [12]:

a. Established models of distributed generation systems in two levels: component-level that includes renewable energy converters, storage, etc and a system-level with models of control, operation and optimization configuration of the new strategies for generation and dispatching.
b. Forecast about energy production from renewable DG sources and simulation of future weather conditions.
c. A new power production schedule to meet requirements, thus traditional unit commitment should be reconsidered.
d. Adjustment of power flow among DGS.
e. Proper dispatching and management strategies in order to guarantee efficient operation of DGS. These could integrate local thermoelectric demand, weather conditions, pricing, fuel consumption, power quality requirements, demand side management, and the level of congestion to make decisions.
f. Appropriate optimization algorithms.
g. Large use of new computer and communications technologies in order to make progress in dispatching automation and integration technology.

h. An integrated training platform to allow users to analyze different network models and operation modes.
i. Finally, it should comply with current standards about dispatching automation technologies such as IEC 61970 standards.

DEMS concepts

This set of aspects expected in a DEMS alters the modular conception of the EMS, generating concepts like the one presented by Schellong in reference [14]. Schellong emphasizes the importance of information systems as the basis for controlling and decision activities in DGS. Thus, asserting that efficient data management and energy data bases are required to optimize the energy generation process and that the energy management system must provide tools for the energy data workflow and the design of information systems. Schellong organizes the DG and storage using the concept of "virtual power station". It represents a multi-fuel, multi-location and multi-owned power station that strongly depends on an applicable control and information system. The heart of the information system in this concept of DEMS is a relational data base that contains all relevant energy data and organizes the information exchanges between the modules, as can be seen in Figure 6.

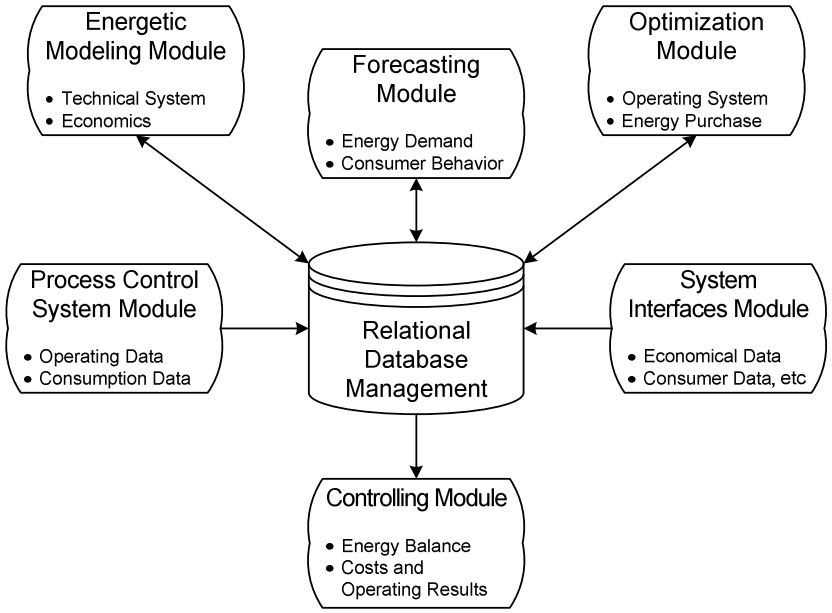

Figure 6 DEMS concept that highlights data management and energy databases importance, adapted from reference [14]

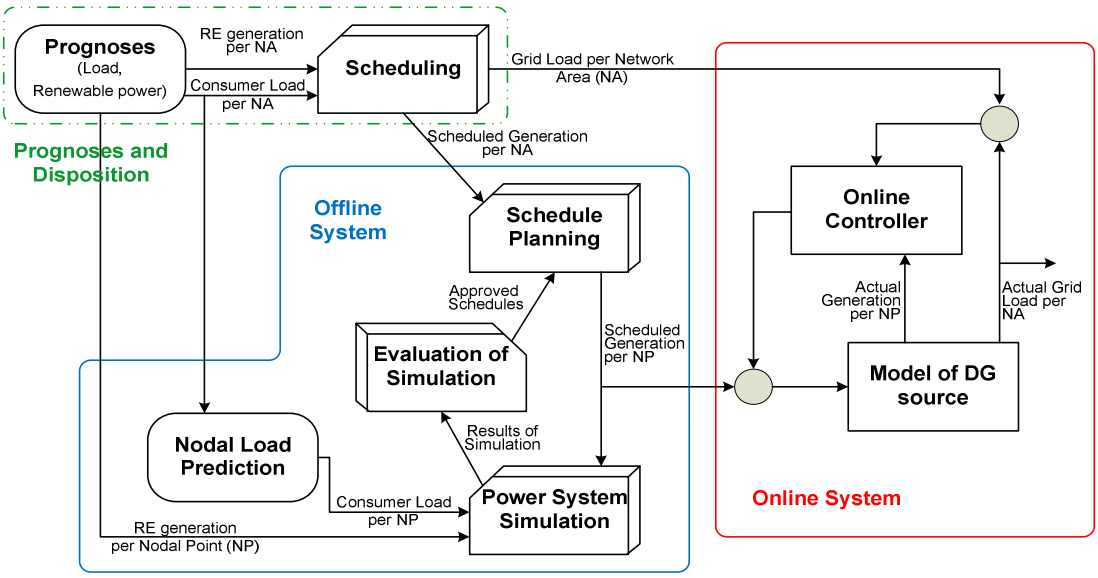

Figure 7 DEMS concept with eight functional parts, based on reference [15]

The DEMS developed in [15] intents to exploit the whole potential of DGS and is composed of eight functional parts shown in Figure 7. The system is divided in two parts, one that beholds the overall network (Prognoses and Disposition) and the other that deals with the investigated scenario using an offline and online system for each subnetwork (nodal point) of the network area.

A licensed DEMS is described in [16]. It is suitable to manage co-generation (electricity and heat), renewable energy converters and load control. It can handle two configurations: offline planning tool and online process system. The former may be used to carry out energy-related economic studies of a DGS while the latter is the platform to perform the actual management of a DGS. Both have similar structure which is based on the function units of forecast, operation planning and online components.

The forecast function predicts the weather, generation and load patterns ahead. The operations planning function carries out the minimization of operating costs through optimal commitment of the available resources and respecting contractual and environmental constraints. Lastly, online components functions perform redistribution of generation and load schedules, generation control and load control in order to maintain the planned and contractually agreed energy exchange. Figure 8 sketches this DEMS and identifies the online functions as exchange monitor (XM), generation manager (GM) and load manager (LM), all working under the online optimization and coordination function (OOC).

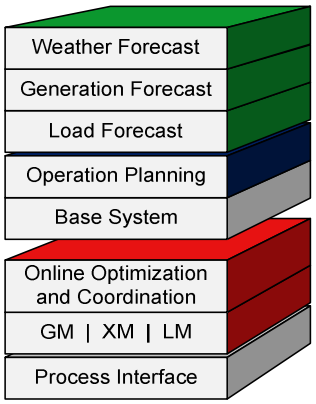

Figure 8 Sketch of SICAM DEMS® concept according to reference [16]

Each of the above DEMS concepts forms the system level of the DGS by slightly altering the general modular structure shown in Figure 5. While maintaining this structure, much more work has been done by research within each one of the Prediction, Optimization and Controlling modules. Several papers are available describing new forecast methodologies, new optimization algorithms and new controlling techniques [17-31]. The majority of these papers use the concept of Microgrid as the framework for the component level of the DGS, framework wherein the modules outcomes are applied.

The concept of Microgrid was created to describe a system where distributed generation sources, storage units and other hardware work together to supply electricity and in some cases also heat to local loads. A Microgrid can operate interconnected to a main distribution grid or in islanded (autonomous) operation mode. This cluster of DG sources operates under the DEMS control, thus a short summary of the current research on the DEMS functional modules follows.

Prediction Module alternatives

Sizing and operational set-points of energy systems depend on the load patterns to serve. In traditional generation systems the simplest load's forecast model is based on historical load data. However, when distributed generation systems that include renewable sources are considered the forecast model becomes more complex. Such prediction model incorporates forecast of the stochastic behavior of renewable energy sources in order to quantify the renewable power generation. Additionally, heat load forecast shall be needed in systems such as Microgrids that look for high energy efficiency.

Forecasting of solar and wind energy use weather forecasts, information regarding time in the day, type of day and season, local meteorological measurements, etc. Large effort has been done to increase the accuracy of this forecast using mathematical tools suitable for dealing with stochastic behaviors. For example prediction models using feed-forward neural networks for solar irradiation or wind speed are discussed in [23] and [30]. Furthermore, Changsong et al. state that factors that influence the character of a renewable energy converter system have to be considered, for example in a PV system such factors are solar irradiation, array transfer efficiency, installation angle, atmospheric pressure, temperature and so on. Therefore, when considering the generation history of a system and its influencing factors a generation forecast can be obtained by training neural network forecasting using past generation data [19, 26].

Hatziargyriou et al. discuss in [21] the forecasting necessity in Microgrids. Depending on the Microgrid operation mode, either grid connected or islanded, the importance of accurate generation forecast changes. The balance of the system is the aim in islanded operation, thus generation and demand predictions are of primary importance. In the case of grid connected, the importance of predictions depends on the driving objective. When it is system-driven, any energy deficit at the microgrid can be covered by the grid then forecasting is less important. In case it is customer-driven, economics matters and the forecasting gain in importance.

Hatziargyriou et al. state that forecasting in Microgrids is mainly short-term with high temporal resolution (e.i 10 minutes) and for the next 1-4 hours. Adaptive fuzzy neural networks are used to forecast demand and generation in the studied Microgrid.

Optimization Module alternatives

In distributed generation systems the power generation dispatch problem may be linked to other objectives besides economics. One of the more interesting seems to be the environmental objective, regarding the current climate change challenge and increase participation of renewable sources in the energy generation mix. In addition to this, the inclusion of storage units also alters the normal structure of the classical unit commitment and dispatch optimization problem.

The objective function of this optimization problem is normally non-linear, discontinuous, of high dimension and when storage included time, inseparability is founded too [13]. Many papers explore different mathematical techniques to solve the optimization problem in DGS. Within the classical techniques are dynamic programming and Lagrangian relaxation, whereas techniques such as genetic algorithms, evolution programming, direct search method, particle swarm optimization, and simulated annealing account for some of the modern stochastic searching optimization techniques [22].

Regardless of the optimization technique used to solve the dispatch problem, the following papers review aims at to pinpoint the structure of the stated optimization problem. Thus, renewable energy addition to the generation dispatch is discussed as well as multi-carriers dispatch, storage inclusion, conflicting optimization objectives, and so on.

A grid connected DGS that includes only renewable energy sources and storage units is presented in [19]. Using a power forecast of three days, the operation of the DGS is maximized regarding the total profit as the objective function. This total profit is made of a time dependent utility energy price function that multiplies to the power bought or sold from/to the utility as function of time as well. Within each optimization step, the information about the next hour power output is employed to define the threshold for charging and discharging rate of the battery, while the power balance and storage states are considered to obey physical constraints. Thus, the optimization defines the hourly power flow direction and amount of flow among sources, storages, loads and grid. The optimization technique used there is intelligent programming with some heuristics.

The optimal dispatch of the coupling between electrical and thermal energy in cogeneration units (CHP) is dealt with in [13]. The islanded system there described includes CHPs, renewable stochastic energy sources, a hydropower plant, and heat and electricity storage units. The optimization function seeks minimization of costs. Costs consisting of operation costs, cost of use (e.g. starting costs of thermal power plants) and penalty costs (e.g. fine for violation of soft restrictions such as minimum running time of a thermal power plant). The optimization is performed in steps of 15 minutes for a horizon of 24 hours using forecast of loads and renewable energies with the same step span. Energy from renewable sources is used as available and other many rules of

common sense are also implemented. The complex optimization problem is solved with evolutionary algorithms, resulting in the proposal of switching schemes of adequate quality for the thermal units and loads.

The optimization problem for a grid connected Microgrid is considered in [21]. Within a hierarchical decision making process, micro source controllers and local micro load controllers execute the demands that a Microgrid System Central controller (MGCC) has reckoned as optimal. The MGCC acts as a market operator, using energy prices of the market, bids of the micro-sources, suggested limits of production, and demand side bidding for "low" and "high" priority loads in order to solve the unit commitment and economic dispatch problem. MGCC can operate under two market policies each one with different optimization objective function. In the first policy, the aim is to satisfy the local energy demand using its local production, when financially beneficial, without exporting power to grid and importing just if power balance cannot be achieved with local resources. Therefore, its objective function looks for minimization of operational costs of the Microgrid. The second policy aims to maximize the value (difference between income and expenses) of the Microgrid through its participation in the energy market of the distribution area, buying and selling active and reactive power to the grid.

The optimal operation of a multi-carrier energy system with storage devices is investigated in [17], through modeling of the couplings between electricity and gas systems with the energy hub approach. In order to cope with the dependency between consecutive time steps that storage devices cause, the optimization is carried out over multiple time steps. A central controller defines the set-points of the energy generation units of the energy hubs via an optimization-based control strategy named Model Predictive Control (MPC). The MPC combines optimization and control at each time step. It means that MPC first measures the current state of the system and then computes an optimal control actions to take regarding the best performance that a prediction horizon gives according to a given optimization objective function. Thus, the set-points for step k are found and this cycle is repeated for the next step. For the case study of three energy hubs, each one with CHP, furnace and heat storage presented in [17], the objective is to minimize the energy costs considering characteristics of the transmission infrastructures, dynamics of the storage devices, and load and price profiles. It is claimed that a prediction horizon of 5 time steps (one hour each step) is a good trade-off between control performance and computational effort.

The inclusion of power generation by renewable sources in the dispatch problem is specifically treated in [22]. The economic dispatch model proposed uses conventional generators and wind energy sources. The model aims the minimization of an objective function that includes: 1) a cost term as function of generated power for each conventional generator, 2) a cost term as function of the scheduled (forecasted) wind power for each wind turbine, 3) a penalty cost term for not using all available power from each wind turbine which is function of the available wind power minus the schedule wind power, and 4) a required reserve cost term, which is a penalty associated with the overestimation of the available wind power. The inclusion of the cost term 2) depends on the ownership of the wind turbines, if the utility owns the wind turbines this cost is zero and the utility will want to use all available wind energy. The available wind power is a random variable that follows a Weibull probability density function. Among the constraints, the conventional power generation plus the wind power generation equals the load. The use of penalty costs gives a good picture of the monetary burden that the unpredictability of wind power represents.

In [28] and [29] Warsono et al. also discuss an economic dispatch formulation that takes account the inclusion of renewable energy power systems. Using wind energy, two approaches for the economic dispatch problem are treated with the same objective function, minimization of power and reserve costs. In the "negative load" approach the forecasted wind power is subtracted from the load demand, thus producing a new load demand that is used in the economic dispatch problem.

The “inclusive” approach incorporates the wind turbines in the calculations with the intention of use it as much as possible. For this second approach a wind cost function that bears the high capital cost and low operational cost of the wind turbines is assumed.

The case of economic-environmental dispatch problem is analyzed in [18] for a system that includes six conventional generators plus wind and solar energy converters. A multi-objectives optimization function aims to minimize a fuel cost function and an emission function, while extracting the maximum power from the renewable sources. From the total load demand the generation of wind and solar sources is extracted, and this remaining total demand is distributed among the conventional generators. The remaining total demand and the renewable power generation (from wind and sun) are determined by using a neural network that takes account for the variation of wind speed, solar radiation, and total load demand. In order to solve the multi-objectives optimization dispatch problem, the authors use a Strength Pareto Evolutionary Algorithm to obtain the non-dominated solutions of the problem.

Controlling Module alternatives

The controlling module is in charge of maintaining the state variables of the system (e.g. frequency and voltage in an electrical system) running properly, it means that decisions about power generation need to be carried out. How to structure this task has a common consensus among the different proposals for controlling DGS, it is a hierarchical control architecture alike to the one used in the traditional EMS. For example, Ortjohann, et al. in [27] propose a three level hierarchical control formed by unit controls, local controls, and a main supervisory control. All of them operating in a system with several Microgrids working in parallel with each other and with the main grid. In this way, the unit control responsibility is to maintain frequency and voltage within acceptable ranges while preventing that a single generation unit takes the whole load on its own. The local control boundary action is the Microgrid and its role is to bring system frequency back to the nominal value and exchange power between the tie lines. Finally, the main supervisory control manages the entire system, through monitoring, optimization and dispatching of power via communication to local controllers, and therefore to unit controllers, of the actions to take.

Distributed generators mainly interface with other generation units by means of power electronics interfaces, i.e. power inverters. Therefore control strategies, at the unit control level, for the operation of these electronics components have been described in several papers. Considering the function that the inverter will accomplish in the grid and the kind of distributed generation source behind it, an inverter can operate under grid-forming, grid-supporting or grid-parallel inverter methodology [25, 27].

A grid-forming inverter is thought to establish and maintain the frequency and voltage of the grid, to achieve this, a frequency-active power droop and a voltage-reactive power droop control strategies are implemented in the inverter’s controller [20, 25, 27, 31]. Since these strategies emulate the control operation of a synchronous generator, a Microgrid can operate safely in an islanded situation without concerns that load variations or contingencies draw frequency and voltage out of their normal ranges. Furthermore, these control strategies rely only in local information of the frequency and voltage at the unit terminals, which make them robust and fast.

In grid-supporting inverter operation, the distributed generator’s inverter injects a preset amount of real and active power to the grid. The power injection is executed by the inverter’s controller while the values of real and active power that are not fixed in time and vary with relation to the requirements of the system are defined by the local and/or main control. For instance, a new

setpoint for the injection of real power could be transmitted either by the local control to bring the frequency to normal or by the main control to comply with some optimization target.

The above inverter methodologies are suitable for dispatchable distributed generation sources. Wind and solar energy sources do not fall into this category, thus their inverters operate based on optimal power generation in order to deliver the maximum available power to the grid. This is the operation methodology of the grid-parallel inverter.

Although voltage droop characteristic is the more accepted control strategy for reactive power, [24] defines other two control strategies. Being the first one voltage regulation control strategy, therein the reactive power is controlled to regulate the voltage in the grid coupling point through the error formed between the terminal voltage and a voltage reference. Power factor correction is the other control strategy. It is used to compensate for a local load power factor by way of relating (through a compensation factor) the load power factor and a desired power factor. Consequently the compensation factor impacts in the reactive power dispatched.

Zilong, et al. demonstrate in [31] the possibility of frequency and voltage droop control strategy for inverters of wind and solar energy sources. This is achieved by creating clusters, each one made of a renewable energy source and a battery stack connected in parallel. The parallel connection takes place at the DC link of these components which in turn connects to the DC side of the inverter. Thus, the battery stack allows power dispatch while maximum harvest of renewable energy is kept.

CHAPTER 3

Thesis Problem Statement and Optimization for Energy Dispatch

The first part of this chapter describes the problem to be solved with this thesis work in detail. The second part presents the proposed answer of a joint-collaboration work, published in [32] and that was developed during the first stage of this thesis. This collaboration tackled the challenge of including storage in the optimization problem for unit commitment and optimal dispatch of multiple energy carriers in distributed generation systems.

Problem Statement of the Thesis Project

The increasing demand for developments in energy efficiency, the daily addition of distributed generation systems to current electricity grids, the unpredictability of continuous wind and solar energy flows, the aim to achieve low production costs, and the new environmental regulations that ask for greenhouse emission reductions are just a few of the reasons to create innovative approaches in the energy generation field and its management.

The PhD research project "Intelligente energiehuishouding op wijk- en woningniveau" which is presently carried out in the Electrical Power Systems group of the Electrical Sustainable Energy department at TU Delft studies the integration of decentralized and renewable technologies at a district level, incorporating aspects related to energy management. Hence this research project includes investigation on the management of DGS energy systems.

The adopted management structure for decision and control in the operation of a distributed multiple energy conversion and supply system resembles the EMS described in Chapter 2. The modular EMS structure depicted in Figure 5 is adapted to incorporate the management traits that are found in a distributed generation system that includes multiple energy carriers and converters, stochastic renewable energy sources, and storage devices. Figure 9 shows the modular structure of this management process, the distributed energy management system (DEMS).

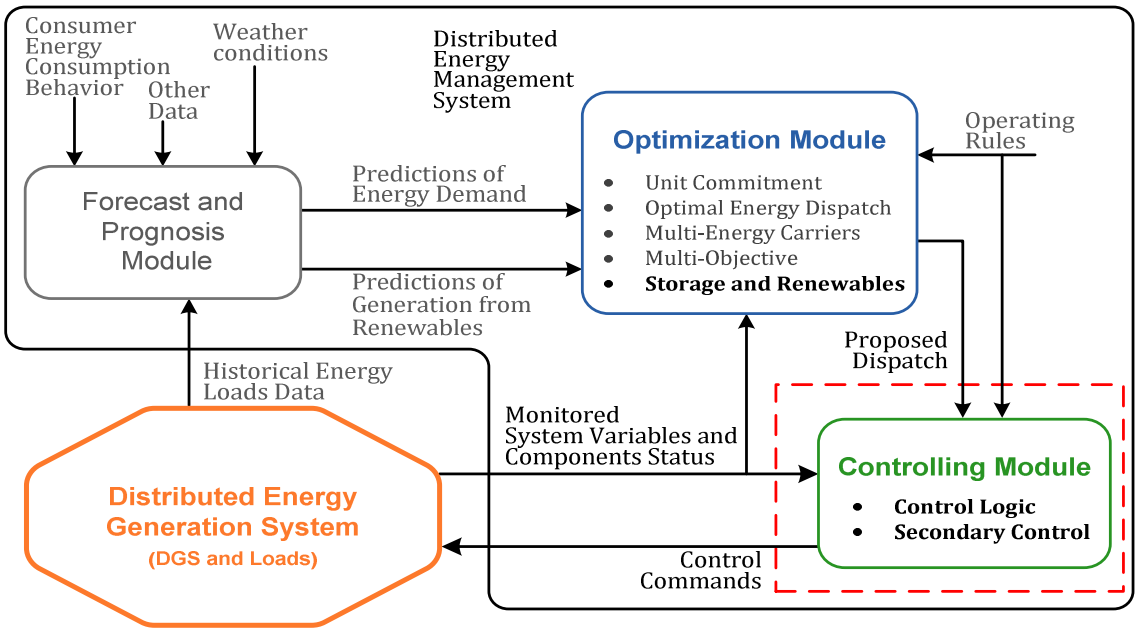

Figure 9 Modular structure of a Distributed Energy Management System (DEMS)

Within this PhD research, ***the study of the DEMS's control module in order to visualize entirely the performance and behavior of DGS operating under DEMS is stated as the problem to be answered by this MSc thesis project***. The result of this project shall be a stable, robust and simple as possible control strategy that satisfies the aims established for the DEMS.

The solution of this problem starts by understanding how the DEMS's control module interacts with the system operator, the optimization module and with the DG system's components through the flowing data signals:

- Operating Rules are provided by the system operator based in the aims for the DGS.
- Proposed Dispatch signal contains an array of setpoints for optimal operation of the DG components.
- Monitoring and Control signals are interchanged between each of the components of the DGS and the control module.

This exchange of data towards and from the control module implies that the above signals must be available in order to asses a suitable control strategy for the DEMS's control module. Operating Rules are taken straight forward from the actual rules that steer the traditional power system, plus the additional needs to incorporate distributed sources of energy. For the Proposed Dispatch signal, the control module requires that the optimization module resolves a unit commitment and optimal energy dispatch problem that includes multi-energy carriers (e.g. electricity, heat, hydrogen, etc), multi-objectives (e.g. economic or/and environmental) and that can deal with the inclusion of random renewable energy sources and storage devices.

In regards to the Monitoring and Control signals, the DEMS's control module expects to send commands that govern the energy dispatch of each one of the energy supply sources in order to satisfy the energy demand properly. At the same time it requires to receive system variables (e.g. voltage, temperature, torque, pressure, etc) and operation status of the controlled and uncontrolled DGS's components in order to decide the next control action to take. In response to this need, it is proposed to develop a simulation platform where models of energy conversion devices, energy storage devices, and energy loads interact each other through variables representing their particular energy domain, e.g. voltage and current for electricity or temperature and heat flow for thermal energy.

In order to carry out this project a representative DGS was chosen. It is an autonomous distributed generation system that includes a renewable energy source, storage devices and has load demands for electricity and heat.

Structure of the Distributed Generation System

The chosen distributed generation system to model comprises two kinds of energy in the demand side: residential and commercial low voltage electrical load and heat load in the form of district heating for room heating and service water heating. Whereas the primary energy sources that feed the input side of the energy converters are natural gas and wind speed. Thereby options for energy converters that suit these energy forms constraints are combined heat and power generators (CHP), wind turbines and boilers.

Figure 10 shows a sketch of the modeled distributed generation system. Three CHPs increase supply reliability and add maneuverability to their operation. The heat and electricity storage devices are added to enhance the flexibility of the system, allowing for example store heat from the CHP when surplus is produced due to a high electricity demand, this stored heat in turn can be used to

cover a scheduled heat demand without burning natural gas in the boiler. Thus environmental and economic savings can be achieved.

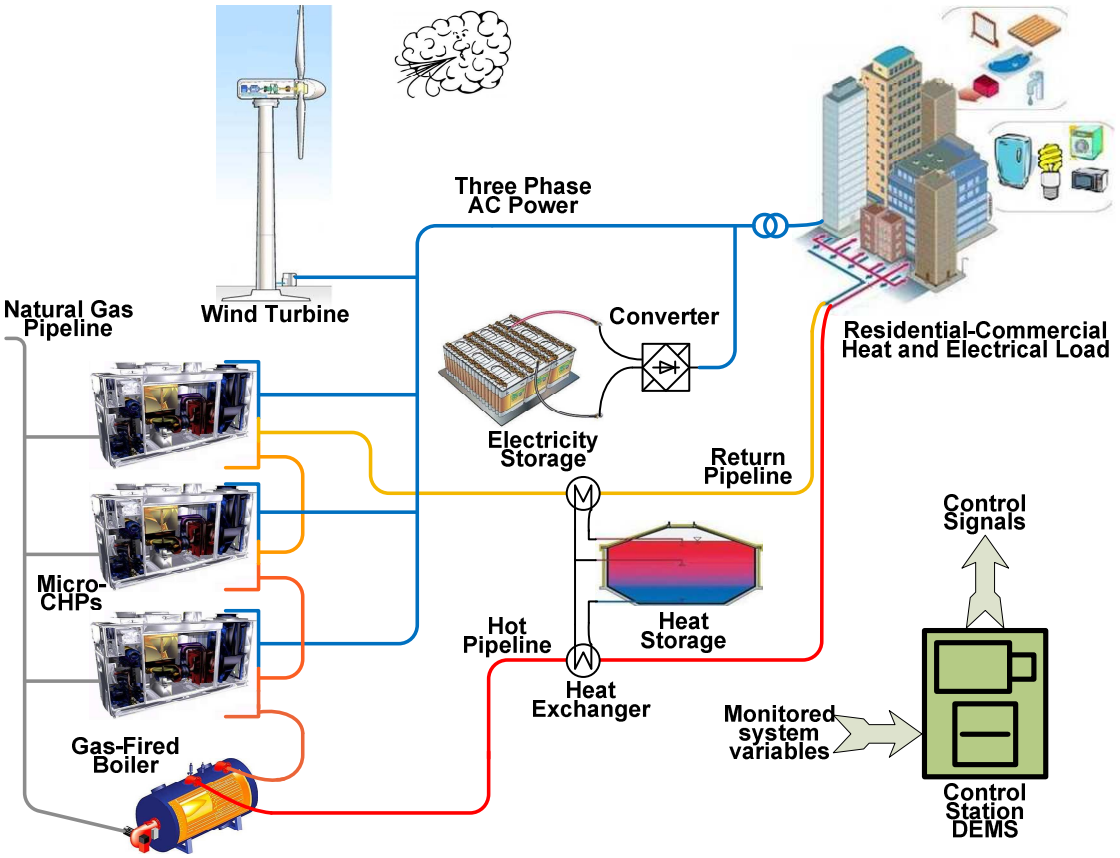

Figure 10 Sketch of the studied distributed generation system

Regarding the electrical part of the DGS model (blue lines in Figure 10), the selected operation mode of this DGS is autonomous (i.e. non connected to a main electrical grid) and its electrical network is made of a three phase generation and load. The power lines of CHPs, wind turbine and electricity storage are connected each other without considering any transformer as interface because this adds few to the research purpose but increases the model's complexity unnecessarily. As the electrical load contemplated for this research belongs to a residential-commercial district, the electrical part of the DGS only considers active power for the modeling. Moreover, power losses due to transmission are neglected.

The heat part of the DGS model (red-orange lines in Figure 10) consists of a district heating system (introduced in chapter 1). The generated heat is transported by hot water through a pipeline with indirect connection at the load side and a return pipeline is included to close the cycle. A cascade configuration of the heat sources (CHPs and boiler) heats up the return water, while the heat storage device takes or gives heat from the hot water pipeline or to the return water pipeline respectively. Since the research's interest is on the heat flows, the pressure in the pipes and effects of pumps are not taken into account and therefore the mass flows are thought to keep an ideal pressure always. Conversely to the electricity transmission losses case, the heat losses throughout the pipelines caused by the effect of ambient temperature are considered.

About the primary sources of energy, the provision of natural gas is given as needed by the DGS. No constraints about its amount, quality or delivery are part of this project. Wind speed patterns that represent the average wind profile in a specific location are given and used without alterations.

The control station carries out the control strategy that will achieve a fair realization of the system objectives. The model includes two levels of control. A primary control level operating in a fast manner is embedded in the components model. Its function is to stabilize the system variable states (frequency, voltage, temperature). A secondary control level, located in the control module, establishes the system condition by monitoring the state of the system variables and status of the DGS's components. These measurements along with a programmed control logic generate control commands. These commands are received by the DGS controllable components wherein they modify the component's operation accordingly. Thus, the secondary control corrects for deviations of the system variables in order to keep the system goals.

Unit Commitment and Optimal Energy Dispatch of the DGS

This thesis work assumes that predictions of energy loads and of generated energy from renewable energy sources for the DGS are given. Therefore the inputs to the DEMS's optimization module are known. As mentioned above the optimization module must be able to minimize the objective function of a DGS that includes multi-energy carriers, distributed generators, renewable sources and storage devices.

The optimal energy dispatch of multi-energy carriers with distributed generation and storage has been studied by Geidl [3], proposing the Energy Hub concept (introduced in Chapter 1), meanwhile Ramirez-Elizondo extended that work to include unit commitment of DGS without including storage or renewable sources [7]. Hence there is a gap to be covered in order to have a suitable optimization method for the operation of the DEMS's optimization module.

The solution of unit commitment is carried out applying Forward Dynamic Programming technique. This solves first the optimal dispatch problem at each time period of operation several times, each time committing different units and storing a pre-determined number of best solutions. Afterwards this technique determines the best set of units to commit in order to minimize the desired objective function. Due to the fact that the inclusion of storage in the system implies time dependability expressed on using the previous storage status to reckon the current, the straight forward application of forward dynamic programming technique is not possible It is because at each time period the pre-determined number of best solutions would be stored for each one of the previous storage status, thus making grow exponentially the number of best solution to save at each time period. Hence a technique to determine the unit commitment for systems that include storage devices is proposed.

A Technique for Unit Commitment in Multi-Energy Carrier Systems with Storage

The framework of unit commitment that is used in this technique follows the description presented in [7]. The problem statement that is used to solve a multi-energy carrier optimal dispatch problem without storage for a defined operating point is from [3] and its storage included version was introduced in Chapter 1 as Energy Hub concept. The multi-carrier unit commitment problem will be solved using the forward dynamic programming method according to [6].

The proposed method is depicted in Figure 11. At first, the unit schedule is obtained after the program runs the multi-carrier unit commitment problem without considering storage, just as described in [7]. This first schedule will then be considered as the starting point for Step 2.

At Step 2, the storage devices are included as part of the system, as described in Chapter 1. At this stage, the program assigns a new dispatch to the scheduled generating units and the storage devices. Storage devices will contribute to peak-shaving. Thus, if there are generating units that may be discarded after the inclusion of storage, it is expected that these units will dispatch at minimum capacity at this step.

At Step 3 a fictitious bidirectional load is included instead of the storage devices. This bidirectional load is loaded in accordance to the power values of the storage devices that were calculated in Step 2 for each time period. The program runs the multi-carrier unit commitment again and a new schedule is obtained. It is expected that the units that were brought to the minimum capacity in Step 2, will now be turned off, if no minimum up or minimum down constraints are violated.

Step 4 runs a new multi-carrier optimal dispatch, including storage. This is considered as the end solution.

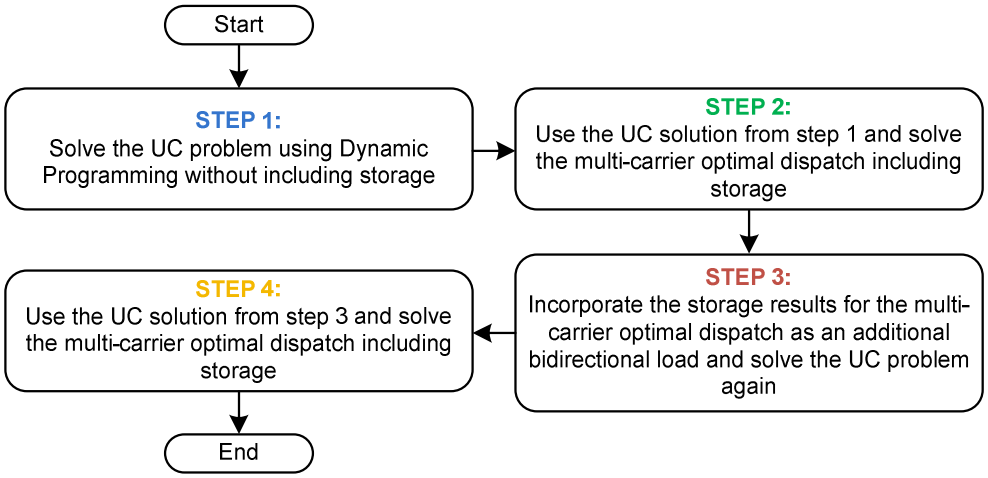

Figure 11 Steps to solve unit commitment of DGS that includes storage devices

As a result of this work, a co-authored paper about this technique appears in the conference proceedings of the 9th IEEE International Conference on Environment and Electrical Engineering 2010 [32].

Optimization Technique applied to the DGS

The mathematical model of the studied DGS according to the Energy Hub approach for optimization is developed next. It follows the framework for energy hub from Chapter 1 and the unit commitment from [7] in order to apply the above discussed technique. Figure 12 sketches the DGS according to the energy hub concept.

The formulation of the optimization problem to solve is stated as:

Economic Objective Function: $\mathcal{F} = aP_g + bP_g^2$

Equations:

$$\mathbf{L} = \begin{bmatrix} L_e \\ L_h \end{bmatrix} \qquad \mathbf{P} = \begin{bmatrix} P_g \\ P_{wnd} \end{bmatrix} \qquad \dot{\mathbf{E}} = \begin{bmatrix} \dot{E}_e \\ \dot{E}_h \end{bmatrix}$$

$$\mathbf{C} = \begin{bmatrix} w_1 v_1 \eta_{g-e}^{CHP-A} + w_2 v_2 \eta_{g-e}^{CHP-B} + w_3 v_3 \eta_{g-e}^{CHP-C} & 1 \\ w_1 v_1 \eta_{g-h}^{CHP-A} + w_2 v_2 \eta_{g-h}^{CHP-B} + w_3 v_3 \eta_{g-h}^{CHP-C} + w_4 v_4 \eta_{g-h}^{fur} & 0 \end{bmatrix}$$

$$\mathbf{S} = \begin{bmatrix} \frac{1}{e_e} & 0 \\ 0 & \frac{1}{e_h} \end{bmatrix}$$

Constraints: They are the same that in [7]

w_x is the status binary variable that equals to 1 when the unit is ON and 0 when it is OFF. The inclusion of wind power is dealt with through the "negative load" approach stated in [28] and discussed in Chapter 2.

This optimization problem is implemented in the optimization modeling software AIMMS (Advanced Integrated Multidimensional Modeling Software) for its solution.

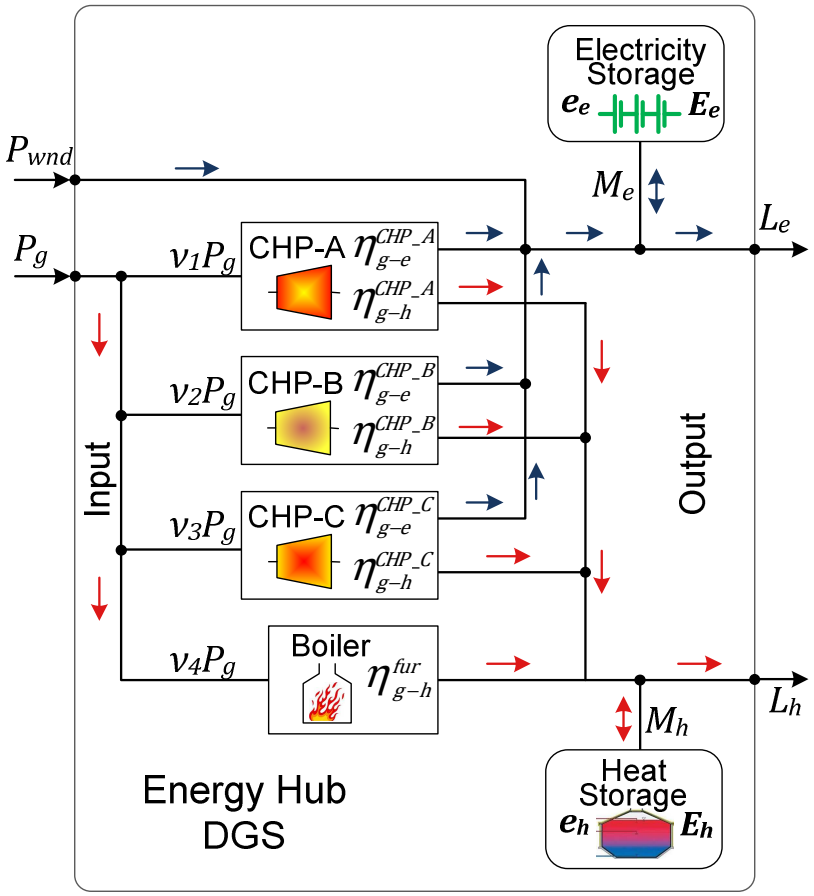

Figure 12 Energy hub block diagram for the studied DGS

CHAPTER 4

Modeling of DGS Components

The performance evaluation of a designed Distributed Energy Management System (DEMS) demands a suitable model of the Distributed Generation System (DGS). Depending on the intended research, a basic representation of the DGS that just takes into account the efficiency of its components may be enough, such in the case of assessing the optimization module of the DEMS (see chapter 3). Nevertheless, a proper research on the operation and control of an energy conversion and supply system under a DEMS demands a more detailed modeling of such system's components.

As the main objective of this thesis work is the design of a control strategy for the optimal operation of the DGS under an energy hub approach, the components of the studied DGS (see Figure 10) include the energy hub elements (energy converters and storage devices) and the load components (electrical load and heat load) are modeled at the extent of a fair characterization of their slow dynamic behavior. Hence, this chapter presents the models used to describe each one of the components of the DGS through implementing them on the model-based design environment MatLab®/Simulink®.

Modeling of Combined Heat and Power (CHP) generator

Thermal processes for electricity generation always yield heat as a by-product, which is commonly dumped into the atmosphere as wasted energy. However, when this generated heat is employed usefully such as in producing hot water, space heating or in some industrial application, the generation system, this way formed, is called combined heat and power. Such configuration makes an efficient use of its primary source of energy, achieving total energy efficiency of up to 90% [33].

Overview of CHP

The current interest on CHP generation lies in its potential in distributed generation systems, owing to its high efficiencies and relatively low carbon foot-print. Hence, CHP is seen as a significant emission-control strategy. Europe in 2001 met 10% of its heat and electricity demand with CHP and expects by 2010 to produce 18% of its electricity by CHP [34]. Currently, EU countries like the Netherlands and Finland rely on CHP to cover the 60% and 25% of its electricity demand respectively. In contrast, in the USA only 3.5% of its power demand was supplied by this means in 2002 [33, 35].

Almost any electricity generation technology can be adapted to work as CHP. It includes prime movers such as reciprocating engines, steam turbines and gas turbines, and electrochemical converters like fuel cells. So a large option of primary energy resources is possible ranging from natural gas, biogas and landfill gas to ethanol, methanol, kerosene, propane, diesel and hydrogen [36]. Nevertheless, gas turbines running by natural gas are the leading technology for CHP applications.

The DGS of this research project takes advantage of CHP based on gas turbines with sizes under 250kWe. Combustion turbines in this power range are known as micro-turbines (micro-CHPs) which operates at high speeds up to 120000rpm [33]. Some designs incorporate the turbine components and the electricity generator on a single shaft. Others utilize a split-shaft design where a power turbine rotates a conventional electricity generator through a gearbox [37]. This thesis work uses this later design coupled to a synchronous generator.

The electrical efficiency of the micro-CHP depends on the heat quality needed. With high-grade heat quality (high temperature), steam can be produced at the expense of less electrical generating efficiency. Conversely, low-grade heat quality, useful for water and space heating, allows the

obtention of electricity efficiency between 20 to 30%. However this efficiency is lower than that of a heavy duty gas turbine (30% to 39%) [33].

The advantages of micro-CHP over other technologies for small-scale power generation are its compact size and lightweight per unit power, small number of moving parts, relative low noise and vibration level, low emissions, multi-fuel capability, little use of lubricating oil and low maintenance cost, additionally its delivery time is relatively short and its installation is fast. Disadvantages include lower electrical efficiency in its basic configuration than other small generation options. However it is currently challenged for power gas turbine derived from high-efficiency aero-engines technologies. Other disadvantage is that its efficiency decreases at partial load and that micro-gas turbine may require power conditioning before connection to grid. A non-technical barrier is that its maintenance requires highly specialized personnel and another that its investment payback period could be high [34].

Three main components are part of a CHP generator: a gas turbine that burns fuel and produces rotational energy, an electricity generator and a heat recovery system that transfers heat from the turbine's exhaust gases into a working fluid (normally water).

Operation Principle and Components of Micro Gas Turbine

A gas turbine harnesses the energy contained within an air-mass flow (potential and kinetic energy of gases under pressure) to generate rotary motion. Either it is a heavy duty gas turbine or a micro gas turbine, its principle of operation is governed by the thermodynamic Brayton cycle. Figure 13 illustrates an ideal Brayton cycle consisting of four internally reversible processes. The first process going from point 1 to 2 is an isentropic (constant entropy) compression of the mass flow and then from 2 to 3 a constant pressure with heat addition process occurs. The next process (3 to 4) is an isentropic expansion where work is performed by the mass flow. Finally, the realization or not of the constant pressure heat rejection process (4 to 1) defines whether the gas turbine operates in either closed cycle or open cycle [38-39] .

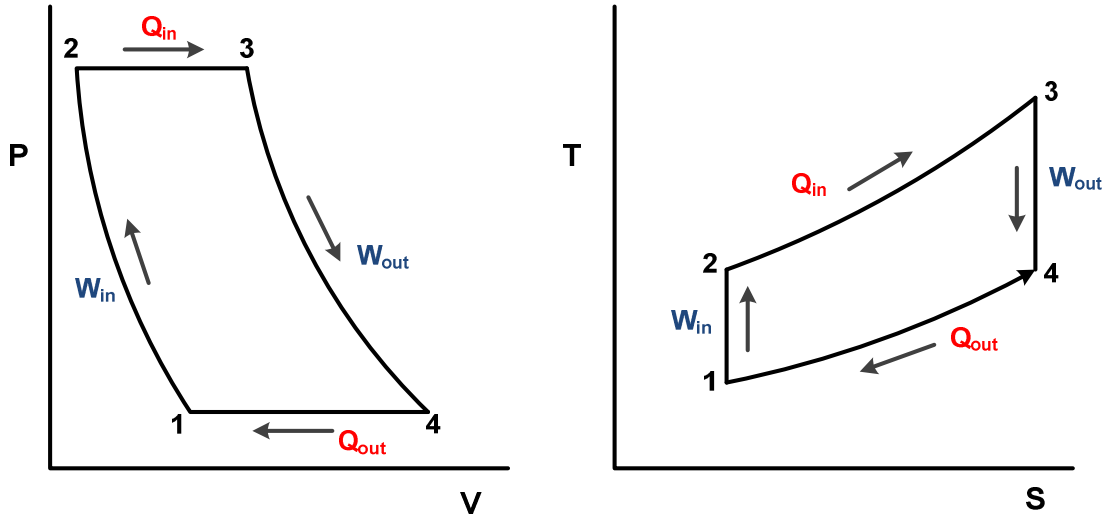

Figure 13 Pressure-Volume and Temperature-Entrophy diagrams of an ideal Brayton cycle

Considering Brayton cycle processes in steady-flow and neglecting changes in kinetic and potential energy, the thermal efficiency of the open cycle is given by [38]:

$$\eta_{th,open} = 1 - \left(\frac{1}{r}\right)^{\frac{(\gamma-1)}{\gamma}}$$

Eq. 8

where r is the pressure ratio: $r = \frac{P_2}{P_1}$; and γ is the specific heat ratio: $\gamma = \frac{C_p}{C_v}$. When the gas turbine works in a closed cycle its efficiency becomes [34]:

$$\eta_{th,closed} = 1 - \frac{r^{\frac{(\gamma-1)}{\gamma}}}{t}$$

Eq. 9

where t is the temperature ratio: $t = \frac{T_3}{T_1}$.

The Brayton cycle carried out by the components of a gas turbine is depicted in the Figure 14. Air at ambient temperature and pressure enters an axial compressor (centrifugal compressor in micro-turbine case) that raises air's pressure by 15 to 25 times along with air's temperature to about 400 to 465°C. The compressed air passes through a recuperator (heat exchange with exhaust gases) where it gains heat before entering the combustor. The primary zone of the combustor chamber mixes a portion of the air flow with high pressure fuel (e.g. natural gas) and ignites it. Straight away, the hot combustion gases pass through the combustor's dilution zone that mixes them with the remainder air flow in order to keep them in a suitable temperature for the turbine's blades, 1370 to 1427°C (around 927°C for micro-turbine). The resulting gases go in a row of turbine's stationary blades (nozzles) that convert the high-enthalpy gases to high velocity and then this energy is transformed to rotary motion by the turbine's moving blades. This rotary motion turns a shaft that in turn drives the compressor and in single shaft turbine configuration the rotor of the electricity generator as well. The expanded exhaust gases leaving the turbine at around 482 to 638°C are fed through the recuperator into the heat recovery system for CHP application [34, 38-40].

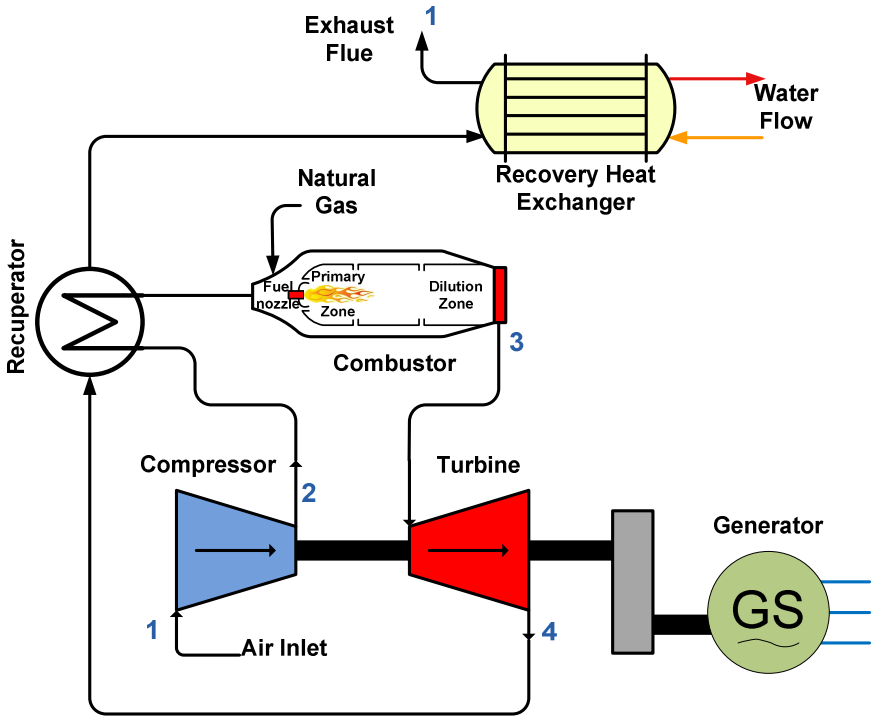

Figure 14 Schematic of micro-CHP gas-fired generator

Model of Micro Gas Turbine

As the research intent is to formulate a control strategy that achieves an optimal energy dispatch of the combined operation of distributed generators, the micro-turbine operation is well enough described by its slow dynamics under normal operation. It means to neglect its fast dynamics at start-up, shutdown, faults, and so on. Thereby the simplified single-shaft gas turbine representation provided by Rowen [41] is quite appropriate. This per unit Rowen's model has been used for several other authors to study turbine's governor options and to characterize other gas turbine configurations, for example in [42] a twin-shaft turbine, in [43-44] a PID-droop governor and in [45-46] a micro-turbine.

The micro-turbine employed here has a split-shaft design where a turbine drives the compressor and a power turbine propels a synchronous generator. Argued by [37], this turbine is suitable to be modeled as an single-shaft turbine. Therefore, a reduced per unit Rowen's turbine model that considers neither temperature control nor acceleration control is depicted in Figure 15 and detailed afterwards.

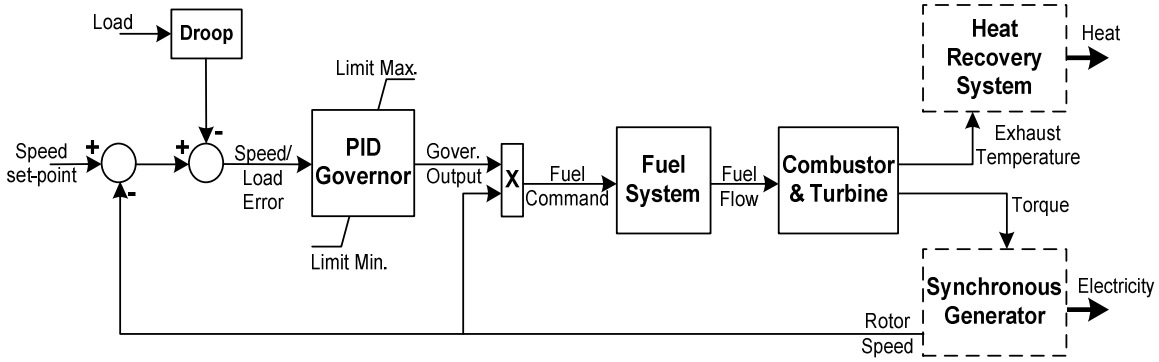

Figure 15 Block diagram of reduced gas turbine model

Fuel system

The fuel flow injection (F_f) in the combustor chamber is accomplished by two valves in series and is proportional to the product of the governor output times the per unit mechanical rotor speed (ω_m). In this simplified model, the valve position is kept proportional to the gas flow command (F_c) and thus only two time constants are important to model the gas injection. One (T_V) corresponds to the valve positioning system and the other (T_A) is associated with the fuel actuator manifold and downstream piping. The transfer functions for these are shown in Figure 16.

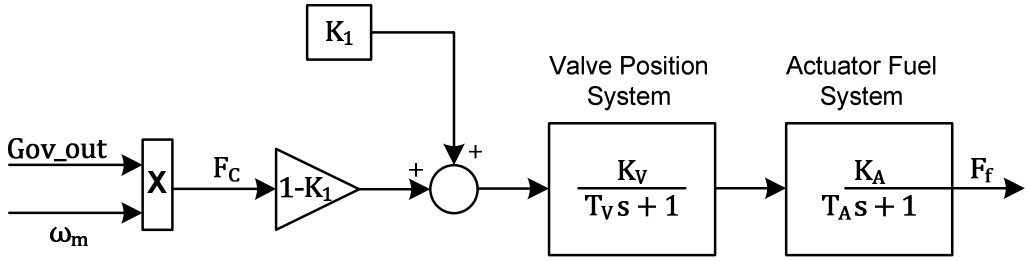

Figure 16 Block diagram of the gas turbine Fuel System

Where, the gains K_V and K_A are of unit value and the per unit value of Gov_out corresponds directly to the per unit value of the mechanical power of the turbine at steady state. Notably, the gas

turbine needs a considerable amount of fuel to maintain operation at nominal speed no-load condition, reaching amounts of around 23% of rated fuel. In order to model this trait, the flow command is scale by 1-K_1 and then added to K_1, where K_1 equal to 0.23.

Compressor-Combustor-Turbine

In order to characterize the dynamics of the compressor-combustor-turbine assembly, three transport delays can be associated with each of its parts:

a) T_{CR} is a small transport delay linked to the combustion reaction time,
b) T_{CD} is a time lag associated with the compressor discharge volume, and
c) T_{TD} is a transport delay to convey the gas from the combustion system through the turbine.

Figure 17 depicts the block diagram of this assembly. The turbine torque and exhaust temperature as function of the fuel flow and turbine speed are described by the following linear equations [41]:

Turbine Torque: $$\boldsymbol{Torque = 1.3(F_f - 0.23) + 0.5(1 - \omega_m)}\ \text{[p.u]} \qquad \textbf{Eq. 10}$$

Turbine Exhaust Temperature: $$\boldsymbol{T_{Et} = T_R - 390(1 - F_f) + 306(1 - \omega_m)}\ [°C] \qquad \textbf{Eq. 11}$$

where, T_R stands for rated exhaust temperature of the turbine. The subtraction of 0.23 from fuel flow accounts for the self-sustaining fuel amount that characterizes the gas turbines. Thus, the power to fuel characteristic rises linearly from 23% of gas consumption at no-load (no torque) to rated consumption at rated power output. This equations accuracy is within 5% at part-load for the torque and somewhat less for the exhaust temperature.

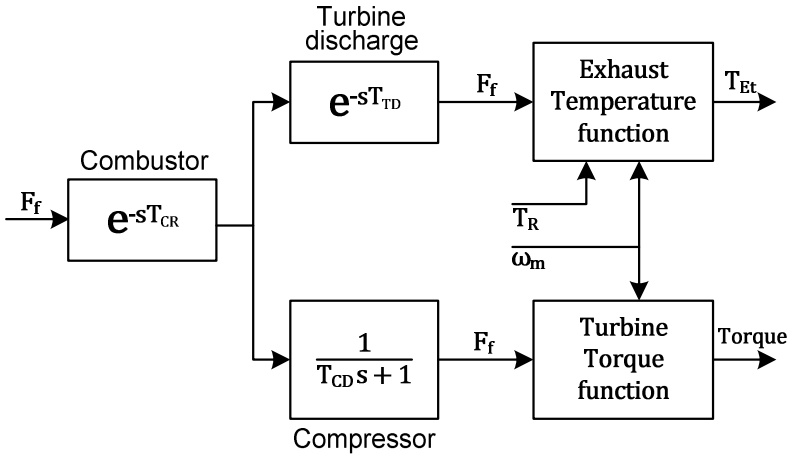

Figure 17 Block diagram of compressor-combustor-turbine assembly

Internal control system (primary control)

The gas turbine uses a Woodward governor that consists of a Proportional-Derivative-Integral (PID) controller that operates on the speed/load error input signal to command the fuel injection as shown in Figure 18. PID controllers have robust performance in a wide range of operating conditions and appealing functional simplicity, being particularly useful for reducing steady state error and improving the transient response [47]. Each of its terms works as follow [48]:

- The proportional term corrects the output in proportion to the input error, thus providing stability but introducing an offset (steady state error).

- The integral term acts on the error duration and its magnitude, accelerating the output respond pace towards the set-point and eliminating the offset. However, it causes the respond's present value to overshoot the set-point value.
- The derivative term changes the output respond proportionally to the rate of change of the input error. It reduces the overshoot and stabilization time but might lead to system instability due to noise amplification of the error input signal.

The PID controller performance is adjusted by tuning its gains (K_P, K_I, K_D) accordingly to the desired respond of the gas turbine-synchronous generator set. This respond is expressed by the stabilization time, maximum overshoot and steady state error of the rotor speed which works as the feedback variable. The PID gains were determined by using the method suggested in [49] with a step signal as system load input and are listed in Table 1.

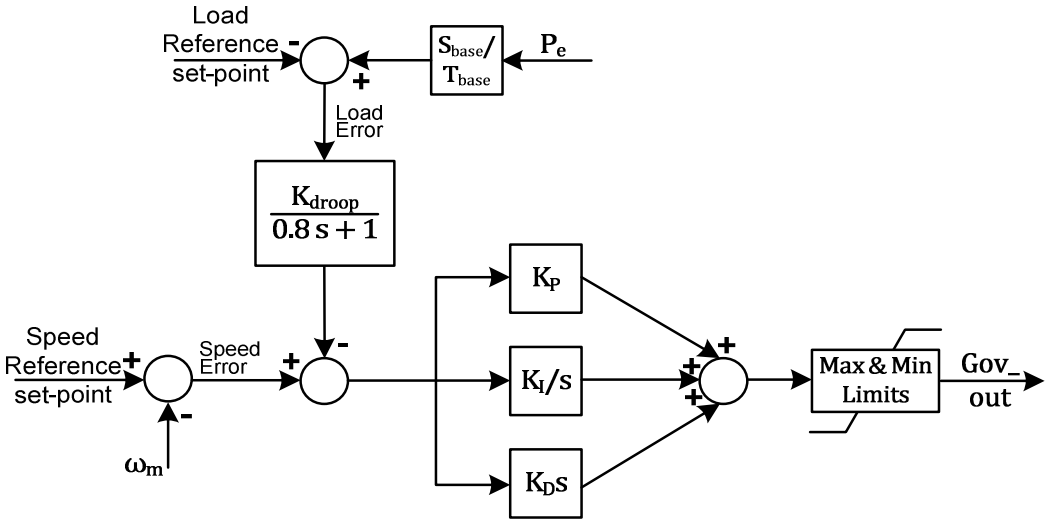

Figure 18 Block diagram internal control system of the micro-CHP

The speed error is made of the speed reference kept at unit value minus the per unit value of the actual rotor speed (ω_m, frequency) taken from the synchronous generator model. If the PID controller is only fed by this speed error, the generator works in isochronous mode making the rotor speed's steady state error zero. However, in this operation mode, parallel connection of two or more generators is not possible because they will "fight" each other to control the frequency when changes in load occur.

In order to operate in parallel, generators work in droop mode at which there will always be a unique frequency to share load changes among them [6]. In this mode, the scaled per unit electrical power (P_e) is used as feedback signal and added to the speed error through a droop gain-filter block. The droop gain (K_{droop}) is 4%, typical value, meaning that a hundred percent change on the output power will result in a four percent change in the frequency. Therefore, in this operation mode a frequency deviation from its reference is inherent and must be corrected. The load reference set-point executes this correction action through changing the operating point of the governor, so reference frequency can be established at any desired power output. By adjusting the load reference in each generator, a scheduled generation dispatch can be implemented while holding the system frequency close to its reference.

Finally, limits are imposed to the governor output signal. The minimum limit accounts for the unique gas turbine capability of transiently absorbing power from the connected system while

maintaining fuel burning in the combustor [41]. The maximum limit acts like an engine temperature control.

Model of Synchronous Generator

A synchronous generator is an electric machine that converts rotary mechanical power into electrical power. This conversion takes place by applying a DC current to the generator rotor winding (field winding) which is turned by a prime mover, thus producing a rotating magnetic field. In turns, this field induces a three-phase set of voltages within the stators windings of the generator.

The generator model is represented in the dq0 (direct-quadrature-zero) coordinates aligned to rotor d and q axes. This eliminates the dependence of inductances on rotor position and simplifies its analysis. In this model rotor variables are reduced to stator variables. The equivalent electric circuit of the salient-two-pole pairs with damping winding used in this work is shown in Figure 19.

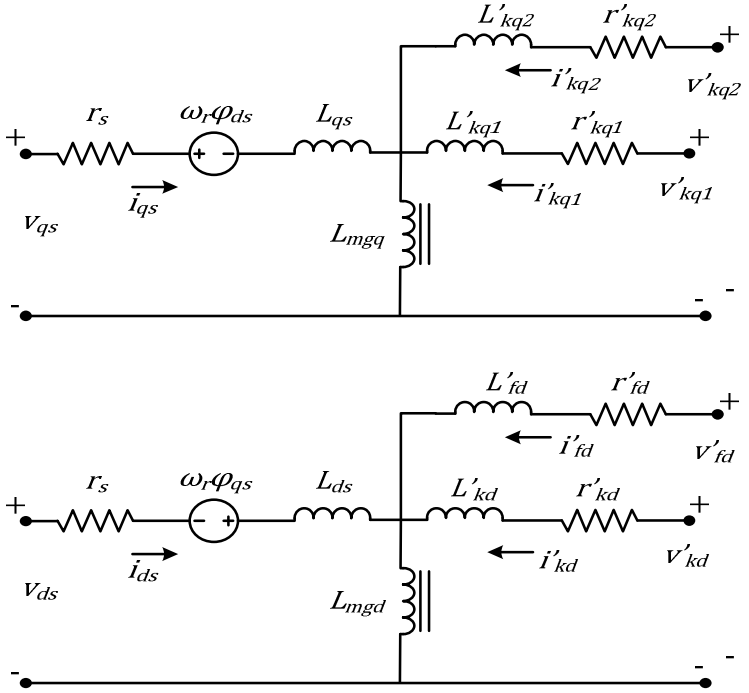

Figure 19 Equivalent circuit of synchronous generator according to [50]

The set of equations that considers the electrical dynamics of the stator, field and damper windings to model the synchronous generator are listed below together with the electro-mechanical rotor equation.

$$v_{qs} = r_s i_{qs} + \omega_r \varphi_{ds} + \frac{d\varphi_{qs}}{dt}; \quad \varphi_{qs} = L_{qs} i_{qs} + L_{mgq} i'_{kq}$$

$$v_{ds} = r_s i_{ds} - \omega_r \varphi_{qs} + \frac{d\varphi_{ds}}{dt}; \quad \varphi_{ds} = L_{ds} i_{ds} + L_{mgd}\left(i'_{fd} + i'_{kd}\right)$$

$$v'_{fd} = r'_{fd} i'_{fd} + \frac{d\varphi_{fd}}{dt}; \quad \varphi'_{fd} = L'_{fd} i'_{fd} + L_{mgd}(i_{ds} + i'_{kd})$$

$$v'_{kd} = r'_{kd} i'_{kd} + \frac{d\varphi'_{kd}}{dt}; \quad \varphi'_{kd} = L'_{kd} i'_{kd} + L_{mgd}\left(i_{ds} + i'_{fd}\right)$$

$$v'_{kq1} = r'_{kq1} i'_{kq1} + \frac{d\varphi'_{kq1}}{dt}; \quad \varphi'_{kq1} = L'_{kq1} i'_{kq1} + L_{mgq} i_{qs}$$

$$v'_{kq2} = r'_{kq2} i'_{kq2} + \frac{d\varphi'_{kq2}}{dt}; \quad \varphi'_{kq2} = L'_{kq2} i'_{kq2} + L_{mgq} i_{qs}$$

$$\Delta\omega(t) = \frac{1}{2H} \int_0^t (T_m - T_e)\, dt - K_k \Delta\omega(t)$$

Eq. 12

Where *v, i, r, L, ω, φ, t, H, T, K* stand for voltage, current, resistance, inductance, speed, flux linkage, time, inertia, torque, damping factor respectively. While the suffixes *q, d, s, r, f, mg, k, m* and *e* stand for d and q axis quantity, stator and rotor quantity, field quantity, magnetizing inductance, damper winding, mechanical, and electrical quantity respectively.

A built-in model of synchronous generator found in MatLab/Simulink/SimPowerSystems® is used in this thesis work. Further, it connects to an excitation system model (also built-in) to provide field voltage while regulating the generator terminal voltage in order to keep a reference. Lastly, the built-in generator's mechanical power input connects with the gas turbine's torque output through the power-torque relation: $P_m = T_m * \omega_m$ **Eq. 13**

Model of Exhaust Heat Recovery System

This part of the micro-CHP consists of a shell and tube heat exchanger in counter-current configuration. Here, the exhaust gases flowing out of the recuperator are transported to the hot-side intake of the heat exchanger where they increase the temperature of the water circulating through the exchanger's cold-side before being released to the atmosphere. Figure 20 shows the block diagram of this system.

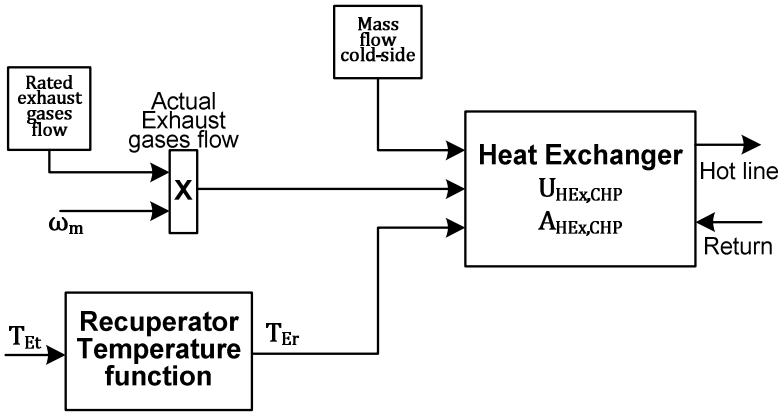

Figure 20 Block diagram of the exhaust heat recovery system

Equation Eq. 14 reckons the exhaust gases temperature (T_{Er}) that leaves the recuperator and goes toward the heat exchanger. This temperature is a linear function of the turbine exhaust temperature and the ambient temperate (T_{Amb}). The coefficient resulted from considering the inlet and outflow exhaust heat at rated values of turbine exhaust temperature, recuperator exhaust temperature and exhaust gases mass flow taken from the micro-CHPs datasheet.

$$T_{Er} = 0.405(T_{Et} - T_{Amb}) + T_{Amb} \quad [°C].$$

Eq. 14

In the heat exchanger model the recuperator exhaust temperature, the actual exhaust gases mass flow and the cold-side water mass flow with its return inlet temperature make up the variables that model the heat exchange between the exhaust gases and the incoming water. They determine

the amount of temperature (heat) gained by the water at the output connection (hot line) of the heat exchanger cold-side. The heat exchanger works at counter-current and employs the logarithmic mean temperature difference (LMTD) as driving force for heat transport. This transport takes place through the contact area ($A_{HEx,CHP}$) between the hot-side and cold-side chambers of the exchanger. The thermal resistance to the heat transfer is expressed by an overall heat transport coefficient ($U_{HEx,CHP}$) where the convective heat transfer mechanism dominates. A detail description of the heat exchanger modeling shall be discussed in the modeling of heat components section.

Integral model of the micro-CHP in Simulink

Each of the above micro-CHP components' models makes up a subsystem in its Simulink representation for this thesis work. This modeling effort takes advantage of Simulink mathematical operations and signals together with the Simulink/Simscape® modeling software for multidomain physical systems. Simscape creates network representations of the system using the Physical Network approach. According to this approach, each system is represented as consisting of functional elements that interact with each other by exchanging energy through their ports [51]. Connecting the Simscape blocks ports together is analogous to connecting real components. Thus, describing the physical structure of a system rather than the underlying mathematics. From this physical structure, Simscape automatically constructs the equations that characterize the behavior of the system.

Two physical domains apply for the micro-CHP modeling and in further models in this thesis. Each domain has one across variable and one through variable, in the electrical domain these are voltage and current respectively. Meanwhile, heat flow and temperature hold for the thermal domain. An important feature of the Physical Network approach is that automatically resolves all the traditional issues with variables, directionality, and so on. Figure 21 shows the micro-CHP subsystems that form this model.

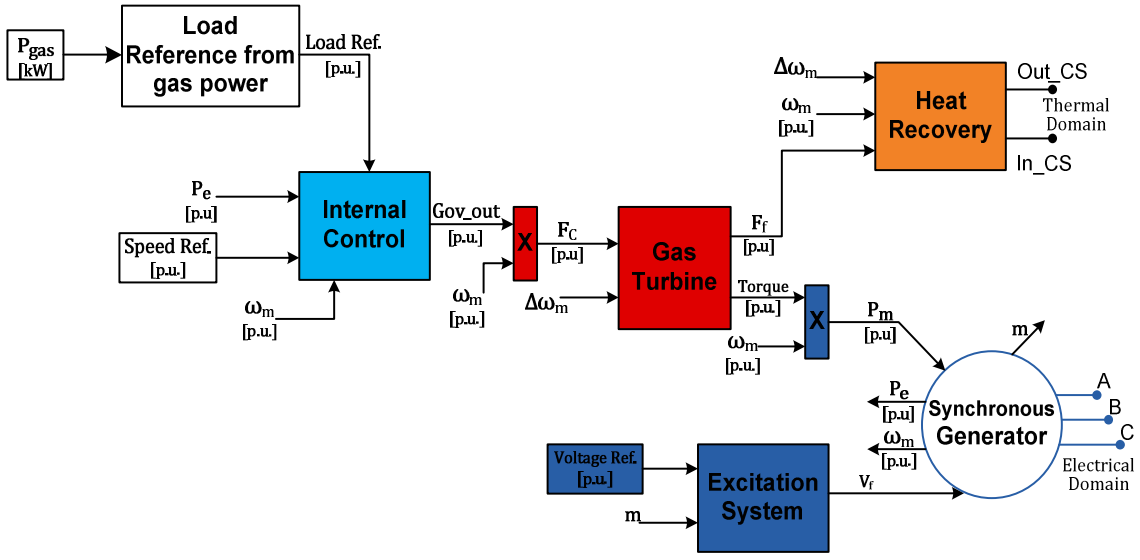

Figure 21 Simulink subsystems of micro-CHP model

As discussed earlier, the load reference is the main means for controlling the electrical power dispatch of the micro-CHP. This thesis work defines the load reference set-point as the amount of power that the system should convert every specific instant in order to have the desired electrical

power at the micro-CHP terminals. Therefore, the load reference set-point takes into account the conversion efficiencies in the system.

The subsystem "load reference from natural gas power set-point" accomplishes the task of converting the dynamic natural gas power set-point (P_{gas} in kilowatts) into the load reference signal used by the micro-CHP per unit model. This task entails the knowledge of the micro-turbine efficiency (η_{Turb}), the electrical generator efficiency (η_{ele}) and the micro-CHP heat rate (HR), the latter is the energy from the fuel used in the turbine to produce one electrical kW-h when operating at rated values. In the heat rate value, the presence of the turbine heat recuperator is considered.

P_{gas} is primarily given by the DEMS's optimization module (which reckons it by considering the CHP electrical efficiency (η_{CHPele})) through the control station. As the gas-turbine dynamic model does not consider turbine's efficiency, the fuel command (F_C in p.u) is directly proportional to the mechanical output power (P_m in [p.u]). Meaning that the load reference represents the per unit amount of mechanical power to convert into electricity. Therefore, micro-turbine efficiency is used to obtain Load Ref. in per unit from P_{gas}.

Regarding the 23% of rated fuel used for turbine self sustaining and the found non linearity of the built-in synchronous generator efficiency, the equations used in the Load reference from power gas subsystem are:

$$\boldsymbol{\eta_{CHPele} = \eta_{Turb} \cdot \eta_{ele}} \quad \textbf{Eq. 15}$$

$$\eta_{CHPele} = \frac{P_{gas} - 0.23 \cdot P_{gas-rated}}{0.77 \cdot HR \cdot P_{gas}}; \quad or \quad \eta_{CHPele} = \frac{P_{gas}[p.u] - 0.23}{0.77} \quad \textbf{Eq. 16}$$

$$\eta_{Turb} = \frac{P_{gas} - 0.23 \cdot P_{gas-rated}}{0.77 \cdot HR \cdot P_{gas} \cdot \eta_{ele}}; \quad or \quad \eta_{Turb} = \frac{P_{gas}[p.u.] - 0.23}{0.77 \cdot \eta_{ele}} \quad \textbf{Eq. 17}$$

$$\eta_{ele} = 0.623P_{ele}^3 - 1.34P_{ele}^2 + 0.965P_{ele} + 0.729; \quad P_{ele}\ in\ p.u \quad \textbf{Eq. 18}$$

$$Load\ Ref._{.[p.u.]} = \eta_{Turb} \cdot \frac{P_{gas}}{P_{gas-rated}} \quad \textbf{Eq. 19}$$

generator efficiency, η_{ele}, is applicable only for electricity yield above 10% of rated.

Table 1 summarizes the parameter values used for the general micro-CHP model. They were collected from references [41, 43-44, 46] . Refer to Chapter 5 on the specific values for each one of the micro-CHPs' parameters used in this thesis work.

Name	*Abbrev.*	*Value*	*unit*
Rotor Speed Reference	Speed Ref	1	p.u.
Internal Control System			
Droop gain	K_{droop}	0.04	p.u.
Proportional gain PID	K_P	3.6	
Integral gain PID	K_I	3.2	
Derivative gain PID	K_D	0.6	
Maximum Limit Governor output	Limit Max	1.3	p.u.
Minimum Limit Governor output	Limit Min	-0.1	p.u.
Gas Turbine			
Min. fuel rate for no-load operation	K_1	0.23	p.u.
Gain actuator system	K_A	1	
Gain valve position	K_V	1	
Actuator system time constant	T_A	0.04	s
Valve position time constant	T_V	0.05	s
Compressor discharge time lag	T_{CD}	0.2	s
Combustion reaction transport delay	T_{CR}	0.01	s
Turbine transport delay	T_{TD}	0.02	s
Synchronous Generator			
Voltage Line-neutral	V_{nom}	230	Vrms
Frequency nominal	f_{nom}	50	Hz
Pole pairs	p	2	pairs
Generator efficiency fix	η_{ele_fix}	0.96	p.u.
Exhaust Heat Recovery System			
Specific heat capacity of exhaust gases	c_{p_exh}	1000	J/kgK
Specific heat capacity of water	c_{p_water}	4180	J/kgK

Table 1 Summary of common parameters for the micro-CHPs model

Modeling of Wind Turbine

In the last decade conversion of wind's kinetic energy into electricity has become in the leading renewable energy technology with more than 159 GW installed capacity by the end of 2009 [52]. The horizontal axis wind turbine (HAWT) is the established technology that dominates the market. With on-shore and off-shore applications, HAWT technology has a wide generation capacity ranging from few tens of kilowatts to the current largest turbine of seven megawatt. HAWT is a sophisticated engineering device that combines knowledge from aerodynamics, mechanics, civil structures and electrical field.

The major components of a HAWT are rotor consisting of hub and blades; drive train made of low-speed rotating shaft, gearbox and high-speed rotating shaft; generator and power converter; tower and foundation; and finally controls. Figure 22 sketches these components.

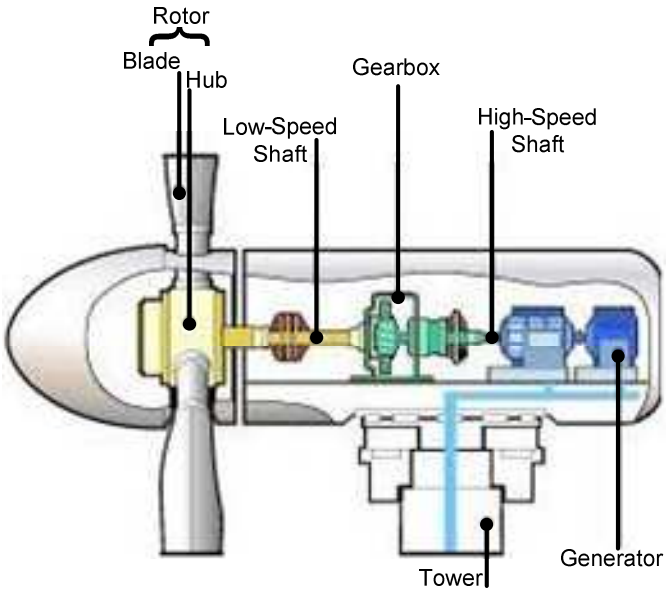

Figure 22 Schematic of a Horizontal-axis Wind Turbine

The aerodynamically designed rotor's blades capture the wind's kinetic energy, converting it to rotational mechanical energy that is transmitted to the gearbox by the low-speed shaft. The gearbox transforms its lower speed input to a higher speed output that connects to the high-speed shaft which turns the rotor of an electricity generator. Thereby ending the conversion path from wind speed to electricity. Further, suitable control strategies steer the electricity generation in order to maintain specific requirements by using power electronics converters and control devices. In this thesis work a three bladed variable-speed pitch controlled HAWT working in optimal power generation mode in order to deliver the maximum available power to the grid is considered.

Operation Principle of HAWT

The energy conversion process of a horizontal axis wind turbine uses the basic aerodynamic force of lift to produce a net positive torque on a rotating shaft [53]. The amount of this produced mechanical power is a function of several factors including wind speed, rotor's diameter and aerodynamic efficiency. Using the conservation law of linear momentum over an air flow stream that passes across the area swept by the HAWTs' rotor blades leads to the following expression describing the power extracted from wind:

$$P_m = \frac{1}{2}\rho\pi R^2 C_{p(\theta,\lambda)} U^3$$

Eq. 20

where P_m stands for mechanical power in watts, ρ is the specific density of air in kg/m^3, R is the rotor radius in meters, U is the wind speed in m/s, C_p is the power coefficient, θ is the pitch angle and λ is the tip speed ratio.

Eq. 20 describes the power performance versus wind speed curve (power curve). Each wind turbine has a characteristic power curve and from it predictions about energy production can be drawn. Another important speed – power relation for describing the wind turbine operation is the electrical power versus generator (rotor) speed curve, a set of this curve for various wind speeds is shown in Figure 23. Both characteristic curves are based in the aerodynamic performance of the blades airfoil.

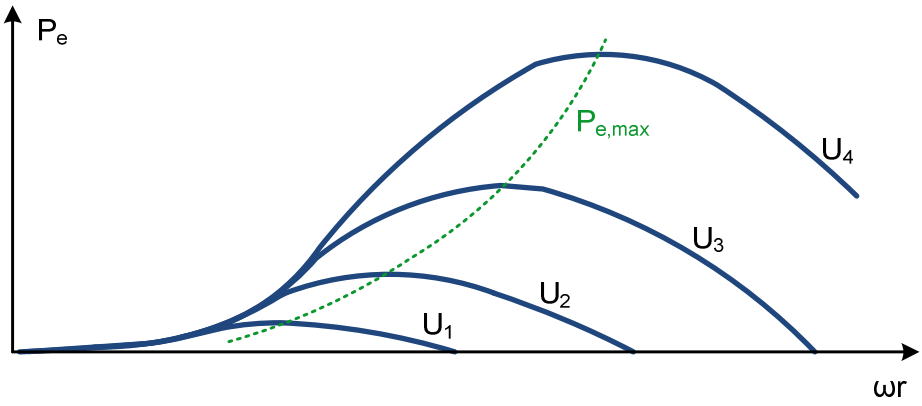

Figure 23 Electrical power versus rotor speed curves for four different wind speeds

The power coefficient or aerodynamic efficiency (C_p) that appears in equation Eq. 20 represents the fraction of the power in the wind that is extracted by the rotor. It characterizes the performance of the wind turbine rotor and is inherent in each wind turbine's aerodynamic design, having a theoretical maximum of 59.3%. C_p can be expressed as a function of the tip speed ratio (TSR or λ) and of the pitch angle in the particular case of the variable-speed pitch controlled wind turbine. TSR is defined as the ratio between the blade tip linear speed to the wind speed:

$$\lambda = \frac{\omega_r R}{U}$$

Eq. 21

where ω_r is the angular rotor speed in rad/s.

TSR allows characterization of a wind turbine through the C_p for any combination of rotor speed to wind speed. It results in a C_p vs λ curve that is obtained analytically or experimentally for each turbine model. Particularly, it identifies a maximum power coefficient ($C_{p,max}$) that corresponds to an optimal tip speed ratio (λ_{opt}). Thus, every wind speed has a rotor speed that gives the optimal TSR and produces the maximum energy extraction from wind.

The pitch angle (θ) refers to the possibility in a variable-speed HAWT to tilt the rotor blades in order to modify the force of lift. As the power coefficient is also a function of the pitch angle, an optimal pitch angle (θ_{opt}) exists for the maximum power coefficient at optimal tip speed ratio. Normally θ_{opt} is the fixed reference and a pitch angle increment results in loss of lift force. As a consequence the power extracted from wind decreases. Figure 24 depicts a C_p vs λ curve for different pitch angles, with θ_{opt} being zero degrees.

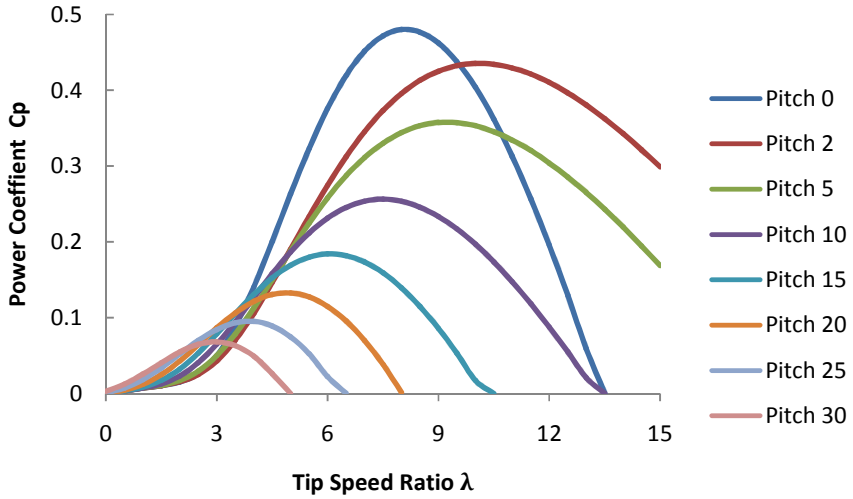

Figure 24 C_p vs λ curve for different pitch angles used in this HAWT model

Control of Variable-speed pitch controlled HAWT

Considering the operation principle of a variable-speed HAWT a control strategy can be generated to follow a desired operational characteristic. In [54] Hansen describes a control method that allows the wind turbine to operate with optimum power efficiency over a wide range of wind speeds. A modified version of this control method, implemented in [55] and in this thesis work, takes the actual generator rotor speed to give an electrical power generation reference that follows the desired operational characteristic of the HAWT. It has two control strategies depending on the operation region of the wind turbine:

1. **Power optimization strategy** takes place in the region below rated wind speed and where the energy capture is optimized. This region is divided in three zones.
   A) In this zone the optimal power is achieved by following the expected aerodynamic efficiency profile at low wind speeds. It keeps the optimal pitch angle and varies the rotor speed above its lower limit through adjusting the generator torque. This result in a TSR non optimum but enhances the energy capture.
   B) Here the energy capture is optimized by keeping a $C_{p,max}$ along the zone. It means to keep the pitch angle at optimum and tune the tip speed ratio to its optimal value over different wind speeds by adapting the rotor speed. The tuning is done by using a reference rotor speed ($\omega_{r,ref}$) obtained from equation Eq. 21 for λ_{opt}. The maximum power is achieved by tracking the reference rotational speed and given by the expression in equation Eq. 22.
   C) In this zone the rotor speed oscillates from around 90% of the nominal speed to the nominal rotor speed and the power extracted is less than the rated. The optimal power is obtained by operating the wind turbine close to its rated rotor speed and by using pitch angle control. This zone enables a smooth transition between the power optimization strategy and the power limitation strategy.

2. **Power limitation strategy** applies for wind speeds above rated and its aim is to keep the wind turbine power at its nominal value, thus preventing any overheat of the generator. The power stays at its rated value for any wind speed above the nominal by means of

increasing the pitch angle. This increment mainly shrinks the height of the C_p vs λ curve (see Figure 24), thus given a C_p lower than the one that would be obtained in the C_p vs λ curve at optimal pitch angle for the same reckoned λ. In this operation zone the rotor speed varies from its nominal to its maximum, which normally occurs at 1.2 times the nominal value.

$$P_{max} = \frac{1}{2}\rho\pi R^5 \frac{C_{p,max}}{\lambda_{opt}^3}\left(\omega_{r,ref(U)}\right)^3$$

Eq. 22

Figure 25 shows the mechanical power versus wind speed curve of the HAWT implemented in this thesis work after above control strategies has been applied to the wind turbine operation. The discussed control zones depict in terms of wind speeds. The cut-in wind speed is a characteristic of the each wind turbine and depends on the rotor inertia. At this wind speed the mechanical power is near zero and the rotor speed is at its minimum. At the other end of the curve, cut-out wind speed is limited by the engineering design and safety constraints.

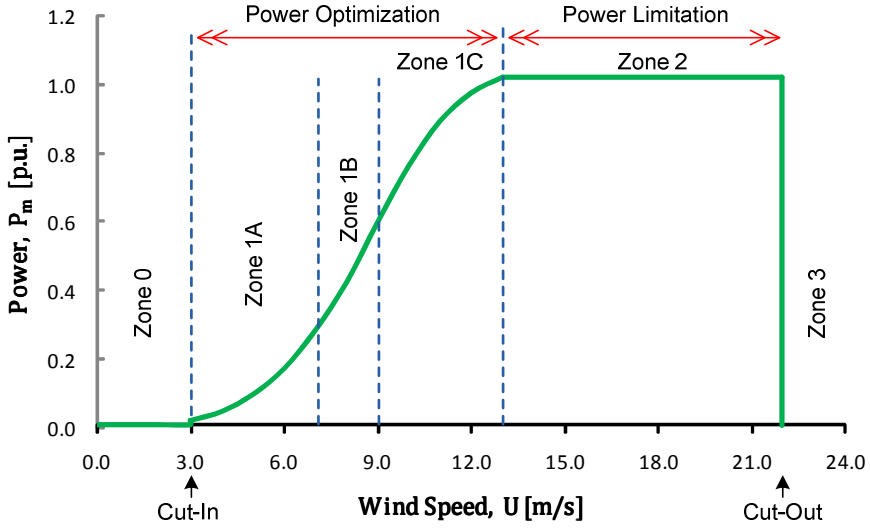

Figure 25 Power curve for the variable-speed pitch controlled HAWT with control zones and regions

Implementation of HAWT model in Simulink

A block diagram for the implementation of a general HAWT model that follows the above discussion along with the model representation of variable-speed HAWT for power system dynamics simulations presented by Slootweg, et al. in [55] is shown in Figure 26. This model representation fits well for any generator technology used in the variable-speed HAWT and is restricted to active power control only. In the context of this thesis work the data sheet and power curve of an Enercon E33 [56] wind turbine are used like frame to specify a per unit model able to extend to smaller wind turbines.

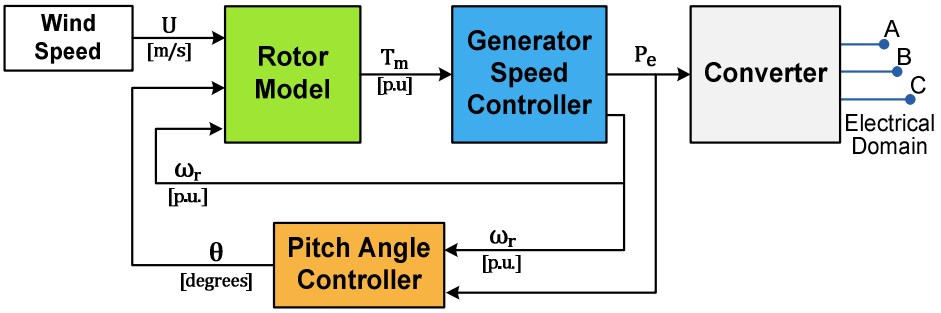

Figure 26 Block diagram of subsystems for the variable-speed HAWT model

Rotor Model

The modeling of the wind turbine rotor is based on equation Eq. 20 and Eq. 21 which are implemented in a per unit based. The rotor model has the wind speed (U), pitch angle (θ) and rotor speed in per unit (ω_r) as variable inputs and the mechanical torque in per unit (T_m) as output. The power coefficient (C_p) as function of θ and λ belongs to a numerical approximation taken from [57] and drawn in Figure 24. It has an optimum tip speed ratio of 8.1 and a maximum power coefficient of 0.48. Therefore, reckoning of C_p for any other combination of $C_{p,max}$ and λ_{opt} must firstly scale λ properly before applying it into $C_{p\ (\lambda,\ \theta)}$ equation, which is and expressed by:

$$C_{p(\lambda,\theta)} = C_1\left(\frac{C_2}{\lambda_i} - C_3\theta - C_4\right)e^{-\frac{C_5}{\lambda_i}} + C_6\lambda$$

Eq. 23

where λ_i is:

$$\frac{1}{\lambda_i} = \frac{1}{\lambda + 0.08\theta} - \frac{0.035}{\theta^3 + 1}$$

Eq. 24

The parameters set for this model are listed in Table 2. Additionally, functional blocks to include cut-in and cut-out wind speed limits were added in the rotor model. The shafts dynamics of the drive train are neglected and the rotor is modeled as a lumped mass which inertia adds to the generator rotor inertia in the generator model.

Generator Model and Speed Controller

Using a simplified approach the generator either it is a doubly-fed induction generator, a squirrel cage induction generator or a synchronous generator is modeled as an electrical torque (T_e) source. Therefore, the equation describing the dynamics of this model is the previously introduced electro-mechanical rotor equation (see Eq. 12), which lets determine the actual rotor speed. Here it takes the following form:

$$\frac{d\omega_r}{dt} = \frac{1}{2H}(T_m - T_e)$$

where all values are in per unit except by the inertia that is in seconds. The inertia includes a component related to the generator rotor mass and another belonging to the wind turbine rotor mass.

It is assumed that an electromagnetic torque control device operates in the wind turbine and that its control characteristic follows the power optimization and power limitation strategies. Consequently the per unit electrical power versus rotor speed characteristic curve shown in Figure 27 enables reckoning an optimal electromagnetic torque set point from the actual rotor speed. The following equations describe the per unit power-rotor speed curve in each of its operating zones:

- **Zone 0 ^ Zone 3** $P_e = 0$ **Eq. 25**
- **Zone 1A.** $P_e = -1.761\omega_r^3 + 2.806\omega_r^2 - 0.818\omega_r + 0.08$ **Eq. 26**
- **Zone 1B.** $P_e = \frac{1}{2}\rho\pi R^5 \frac{C_{p,max}}{\lambda_{opt}^3 P_{nom}} \left(\omega_r\, \omega_{r,nom}\right)^3$ **Eq. 27**
- **Zone 1C.** $P_e = 4.217\omega_r - 3.202$ **Eq. 28**
- **Zone 2.** $P_e = 1$ **Eq. 29**

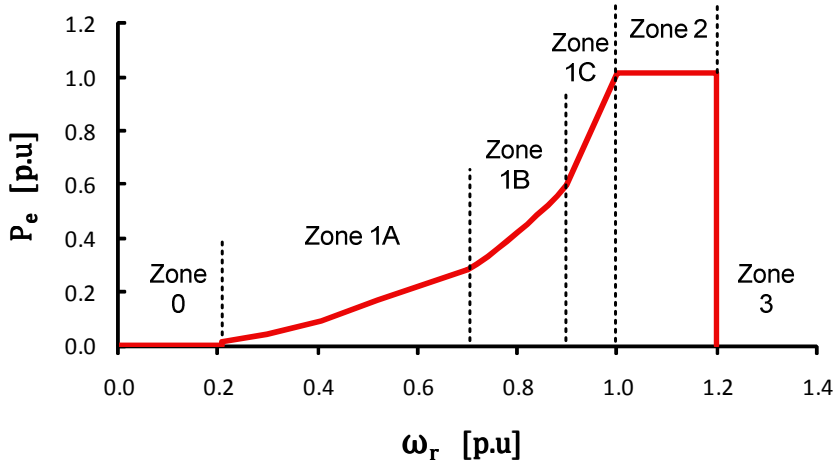

Figure 27 Per unit electrical power versus rotor speed curve following optimal power control strategies

The generator model's block diagram is shown in Figure 28. The electrical power output from the model is in per unit, changed to watts and then connected to a built-in Simulink block (Converter in Figure 26) that transforms the active power signal to the three phase electrical domain of SimPowerSystems.

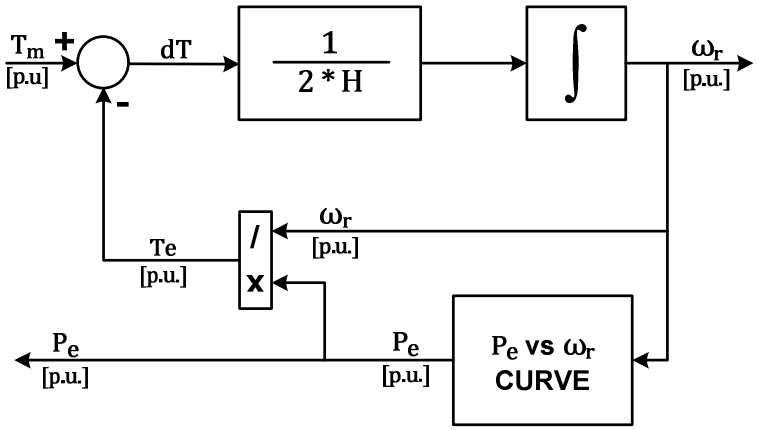

Figure 28 Block diagram of generator model and rotor speed controller for HAWT

Pitch Angle Controller

The pitch angle controller described in [58] and shown in Figure 29 corrects the pitch angle based on the rotor speed error signal. The pitch angle controller operates in zone 1C and 2 with its

own rotor speed reference ($\omega_{r,ref}$) and proportional gain (K_P) values for each zone. The electrical power (P_e) input from the generator model commands which values to use. When P_e equals the rated value, the controller employs $\omega_{r,ref}$= 1 and K_P for zone 2. Whereas, when P_e is lower than rated the values for zone 1C are conveyed to the controller. Since rotor speed at zone 1C begins at 0.9 [p.u.], this is the reference speed taken. Hence, this control limits the generator power in the zones by reducing the power coefficient through modifications of pitch angle from optimal. However, for rotor speeds equal or lower than $\omega_{r,ref}$ of zone 1C, the pitch angle controller sets the angle to its minimum value which corresponds to its optimum.

The controller uses a proportional control with gain K_P which is related to the amount of rotor over speeding for each operation zone. Tuning of the proportional gain was done to find the suitable value. The finite rate of change of the pitch angle ($d\theta/dt$) is taken into account together with pitch angle maximum and minimum values.

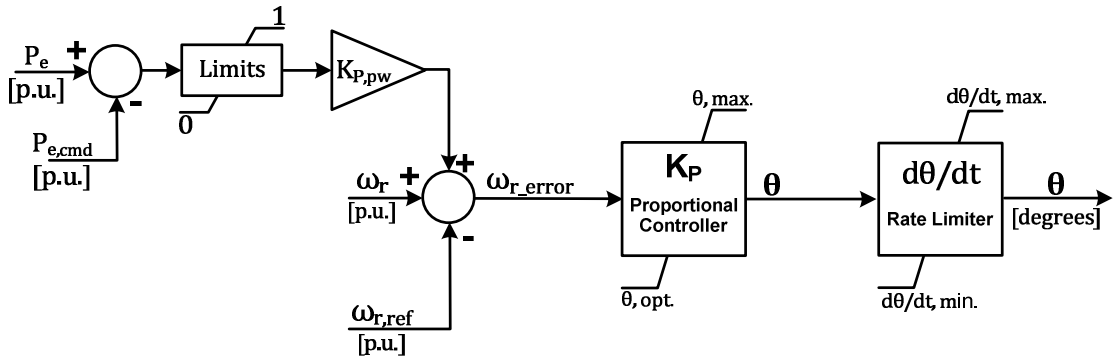

Figure 29 Block diagram of Pitch Angle controller

Additionally, the controller can work to dispatch a specific amount of power based on a user given power reference command (Pe,cmd). It is intended to operate only when the actual power delivered by the wind turbine exceed the demand, cannot be stored or it is not possible to be sold to another network.

Table 2 lists the parameters used in the horizontal axis wind turbine model. Refer to Chapter 5 on the specific values for the rated wind turbine used in this thesis work.

Name	*Abbrev.*	*Value*	*unit*
Rotor Model			
Air density	ρ	1.225	kg/m^3
Cut-in Wind speed	Cut-in	3	m/s
Cut-out Wind speed	Cut-out	22	m/s
Desired characteristic p.u. power at U_{dch}	P_{dch}	0.4182	p.u.
Desired characteristic wind speed	U_{dch}	8	m/s
Maximum Cp at desired characteristic	$C_{p,max}$	0.5	
Optimal tip speed ratio	λ_{opt}	5	
Coefficient 1 for $C_{p(\lambda,\theta)}$ equation	C_1	0.5176	
Coefficient 2 for $C_{p(\lambda,\theta)}$ equation	C_2	116	
Coefficient 3 for $C_{p(\lambda,\theta)}$ equation	C_3	0.4	

Coefficient 4 for $C_{p(\lambda,\theta)}$ equation	C_4	5	
Coefficient 5 for $C_{p(\lambda,\theta)}$ equation	C_5	21	
Coefficient 6 for $C_{p(\lambda,\theta)}$ equation	C_6	0.0068	
Pitch Angle Controller			
Proportional Gain for Zone 1C	K_P, zone 1C	48	
Proportional Gain for Zone 2	K_P, zone 2	250	
Proportional Gain power error	$K_{P,pw}$		
Reference rotor speed for Zone 1C	$\omega_{r,ref}$	0.9	p.u.
Reference rotor speed for Zone 2	$\omega_{r,ref}$	1	p.u.
Maximum pitch angle	$\theta_{,max}$	30	degrees
Minimum (Optimal) pitch angle	$\theta_{,opt}$	0	degrees
Raising pitch angle rate	$d\theta/dt_{,max}$	5	degrees/s
Falling pitch angle rate	$d\theta/dt_{,min}$	-5	degrees/s

Table 2 Summary of general parameters used in the HAWT model

Modeling of Electricity Storage

Electricity will be stored as chemical energy in a stack of deep-cycle lead-acid batteries. This thesis work took advantage of a Simulink built-in battery model described by equation Eq. 30 and Figure 30 to characterize the battery stack.

$$E = E_0 - \frac{K * Q}{Q - it} + A^{-B*it}$$

Eq. 30

where E stands for no load voltage [V], E_0 is constant voltage [V], K is polarization voltage [V], Q battery capacity [Ah], A is exponential voltage [V], B is exponential capacity [Ah^{-1}].

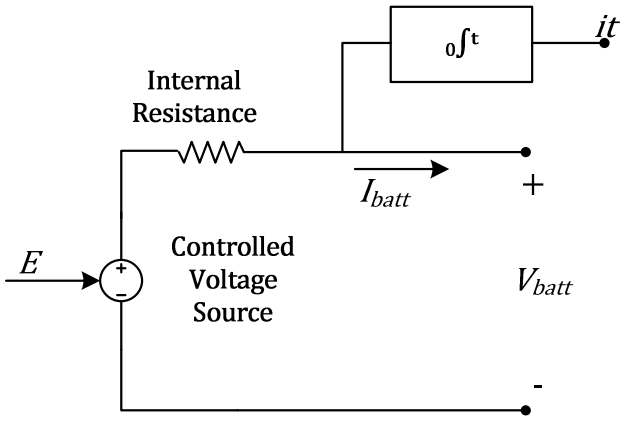

Figure 30 Built-in model of battery in Simulink/SimPowerSystems

A power command from the main control ($P_{e\_st\_cmd}$) charges and discharges the electricity storage by applying a positive or negative current to the built-in battery model respectively. Stand-by losses due to internal resistance of the battery are considered through applying a constant draining power at the battery stack ($P_{e\_st\_loss}$). The electricity storage model also takes into account the efficiency of the power electronics inverter (η_{e_inv}) that transforms the grid AC current into DC and vice versa.

Figure 31 shows the implemented Electricity Storage. The connection to the three phase grid is achieved with a built-in block that changes a power signal into three phase power system variables of voltage and current.

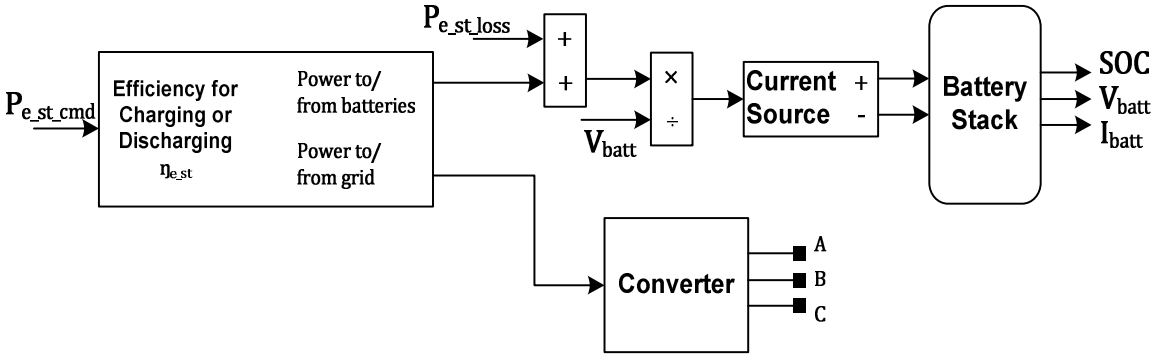

Figure 31 Block diagram of electrical storage model implemented in Simulink

Table 3 lists the parameters for the electrical storage model. They were taken from a commercial battery datasheet found in reference [59].

Name	*Abbrev.*	*Value*	*unit*
Nominal Voltage Battery Stack	V_{batt}	120	V
Full Charge Voltage		104	%
Nominal Discharge Current		10	%
Internal Resistance		0.001	Ohms
Capacity @ Nominal Voltage		60	%
Voltage @ Exponential Zone	$A\%$	103.5	%
Capacity @ Exponential Zone	$B\%$	1.7	%
Efficiency of Power Electronics Inverter	η_{e_inv}	90	%

Table 3 Summary of parameters used in the Electricity Storage model

Modeling of Heat Components

The heat demand in the studied distributed generation system corresponds to district heating purposes only. It means that heat is needed for space heating and tap water heating. The modeled system is a district heating system (DHS) with indirect configuration and return pipeline. The medium that conveys heat is water which is kept at a temperature of 100 degrees Celsius at the hot water pipeline.

The heat components that supply, transport, transfer and demand heat are described through their amount of heat (supplied, lost or demanded), by heat transfer coefficients, by the temperature of the heat transport medium and by the mass flow of the heat transport medium. Pressures in the system are not considered and it is assumed that they keep their normal range. The heat transfer mechanisms of conduction and convection apply for the characterization of the components.

Heat Conduction takes place in a stationary medium in the presence of a temperature difference. Heat is transferred from more energetic to less energetic molecules when neighboring molecules collide. Thus heat flows from a high temperature towards a low temperature [60].

Heat Convection takes place between a surface and a moving fluid at different temperatures.

The heat transfer modeling of the components is based on the law of conservation of energy, the Newton's law of cooling for heat transfer through convection mechanism, and the Fourier's law for heat transfer conduction. The following equations express these laws [60].

Law of conservation of energy in an open system:

$$\frac{dE_t}{dt} = \phi_{m,in} * u_{in} - \phi_{m,out} * u_{out} - \phi_H + \phi_A$$

Eq. 31

where $E_t = \rho * c_p * T * V$ and $u = c_p * T$. E_t stands for energy [J], ϕ_m is mass flow [kg/s], u is internal energy per unit mass [J/kg], ϕ_H is heat exchanged with the surroundings per unit of time [W], ϕ_A is mechanical energy added per unit of time [W], t is time [s], ρ is density [kg/m^3], T is temperature [K], c_p is specific heat capacity [J/kgK] and V is volume [m^3]. Eq. 31 is a balance of the energies performing in a bounded system.

When equation Eq. 31 neglects density and specific heat capacity variation, when the output and input mass flow are equal and when no mechanical energy is added to the system, it turns into:

$$M * c_p * \frac{dT}{dt} = \phi_m * c_p * (T_{in} - T_{out}) - \phi_H$$

Eq. 32

where M stands for mass [kg]. If the system is stationary, the heat exchanged with the surroundings becomes in the heat transferred by the mass flow, thus:

$$\phi_q = \phi_m * c_p * (T_{in} - T_{out})$$

Eq. 33

Newton's law of cooling for stationary heat convection:

$$\phi_q = h * A * dT$$

Eq. 34

where ϕ_q is heat transferred per unit of time [W], h is convective heat transfer coefficient [W/m^{2}K], A heat transfer area [m^2] and dT is the temperature difference that drives the heat transfer phenomena [K].

Fourier's law for stationary heat conduction:

$$\phi_q = \frac{\lambda}{d} * A * dT$$

Eq. 35

where λ is the thermal conductivity [W/mK] and d is the thickness of the material [m].

The models are implemented in MatLab/Simulink through Simscape® Thermal software. Simscape is a physical modeling environment where functional blocks exchange energy through their ports. Simscape Thermal operates in the thermal physical domain and has heat flow and temperature as variables [51]. Additional mathematical formulas and operations for models' implementation and their control are carried out through physical signals instead of Simulink signals, thus allowing a faster execution of simulations. Simscape Thermal is a relatively new and does not offer built-in elements for representation of the intended DHS' components. Therefore, all the heat components models were built using the Simscape foundation blocks for the thermal domain and for physical signals. In this way, these modeled DHS's components can be used as built-in models for other research projects.

Figure 32 depicts the heat components that make up the DHS and how they are interconnected. Only one CHP is depicted due to the others use the same model but with different settings. Additionally the CHP is represented only for its heat recovery heat exchanger.

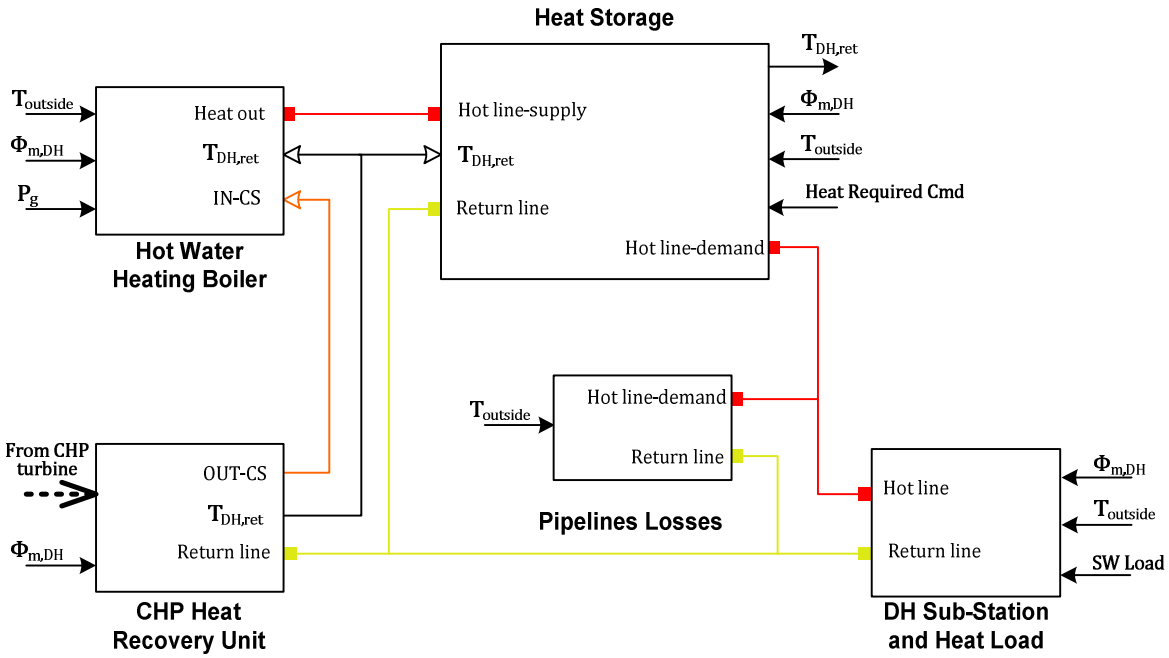

Figure 32 District Heating System Components Interconnection

Model of District Heating Sub-Station and Heat Load

There are two types of heat load in the system. One is the service water heat demand, which represents the amount of heat needed to heat up a desired mass flow of tap water from 15 degrees to 80 degrees Celsius. The other heat load refers to the space heating demand, which is function of the desired indoor temperature, outside temperature and heat losses through the building structure. Each of these heat demands is supplied by its own heat exchanger in the building sub-station. A diagram of a district heating sub-station is shown in Figure 3. In the case of space heating the indoor air mass is heated through radiators that connect to the sub-station space heating heat exchanger. Figure 33 sketches the interconnections among the heat load models, radiator model, sub-station heat exchangers models and controllers.

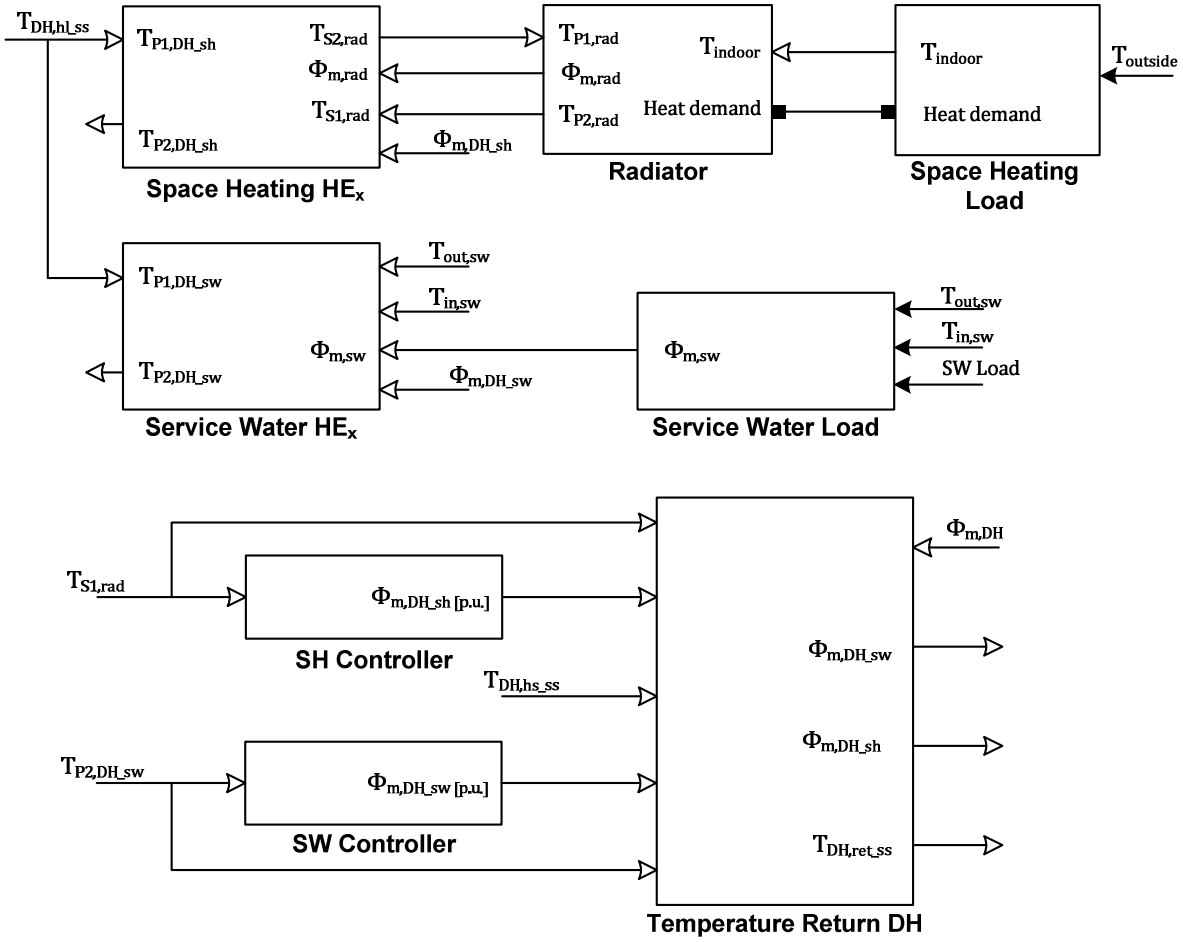

Figure 33 Block diagram of the Interconnection of Heat Load models, Radiator model, Sub-Station components and controllers.

Service Water Heating Load Model

This model transforms the service water heat demand signal in watts to a representative water mass flow through the use of equation Eq. 33. Here, the energy conservation law applies to a system where a flow of fresh water at the system input has a temperature T_{in_sw} of 15 degrees Celsius and its desired temperature at the system output T_{out_sw} is 80 degrees Celsius.

$$\phi_{m,sw} = \frac{\phi_{q,sw}}{c_{p,w} * (T_{in,sw} - T_{out,sw})}$$

Eq. 36

Space Heating Load Model (Building Heat Transfer Model)

The space heating demand represents the desire to maintain a comfortable temperature in the interior of the dwelling at all time. The comfort indoor temperature is selected to be 20 degrees Celsius. In this model, it is assumed that heat flows from the heat sources (radiators) to the dwelling interior heating only the indoor mass of air. Consecutively heat leaves the building towards the exterior through walls, roof and windows. The driver for this heat loss is the temperature difference between the warm building interior to its cold surrounding, T_{indoor}-$T_{outside}$. The loss of heat is mainly limited by the thermal conductivity of the materials that make the dwelling structure. Additionally heat transfer by convection happens between the moving interior mass of air and the interior surface of walls, roof and windows. Convection also takes place in the exterior surface of building's walls, roof and windows in contact with the cold surrounding air.

Here the system to apply the energy balance encloses the heat source, the building structure and its surrounding cold air temperature. Thus, the law of conservation of energy as per reference [61] turns into:

$$M_{air} * c_{p,air} * \frac{dT_{indoor}}{dt} =$$

$$\phi_{q,source} - \left(U_{walls} * A_{walls} + U_{wnds} * A_{wnds} + U_{roof} * A_{roof}\right) * (T_{indoor} - T_{outside})$$

Eq. 37

where U stands for overall heat transfer coefficient which is function of the convective heat transfer coefficient and of the thermal conductivity in accordance with:

$$\frac{1}{U_x} = \frac{1}{h_{air,in-x}} + \frac{d_x}{\lambda_x} + \frac{1}{h_{x-air,out}}$$

Eq. 38

where x stands for either walls, floor or windows.

Figure 34 shows the block diagram for the implementation of this model in Simulink. The heat from the radiator goes to the air mass indoor block and through the daisy chain of heat transfer coefficients and thermal conductivity blocks to the building exterior. The outdoor temperature signal is transformed to a temperature source which port connects to the physical thermal lines that carry heat from inside the building.

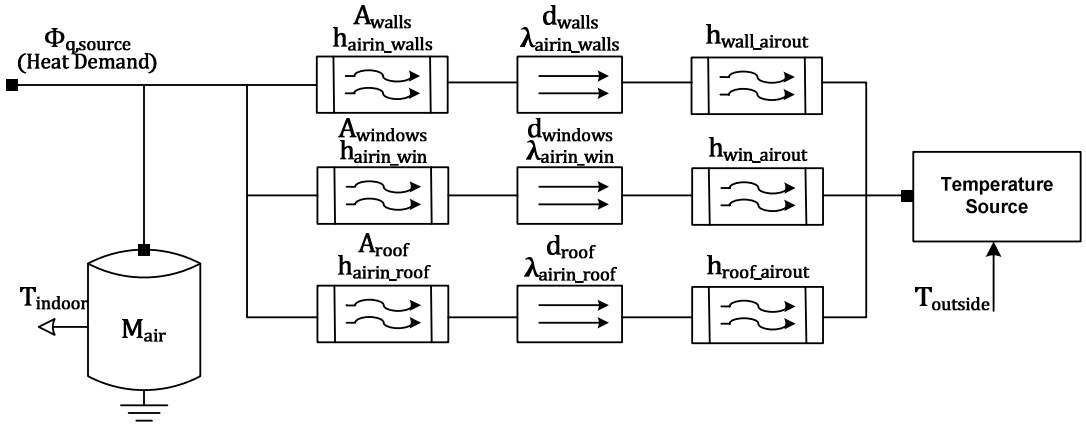

Figure 34 Block diagram of the space heating load model

Radiator Model

The heat transfer from a radiator to the surrounding environment occurs due to conduction of heat through the radiator metal frame, due to force convection of the hot water circulating within the radiator and owing to natural convection of air next to the radiator. These heat transfer mechanisms work all together and have time and space dependency, making of it a complex process where the temperature difference that drives this process changes at every point of the radiator surface. In this heat process the convection mechanism exceeds over conduction's and the ability to transfer heat is expressed through an overall heat transfer coefficient U_{rad}. In order to model this heat transfer process, the most common and accepted method is to use a mean temperature difference as the temperature driver for this process instead of analyzing the temperature difference at each piece of radiator surface [60, 62]. In this case the Logarithmic Mean Temperature Difference (LMTD) expresses well the temperature difference between interior and exterior of the radiator.

LMTD for a radiator is given by [61]:

$$LMTD_{rad} = \frac{T_{P1,rad} - T_{P2,rad}}{\ln\left(\frac{T_{P1,rad} - T_{indoor}}{T_{P2,rad} - T_{indoor}}\right)}$$

Eq. 39

where $T_{P1,rad}$ and $T_{P2,rad}$ are the water mass flow temperatures at the entrance and exit of the radiator respectively.

The boundaries for the energy balance in this process comprise the input and output ports of the radiator and its surrounding mass air temperature. Hence, the balance for energy conservation follows as:

$$M_{w,rad} * c_{p,w} * \frac{dT_{P2,rad}}{dt} = \phi_{m,rad} * c_{p,w} * (T_{P1,rad} - T_{P2,rad}) - U_{rad} * A_{rad} * LMTD_{rad}$$

Eq. 40

Here heat is given by the hot water mass flow ($\phi_{m,rad}$) by means of losing temperature throughout its travel within the radiator. This heat source balances with the heat convection driven by the $LMTD_{rad}$ along the contact area of the radiator (A_{rad}) with its surroundings. The term at the left side of equation Eq. 40 represents the instant change of energy contained in the water mass ($M_{w,rad}$) at the output of the radiator (expressed as change in temperature). It becomes zero at stationary state.

The implementation of this model in Simulink/Simscape is depicted in Figure 35. In the upper part, heat given from the hot water mass flow is injected towards the radiator surrounding air by

passing through the heat transfer barrier represented by the radiator exchange area and its overall heat transfer coefficient in the depicted block. The instant temperature value of the water mass flow at the output of the radiator is acquired from the temperature signal at the radiator water mass block. This water mass is the amount of water that circulate in the radiator per unit of time. As per equation Eq. 40, the heat flow from the water mass flow is balance to the convective heat transfer to produce a change in the temperature of the radiator output water mass flow. All this is shown in the lower part of Figure 35 where the LMTD block implements the equation Eq. 39.

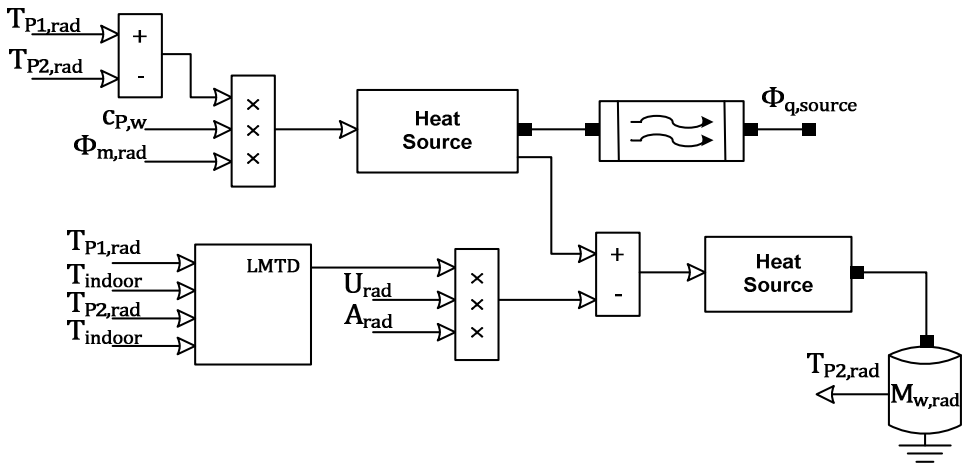

Figure 35 Block diagram of radiator model as implemented in MatLab/Simulink/Simscape

Finally the control to maintain the desired indoor temperature (T_{indoor}) is done by restraining the amount of water mass flowing into the radiator. A proportional control with gain $K_{P,rad}$ performs this task using the temperature error as its input. Its implementation is in per unit and its block diagram is sketched in Figure 36.

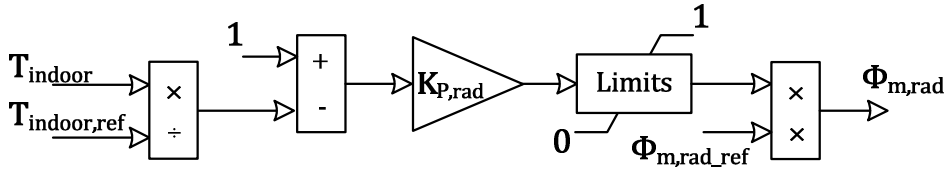

Figure 36 Block diagram of a per unit proportional control for the radiator model operation

Space Heating Heat Exchanger Model

A heat exchanger (HEx) is an efficient heat transfer device that plays a major role in the thermal conditioning of two mediums, with the advantage of keeping them separated from each other. The heat exchangers in the DHS sub-station link the heat supply coming in the form of district heating hot water flow with the heat demanded by the water streaming in the radiators network in the case of the space heating heat exchanger or the tap water heating demand regarding the service water heat exchanger.

The heat transfer mechanisms that occur in a heat exchanger are convection between the hot medium flowing in the HEx hot chamber and the hot side of the solid wall that prevents mixing of the mediums, conduction that takes place between the hot side and cold side of the solid wall, and convection between the solid wall's cold side and the medium streaming in the HEx cold chamber.

Similar to the radiator, in a heat exchanger the temperature difference between its cold and hot side varies in time and place within heat exchanger and thus the LMTD is used to simplify the HEx

model. Two arrangements for medium flow direction are possible, in co-current arrangement the two mediums enters the HEx for the same end and travel in parallel each other to exit at the other end. Conversely in counter-current arrangement the mediums enter the HEx from opposite ends. The counter-current HEx is most efficient [60] and it is modeled in this thesis work. Figure 37 shows a simple scheme of a counter-current HEx.

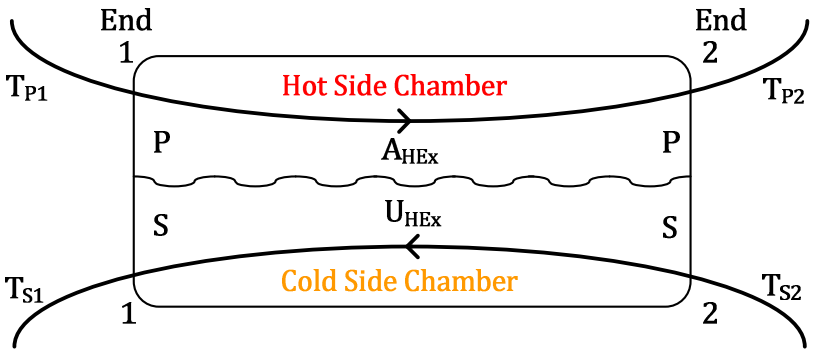

Figure 37 Simple counter-current HEx scheme

The energy balance can be set up at each side of the HEx. Considering the hot side the energy conservation law states:

$$M_{DH\_sh} * c_{p,w} * \frac{dT_{P2,DH\_sh}}{dt} = \phi_{m,DH\_sh} * c_{p,w} * (T_{P1,DH\_sh} - T_{P2,DH\_sh}) - U_{HEx\_sh} * A_{HEx\_sh} * LMTD_{HEx}$$

Eq. 41

Idem for the cold side:

$$M_{S1,rad} * c_{p,w} * \frac{dT_{S1,rad}}{dt} = \phi_{m,rad} * c_{p,w} * \left(T_{s2,rad} - T_{s1,rad}\right) + U_{HEx\_sh} * A_{HEx\_sh} * LMTD_{HEx}$$

Eq. 42

where U_{HEx_sh} and A_{HEX_sh} are the overall HEx heat transfer coefficient and the heat transfer surface of exchange respectively. The sub-scripts mean, DH_sh: belonging to the district heating space heating, rad: belonging to the radiator network system.

The LMTD for the HEx is expressed by:

$$LMTD_{HEx} = \frac{(T_{P1} - T_{S1}) - (T_{P2} - T_{S2})}{\ln\left(\frac{T_{P1} - T_{S1}}{T_{P2} - T_{S2}}\right)}$$

Eq. 43

Equation Eq. 41 describes that the change in time of the medium's output temperature at the hot side of the heat exchanger (T_{P2,DH_sh}) is owed to the heat supplied into the system by the temperature difference between the district heating water mass flow's temperature at the entrance and exit of the HEx hot side chamber (T_{P1,DH_sh} - T_{P2,DH_sh}), and due to the amount of heat transfer out of the HEx hot side chamber driven by the logarithmic mean temperature difference. Similar meaning holds for equation Eq. 42, where a change in medium's output temperature at the HEx cold side (T_{S1_rad}) depends on the amount of heat supplied to the cold side chamber by means of LMTD and the heat gained by the cold side medium when raising its temperature. In both cases at stationary state the left side term of equations becomes zero.

Figure 38 shows how this model is implemented in Simulink/Simscape. The upper part belongs to the modeling of the HEx hot side chamber through the energy balance stated by equation Eq. 41. The actual temperature T_{P2,DH_sh} measured in the hot side water mass block is used to compute the heat supplied to the system by the district heating water mass flowing at the hot chamber. T_{P2,DH_sh} also feeds the LMTD block in order to reckoning the amount of heat that leaves the hot chamber regarding the heat exchange area and the overall heat transfer coefficient. The lower part of Figure 38 describes equation Eq. 42, here the actual temperature of the water mass flowing at the output of the HEx cold chamber ($T_{S1,rad}$) is measured and forwarded to the LMTD block and used to compute the amount of heat demanded by cold side radiator water flow. The inputs and outputs of this model are physical signals of temperature, thus knowing the mass flow's amount of the medium and its specific heat capacity the heat flows can be reckoned for any further use.

The control strategy for the space heating heat exchanger is to keep the temperature of the water mass flow towards the radiator network ($T_{S1,rad}$) near to a reference value. In this system the radiator water mass flow varies so the control's aim is well fulfilled if $T_{S1,rad}$ keeps as much possible its setpoint. The best and simple option found for this controller was a proportional control with $K_{P,sh}$ gain and temperature error made of the setpoint and $T_{S1,rad}$. Its structure is the same as for the radiator control shown in Figure 36.

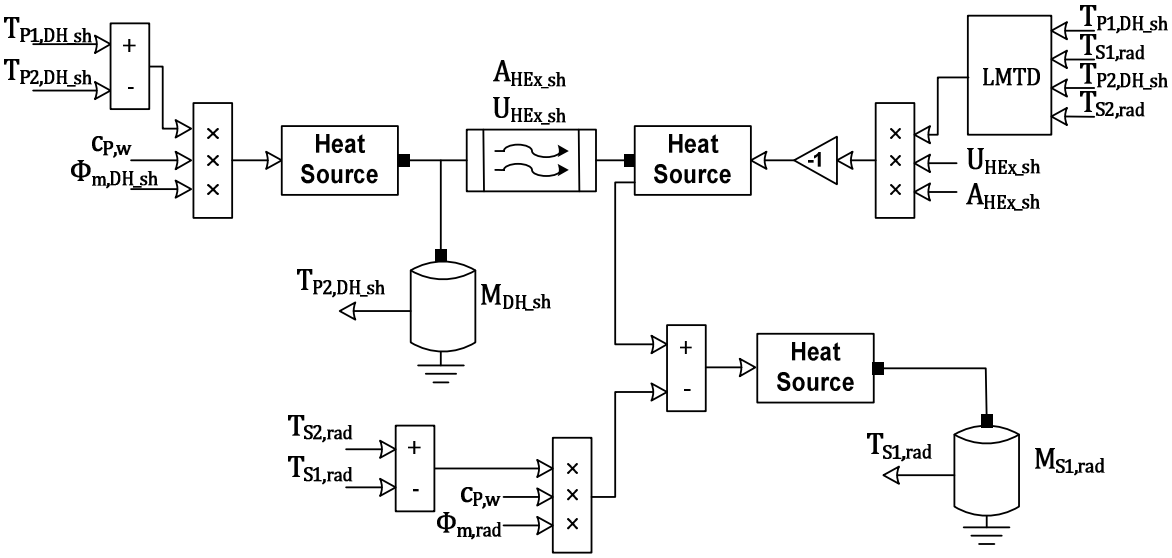

Figure 38 Block diagram of the heat exchanger for space heating implemented in Simulink/Simscape

Service Water Heat Exchanger Model

The heat exchanger for heating service water is modeled simpler than the space heating HEx. The model aims to reproduce the given service water load into the HEx hot side by changing the medium's output temperature and its amount of mass flow. Here, the heat demanded is bounded to two assumed fixed temperatures at the cold side of the HEx, one is the temperature of the service water at the input of the HEx (T_{in_sw}) and the other the desired hot service water temperature T_{out_sw}. Therefore, only the service water mass flow varies to change the heat demand felt by the HEx hot side. The energy balance for this model shall be:

$$M_{DH\_sw} * c_{p,w} * \frac{dT_{P1,DH\_sw}}{dt} = \phi_{m,DH\_sw} * c_{p,w} * \left(T_{P1,DH\_sw} - T_{P2,DH\_sw}\right) - \phi_H$$

Eq. 44

where T_{P1,DH_sw} and T_{P2,DH_sw} are the input and output temperature of the district heating water mass flow that travels throughout the HEx. The sub-script DH_sw denotes pertinent to district heating service water heat exchanger. ϕ_H is $\phi_{q,sw}$ the service water heat load as per equation Eq. 36.

The service water heat exchanger representation in Simulink is depicted in Figure 39. As in the case of the space heating HEx the temperature signals and heat flows account for the energy balance at the hot side chamber stated by Eq. 44. The LMTD is not used because of the fixed temperatures at the HEx cold side, however the effects owing to the overall heat transfer coefficient U_{HEx_sw} and effective heat exchange surface A_{HEX_sw} are characterized for their respective Simscape block.

The control for this HEx is achieved with a proportional controller with gain $K_{P,sw}$ alike to the space heating HEx controller. The control action allows supplying the demanded heat by changing the district heating mass flow intake to the HEx hot side chamber. The monitoring variable is T_{P2,DH_sw} temperature which is compared to a reference in order to generate the error input to the controller.

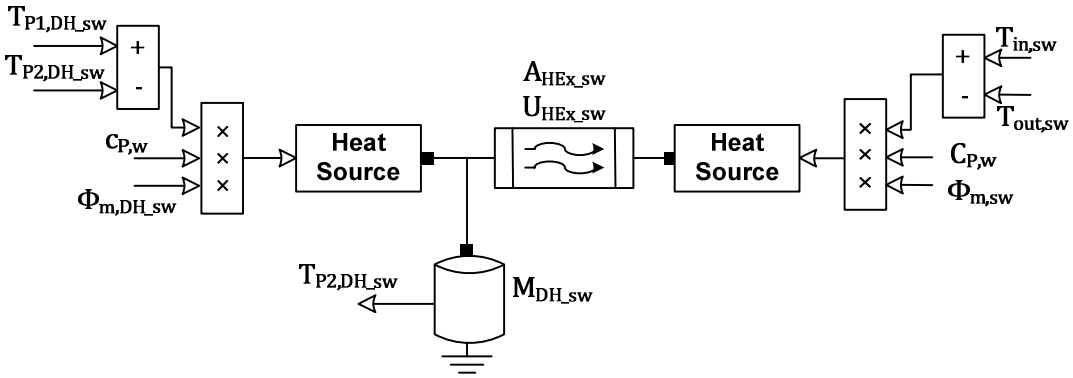

Figure 39 Block diagram of service water heat exchanger

Determining the District Heating Return Water Temperature

The district heating water mass flow that leaves the sub-station and returns to the heat sources has a temperature that depends on:

- the amount of it used for each heat exchanger
- the temperature of it out of each heat exchanger
- and the among of it non use and that was bypass, this assumes that no change in mass flow amount is possible in the district heating main line.

Given this, the district heating return water mass flow temperature at the sub-station outlet ($T_{DH\_ret\_ss}$) is obtained according to equation Eq. 45 as per reference [63]:

$$T_{DH\_ret\_ss} = \frac{\phi_{m,DH\_sw} * T_{P2,DH\_sw} + \phi_{m,DH\_sh} * T_{P2,DH\_sh} + \left(\phi_{m,DH} - \phi_{m,DH\_sw} - \phi_{m,DH\_sh}\right) * T_{DH\_hl\_ss}}{\phi_{m,DH}}$$

Eq. 45

where $\phi_{m,DH}$ is the water mass flow that circulates in the district heating main pipeline, and $T_{DH\_hl\_ss}$ is the temperature of the district heating water mass flow in the hot line at the intake of the sub-station. T_{P1,DH_sw} and T_{P1,DH_sh} equal to it.

Model of Heat Storage

In this thesis work, heat storage is carried out by a sensible heat storage system. In sensible heat storage method the energy is stored by changing the temperature of the storage medium and its amount is proportional to the difference between the storage input and output temperatures, the mass of the storage medium, and the medium specific heat capacity. This system is available for short and long-term storage and is made of a container, input/output devices and the storage medium, which commonly can be water or rocks [64]. In district heating applications a water tank offers the more suitable choice because of the temperature range needed and the high heat capacity of water that is twice that of rocks.

Thereby, the heat storage model characterizes a cylindrical insulated tank of water buried on soil with a heat exchanger that connects to the district heating hot pipeline when charging and to the return pipeline when discharging the storage system. The heat storage operates commanded by an exterior positive or negative signal that informs to the model to charge (+) or discharge (-) it and the amount of heat to be exchanged (ϕ_{q,st_cmd}).

The supply of heat to the return pipeline (storage discharging) is modeled by equation Eq. 33 with T_{in} = T_{st_act} and T_{out} = T_{st_bfr}. The former being the actual value of the storage medium temperature and the latter the reckoned previous temperature of the storage before heat was exchanged, again using Eq. 33. The implementation of this heat exchange process in Simscape considers a functional block representing the HEx overall heat transfer coefficient (U_{HEx_st}) and the effective HEx surface area (A_{HEx_st}). The water stream in the HEx has a constant value $\phi_{m,st}$. The same model applies when charging the storage (removing heat from the hot pipeline).

The storage water tank is assumed to be a continuously stirred tank so the storage medium temperature is homogeneous. The instantaneous change of this temperature happens by action of the actual amount of heat ($\phi_{q,st}$) that is stored or removed in/from the storage medium mass (M_{st}) and this heat flow in turn depends on the HEx efficiency (η_{st}). The model also regards the heat losses due to heat conduction from the tank surface area towards the atmosphere. The resistance to heat transfer mainly happens in the insulating material overlaying the tank and in the soil layer covering it. Therefore convection is neglected due to its small contribution to the heat losses. Equation Eq. 46 describes this energy balance and Figure 40 shows this model block diagram.

$$M_{st} * c_{p,w} * \frac{dT_{st\_act}}{dt} = \phi_{q,st} - U_{st} * A_{st} * \left(T_{st\_act} - T_{outside}\right) \quad \textbf{Eq. 46}$$

where $\frac{1}{U_{st}} = \frac{d_{insulator}}{\lambda_{insulator}} + \frac{d_{soil}}{\lambda_{soil}}$ and $\phi_{q,st} = \eta_{st} * \phi_{q,st\_cmd}$ with the storage efficiency being:

$$\eta_{st} = \begin{cases} \eta_{st,ch}, & \phi_{q,st_{cmd}} \geq 0 \ (charging) \\ \frac{1}{\eta_{st,disch}}, & \phi_{q,st\_cmd} < 0 \ (discharging) \end{cases} \quad \textbf{Eq. 47}$$

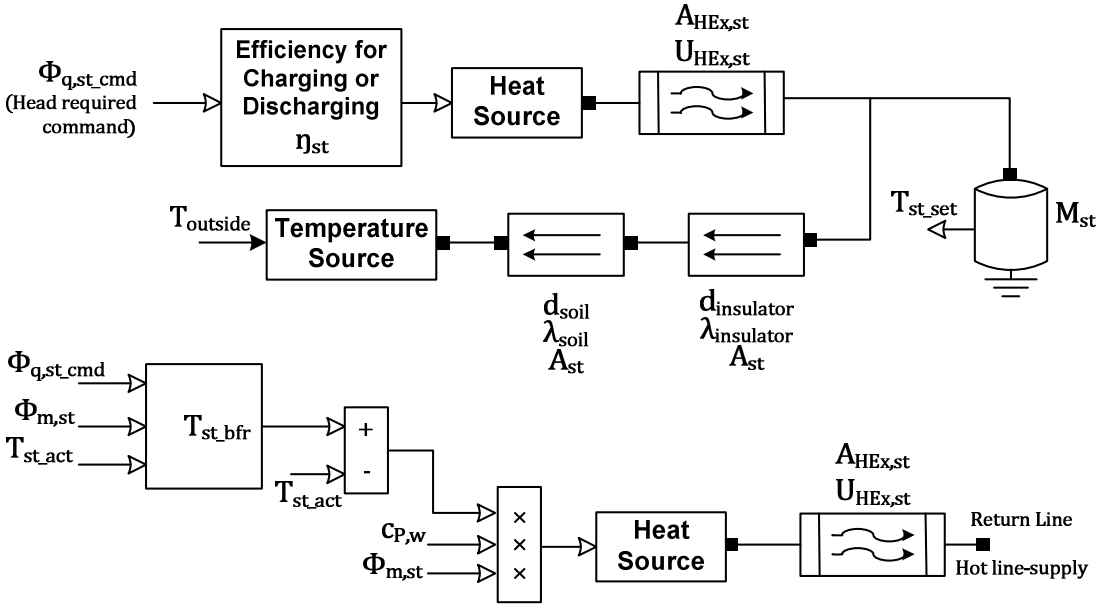

Figure 40 Heat storage model block diagram in Simscape

Model of Hot Water Heating Boiler

A simple boiler model can be reduced to two main parts: the furnace, where fuel is burnt, and the heat exchanger where the hot flue gases exchange their heat with the water circulating at the other side of heat exchanger transfer wall. The boiler model aims to describe the heat injection to the district heating water as a function of:

- the amount of fuel burnt,
- the temperature of the air used for combustion,
- and the lower limit of the flue gases temperature at the boiler exit.

The zero dimensional model described in [65], which applies mass and energy balances and ignores spatial variation of temperatures and heat fluxes is used to characterize the furnace in quasi-stationary state. Further, the predicted combustion temperature that the gases would acquire in the adiabatic process of fuel combustion (adiabatic temperature, T_{aft}) is a function of fuel and air mass flow, temperature of combustion air, lower heat value of fuel (LHV), and of the specific heat capacity of air and flue gases [66]. The calculation of the net heat transfer in the furnace ($\phi_{q,fur}$) requires knowing of the adiabatic temperature and the temperature of the gases at the furnace exit (T_{gfe}) and is described by equation Eq. 48 as per reference [67].

$$\phi_{q,fur} = \phi_{m,gases} * c_{p,gases} * \varphi * \left(T_{aft} - T_{gfe}\right) \quad \textbf{Eq. 48}$$

$$\phi_{m,gases} = \phi_{m,fuel} + \phi_{m,air} \quad \textbf{Eq. 49}$$

$$\phi_{m,air} = \phi_{m,fuel} * AFR * \alpha \quad \textbf{Eq. 50}$$

$$T_{aft} = \frac{LHV + AFR * \alpha * c_{p,air} * (T_{air,outside} - 80)}{(1 + AFR * \alpha) * c_{p,gases}} \quad \textbf{Eq. 51}$$

$$T_{gfe} = T_{aft} * \theta_{fl} \quad \textbf{Eq. 52}$$

Where φ represents 1-radiations losses/100, AFR is the stoichiometric air fuel ratio, α is 1+excess air factor/100 and Θ_{fl} is the dimensionless temperature furnace parameter and is based on experimental data. Equation Eq. 51 must be solved using the British units system.

This set of equations gives the net heat exchanged in the furnace by the combustion of natural gas. They are implemented in Simulink/Simscape and the reckoned heat flow is injected to the district heating hot pipeline through a Simscape functional block representing the effect of the overall heat conduction between the mediums and the effective surface area for heat exchange in the boiler (U_{HEx_boiler} and A_{HEx_boiler} respectively).

Model of Heat Recovery Exchanger in CHP generator

This exhaust gases to water heat exchanger is modeled identical to the discussed space heating heat exchanger, Figure 38. The same modeling equations apply and are shown below with the appropriate subscripts. The variable temperature of the CHP exhaust gases enters the HEx hot chamber input together with the barely fluctuating exhaust gases mass flow ($\phi_{m,gases}$) and with the variable temperature of the district heating return water flow. A daisy chain connection of three of these exchangers, each of them increasing further the temperature of the fixed district heat water flow makes up the CHPs heat section.

HEx hot side:

$$M_{gases} * c_{p,gases} * \frac{dT_{P2,CHP}}{dt} = \phi_{m,gases} * c_{p,gases} * (T_{P1,CHP} - T_{P2,CHP}) - U_{HEx\_CHP} * A_{HEx\_CHP} * LMTD_{HEx}$$

Eq. 53

HEx cold side:

$$M_{water} * c_{p,w} * \frac{dT_{S1,CHP}}{dt} = \phi_{m,DH} * c_{p,w} * \left(T_{s2,CHP} - T_{s1,CHP}\right) + U_{HEx\_CHP} * A_{HEx\_CHP} * LMTD_{HEx}$$

Eq. 54

Model for Heat Losses in Pipelines

The effect of heat losses in pipes has been neglected for the radiator network and sub-station, however the large distances that hot and return water might travel inside the pipelines in district heating application make necessary to consider heat losses in pipelines owing to the temperature difference between the interior and surroundings of the pipes.

The main heat transfer mechanism in this case is heat conduction through the pipe insulator and surrounding soil. The energy balance for this system gives:

$$M_{DH\_w} * c_{p,w} * \frac{dT_{DH\_ret}}{dt} = \phi_{m,DH} * c_{p,w} * \left(T_{DH\_ret\_ss} - T_{DH\_ret}\right) - \phi_{q,DH\_loss}$$

Eq. 55

Where $T_{DH,ret}$ is the temperature of the return water mass flow at the entrance of the first heat supply source, and ϕ_{q,DH_loss} are the heat losses due to conduction given by the temperature difference between the return water and the environment.

$$\phi_{DH\_loss} = U_{DH\_pipe} * A_{DH\_pipe} * LMTD$$

Eq. 56

where $\frac{1}{U_{DH\_pipe}} = \frac{d_{insulator}}{\lambda_{insulator}} + \frac{d_{soil}}{\lambda_{soil}}$ and $A_{DH,pipe}$ is the cylindrical surface at the middle of the pipe insulator material along the whole pipe length.

The implementation of this model in Simulink/Simscape is shown in Figure 41. Having the temperature of the outside air as given and using a Simscape functional block for temperature source, the model uses equation Eq. 55 and regards the overall heat conduction transfer coefficient and surface area of transfer for the insulator and soil in two separated blocks. The same model repeats for the hot water pipe line.

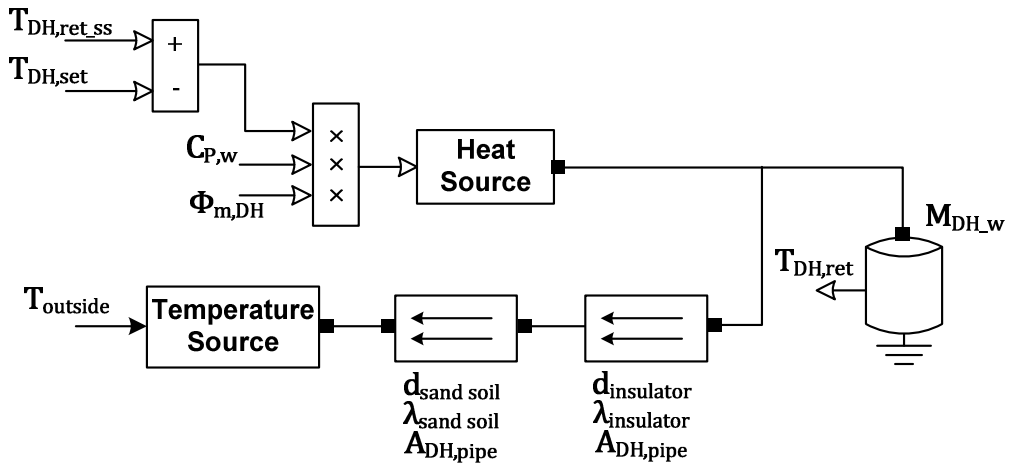

Figure 41 Block diagram of model for pipelines heat losses

Determining the Parameters for District Heating System

Sizing of the DHS components was accomplished through defining a general load pattern for a specific type of consumer, using some rules of thumb, applying the above equations, and by collecting heat parameters (λ, U, c_p , etc) referenced in tables, handbooks and datasheets of commercially available DHS components.

A software program developed by the University of Amsterdam generates load patterns based on a user specified household consumer characteristics. The patterns correspond to the evaluation of a large selection of data corresponding to a large survey. The software outcome is a week load pattern for electricity and gas consumption for heating purposes of a single household. The software distinguishes between a winter and summer load pattern. The consumer characteristics used in this thesis work are:

- Age range of dwellers: < 65 years old
- Number of dwellers per property: 2 to 5
- Type of property: semi-detached; row, between home; and row corner

The gas consumption pattern was modified in order to removed the consumption of it in cooking and further a pattern consumption for heating purposes and another for service water purposes was discerned throughout comparing the summer and winter patterns. It gave that roughly 20% of the load is from service water heating demand.

The maximum load value plus a safety factor was used in sizing the DHS components. For space heating, its maximum load was assumed to be the house heat losses when T_{indoor} = 20 [°C] and $T_{outside}$ = -4. Thus, assuming values for the heat transfer coefficients and thermal conductivity of the materials of the house structure (walls, windows, roof) based on references [51, 68] , and considering that only roof, front and rear sides of the property have direct contact with the outside temperature, the surface area of the house structure and the mass of air contained in it was reckoned.

The radiator heat exchange area (A_{rad}) was obtained using the rule of thumb that a squared foot will emit 170 BTU per hour when the room temperature T_{indoor} = 20 [°C] (70 [°F]) and water temperature entering the radiator $T_{P1,rad}$ = 82 [°C] (180 [°F]) [69]. This rule results in a U_{rad} of 11 [W/m^{2}K] which is in accordance with the range found in [68]. The radiator water mass flow was determined using equation Eq. 33 with the radiator design temperatures shown in Table 4.

Heat exchangers parameters were determined by selecting an appropriate overall heat exchanger coefficient (U_{HEx}) which depends of the heat exchanger model, either shell-tube or plate [70]. And by considering appropriate design input and outputs temperatures and the maximum designed heat transfer capacity. All of them applied to equations Eq. 33 and Eq. 34.

Pre-insulated pipes are considered for the hot and return lines of the DHS. Its diameter depends on the amount of DH mass flow to transport and the required flow speed. It was assumed that each DH pipeline has a length of 1 kilometer and that the DH water flow should cover it in 5 minutes. Knowing the required diameter a pre-insulated pipe model was selected from reference [71] and the pre-insulated pipeline area at middle of the insulator was reckoned.

Heat storage was dimensioned to satisfy a specific heat load during a specific time. The water mass, volume and surface area of the tank needed to fulfill these conditions are found through equation Eq. 33 and the geometry of the tank. The same insulation material used in the pipelines was assumed to cover the tank.

Table 4 summarized the general parameters used in the DHS model. Please refer to Chapter 5 for the specific values concerning to the studied district used in this thesis work.

Name	***Abbrev.***	***Value***	***unit***
Specific Heat Capacity of Water	$c_{p,w}$	4.18	kJ/kg K
Specific Heat Capacity of Air (British system)	$c_{p,air}$	0.24	Btu/lbF
Maximum designed DH Hot line Temperature	$T_{DH\_hl,\ max}$	100	°C
Minimum designed DH Return line Temperature	$T_{DH\_ret,\ min}$	65	°C
Minimum designed outside Temperature	$T_{outside,min}$	-4	°C
Service Water Heating Load			
Designed Input Temperature Service Water	$T_{in,sw}$	15	°C
Designed Output Temperature Service Water	$T_{out,sw}$	80	°C
Space Heating Load			
Heat Transfer Coefficient -indoor air to walls	$h_{air,in\text{-}walls}$	24	W/m^2 K
Heat Transfer Coefficient -indoor air to windows	$h_{air,in\text{-}wnds}$	25	W/m^2 K
Heat Transfer Coefficient -indoor air to roof	$h_{air,in\text{-}roof}$	12	W/m^2 K
Thermal Conductivity walls	λ_{walls}	0.038	W/m K
Thermal Conductivity windows	λ_{wnds}	0.78	W/m K
Thermal Conductivity roof	λ_{roof}	0.038	W/m K
Heat Transfer Coefficient -walls to outside	$h_{walls\text{-}air,out}$	34	W/m^2 K
Heat Transfer Coefficient -windows to outside	$h_{wnds\text{-}air,out}$	32	W/m^2 K
Heat Transfer Coefficient -roof to outside	$h_{roof\text{-}air,out}$	38	W/m^2 K
Radiator			
Maximum designed In Radiator Temperature	$T_{P1,rad,max}$	85	°C

Minimum designed Out Radiator Temperature	$T_{P2,rad,min}$	60	°C
Overall Heat Transfer Coefficient Radiator	U_{rad}	11	W/m^2 K
Space Heating Heat Exchanger			
Maximum designed In HEx Temperature	$T_{P1,DH\_sh,max}$	100	°C
Minimum designed Out HEx Temperature	$T_{P2,DH\_sh,min}$	65	°C
Overall Heat Transfer Coefficient Plate HEx SH	$U_{HEx,sh}$	800	W/m^2 K
Service Water Heating Heat Exchanger			
Maximum designed In HEx Temperature	$T_{P1,DH\_sw,max}$	100	°C
Minimum designed Out HEx Temperature	$T_{P2,DH\_sw,min}$	65	°C
Overall Heat Transfer Coefficient Shell-Tubes HEx SW	$U_{HEx,sw}$	150	W/m^2 K
Heat Storage			
Minimum designed Storage Temperature	$T_{st,,min}$	70	°C
Efficiency at Charging and Discharging H. storage	$\eta_{st,}$	95	%
Thermal Conductivity Polyurethane foam Insulator	$\lambda_{insulator}$	0.023	W/m K
Thermal Conductivity normal soil	λ_{soil}	1.5	W/m K
Overall Heat Transfer Coefficient Plate HEx storage	$U_{HEx,st}$	800	W/m^2 K
Hot Water Heating Boiler			
Specific Heat Capacity of combustion gases	$c_{p,gases}$	1.34	kJ/kg K
Specific Heat Capacity of gases (British system)	$c_{p,gases}$	0.32	Btu/lbF
Air-Fuel ration (Natural Gas)	AFR	17.138	
Excess air factor		10	%
Low Heating Value of Natural Gas	LHV	49200	kJ/kg
Low Heating Value of Natural Gas (British system)	LHV	21156	Btu/lb
Radiation Losses		2	%
Overall Heat Transfer Coefficient Boiler	$U_{HEx,boiler}$	70	W/m^2 K
Pre-Insulated Pipelines			
Thermal Conductivity PUR foam Insulator	$\lambda_{insulator}$	0.023	W/m K
Thermal Conductivity sand soil	λ_{soil}	0.2	W/m K

Table 4 Summary of general parameters used in the District Heating System model

CHAPTER 5

Control Strategy, Simulations and Results

Control Strategy

The operation of the autonomous distributed generation system needs some means to perform the energy dispatch given by the optimization module. Even more, it requires a method of control over the DGS components to keep equilibrium between demand and supply, given the constantly changing loads. Additionally, the load changes must be allocated to the DGS components through some means that ensures their fair division. All this should take place while maintain the quality of the supplied energy, i.e. frequency and voltage in the electrical system and temperature and heat flow in the heat system must keep their specifications.

To accomplish this, a control strategy based on a hierarchical control architecture is selected. As discussed in Chapter 2, research in DGS control strategies agrees that this is a proper option due to its proved robust performance in traditional power systems.

This hierarchical control will handle the following technical and economical objectives for the operation of the DGS.

- *Technical Objective:* provide demanded energy to the varying loads while maintaining system frequency within its specified nominal value (50 Hz) in the case of the electrical system and to maintain temperature of the district heating hot water line within its desired value (100 °C).
- *Economical Objective:* minimize the operative costs. The allocation of the individual generation output of a DGS generator is obtained by adding its optimal economic dispatch (proposed by the optimization module) to its participation on the unpredicted load demand. The latter reckoned using participation factors (pf). In regards to wind energy generation, its maximum possible production is always added to the system.

The proposed hierarchical control structure has two levels of control to perform the objectives:

- *Primary Control.* It is embedded in the DGS components. It assures that each DGS component keeps its assigned control variable as close as possible to its desired setpoint.
- *Main Control.* It is responsible to manage the entire system. It brings the system frequency and district heating hot line temperature to its nominal value. It monitors the distributed generation system and it commands the dispatch of the desired energy output of each controllable DGS component.

Figure 42 sketches this two levels hierarchical control, the location of each controller in the DGS and their role in the studied distributed generation system.

Primary Control

Each of the primary controllers implemented in the DGS is described in Chapter 4. Here a summary to describe their role within the hierarchical control structure is presented.

In CHP generators. The PID governor of each CHP is assigned to control the rotor speed of the generators. It chases the specified rotor speed by changing the fuel injection. Additionally it responds to the load error signal to enable parallel operation with other generators and correction of the system frequency. It also permits to maintain a desired power dispatch. The primary control for the voltage is carried out by the excitation system of each generator; this control is assumed to perform properly in this thesis work.

In Wind Turbine. Two embedded controls operate in the wind turbine. The rotor speed control performs in order to obtain optimal power through changing the rotor speed by modifying the electromagnetic torque. The pitch angle control operates for power limitation. It ensures to maintain the assigned rotor speed by changing the aerodynamics of the wind turbine blades.

In Service Water Heating Heat Exchanger. Its control operates to maintain the desired hot service water temperature by changing the mass flow of hot water in the hot side of the heat exchanger.

In Space Heating. Two embedded controls operate for space heating. The one in the radiator network work keeping the room temperature at the desired level by changing the amount of radiator hot water flowing throughout the radiators. The one in the space heating heat exchanger control the temperature of the water going to the radiators by changing the mass flow of DHS hot water in its hot side.

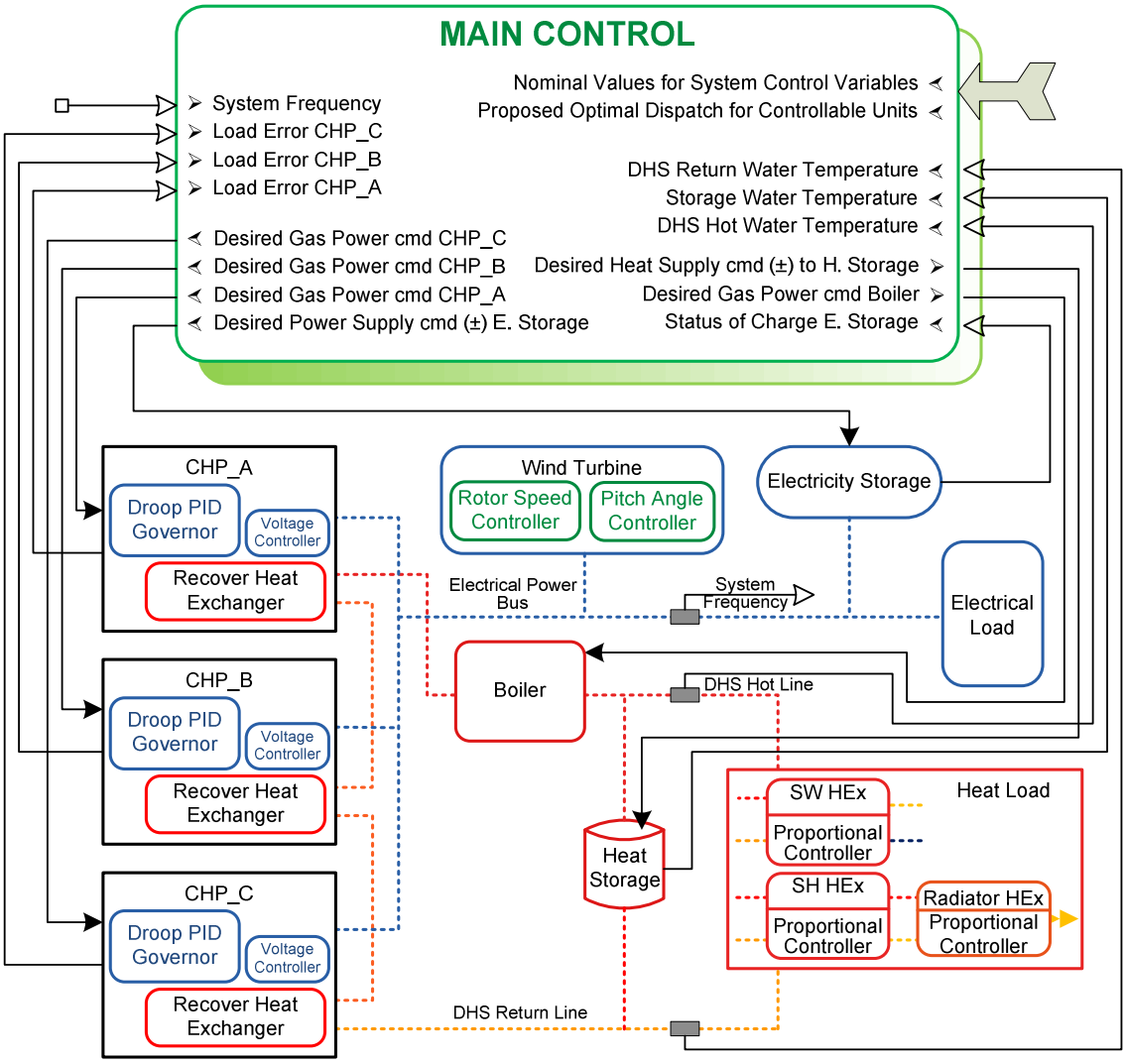

Figure 42 Hierarchical control structure for the control of the DGS

Main Control

The main control performs for the whole system by distinguishing the control actions needed for the heat system and the needed for the electrical system. Given that the energy link between the heat system and electrical system are the CHP generators, the main control only takes corrective actions over the electrical generation of the CHPs, leaving their yielded heat to feed the heat system as an uncontrollable heat source. Alike to the wind turbine generation for the electrical system. This control operation decision is supported by the lack of a generation unit dedicated only for electricity, conversely to the case in the heat system where the boiler is controlled to supply the heat demand without affecting the electricity supply.

Heat System Main Control Structure

In the heat system the energy demand at the supply side is given through the amount of energy that must be added to the DHS return water mass flow in order to reach the specified nominal hot water flow temperature at the entrance of the DHS hot pipeline. The water heating process starts at the recovery heat exchangers of the CHPs and finishes later in the boiler. The heat storage can either supply energy (discharging operation) to the DHS return water or can take energy from the hot water (charging operation) before it enters the DHS hot pipeline.

Taking into account this system operation setup, the main controller performs its duties: allocate the scheduled optimal energy dispatch to the boiler and heat storage unit, and execute corrective actions in order to assure the DHS hot water enters the hot pipeline at the specified temperature (100 °C). The first controller's task is fulfilled quite straightforward for the boiler; however for the heat storage, precaution is taken in order to avoid infringing any physical law of heat transfer. It means determining the possibility of charging or discharging at every instant. Charging is available if the heat storage water temperature is lower than the DHS hot water temperature and discharging is possible if the heat storage water temperature is higher than the DHS return water temperature.

The second controller's task is accomplished by first recognizing the need of a corrective control action. There is a need if the error between the actual DHS hot water temperature at the hot line entrance and its nominal value is different from zero. The sign of the error signal indicates if the correction should be to increase the heat supply (negative sign) or to curtail it (positive sign). The error signal is fed to a proportional controller (proportional gain) in order to determine the amount of energy needed to return the hot water temperature to its nominal value. This energy amount is distributed between the boiler and heat storage unit using participation factors. After calculating the participation of each unit with equation Eq. 58, its energy participation is added to its scheduled optimal energy dispatch and the desired energy command is formed (Eq. 59).

A simple addition works for determining the desired energy command to the boiler. However for the desired operation of the heat storage unit, its required operation mode (charging or discharging) must be firstly recognized. It is carried out by identifying the sign of the energy amount that results from adding the storage participation to its scheduled optimal dispatch. Meaning a positive sign that charging is required and a negative sign that discharging is required. Thus, the control can resolve if the desired storage charging or discharging can take place and send the proper command to the storage unit. Figure 43 shows the flow charge for the operation of the main control logic in its heat system controlling part.

Participation Factors. The predicted optimal operation of the heat system would happen if it operates only with the proposed dispatch from the optimization module. Nevertheless, this optimal dispatch is based in a forecast of demand at discrete periods of time, so the online operation of the system has to correct the mismatch between the forecasted demand and the real demand. In order

to do this, the heat supply must be corrected while somehow keeping the reckoned optimum. The participation of each controllable unit on the supply's correction is performed by "participation factors" determined at each period of time. These participation factors are reckoned using the scheduled optimal dispatch as follow:

$$pf_{cont\_unit} = \frac{Scheduled\ Heat_{cont\_unit}\ [p.u]}{\sum Scheduled\ Heat_{cont\_unit}\ [p.u]} + pf_{min.cont\_unit}$$

Eq. 57

then,

$$Heat\ participation_{cont\_unit} = Heat\ supply\ correction * pf_{cont\_unit}$$

Eq. 58

and, the desired energy dispatch command to each controllable units is:

$$Desired\ Energy\ _{cont\_unit} = Heat\ participation_{cont\_unit} + Scheduled\ Heat_{cont\_unit}$$

Eq. 59

where pf stands for participation factor and the subscript $cont\_unit$ stands for controllable unit. The base of per unit value is the combined nominal heat power of the controllable units.

Additional provisions are taken in reckoning the participation factors. The absolute value of the scheduled heat storage is used in equation Eq. 57. Moreover, if the scheduled heat storage is for charging operation (storage demanding heat) but the main control reports the need of increasing supply, the scheduled heat storage passes as zero to equation Eq. 57. This is done in order to keep its participation at the minimum, because its optimal operation in that period of time is for storage charging. The same applies when it is scheduled to discharge. In that case, if the main control reports that the heat supply should decrease, the scheduled heat storage passes as zero to equation Eq. 57. Finally, a minimum participation factor exists for each controllable unit in order to give more weight to the heat correction in charge of the boiler. Given that the heat storage capacity has limits regarding time span.

Electrical System Main Control Structure

The control strategy chosen for the main control of the DGS electrical system is the Automatic Generation Control (AGC). AGC is a well-known, reliable, and quite proven control system for power generation systems. Its main objectives are to hold system frequency at or very close to specified nominal value, to maintain the correct amount of scheduled power interchange among control areas, and to maintain each unit generating at its most economic value [6]. The first and the last objective of this control system match with the aims of the designed main control, therefore their implementation is adapted in the main controller for the studied autonomous DGS.

Since the governors of each CHP operate in droop mode, a change in load will induce a frequency change (after transient) with a value that depends on the droop characteristics of the governors. This change must be corrected in order to restore the frequency to its nominal value. An integral controller with input the error between the actual system frequency and its nominal value performs this correction.

The most economic value of each unit's generation (desired dispatch) is achieved through adding the scheduled optimal energy dispatch to the reckoned participation of each unit's generation in the correction of the combined error. To force realization of the desired dispatch, the errors between the actual CHP unit's generation and its desired CHP unit's generation add to the frequency error forming a combined error that enters in the integral controller. In order to give more weight to the frequency error, it is multiply by a gain factor before composing the combined error.

Using this allocation of power generation, which depends on the system frequency error and on the scheduled optimal dispatch, the electricity storage is controlled. When no scheduled optimal dispatch is given for the electricity storage, the main controller makes it to discharge any time that the system needs power and commands storage to charge when both the wind energy surpassed the demand and the CHPs have been turn down to minimum. In the case that scheduled optimal dispatch exits, the main controller discerns whether it is for charging or discharging, compares it with the current need of the system (correct to increase or decrease generation) and decides whether the electricity storage intervenes with a minimum participation factor or with a higher participation factor. Alike to the heat storage's logic for determining its participation factor, here a scheduled electricity storage's charging will give a minimum storage's participation factor if the actual system need is for power increment. Whereas a scheduled discharging while the system asks for generation reduction gives the minimum participation factor as well.

The availability for charging or discharging the electricity storage (battery stack) is evaluated before the main controller sends the desired power command to it. The battery stack is available for charging if its State-Of-Charge (SOC) is lower than 104% and it is available for discharging if its SOC is higher than 20%, these limits according to [59]. Fulfilled these conditions the desired electricity storage power command is sent, otherwise the storage is held in stand-by mode.

Participation Factors. They are reckoned using the following equations:

$$pf_{E.Storage} = \frac{Scheduled\ Ele.Power_{E.Storage}\ [p.u]}{\sum Scheduled\ Ele.Power_{cont\_unit}\ [p.u]} + pf_{min.E.storage}$$

Eq. 60

$$pf_{CHP\_x} = \frac{Scheduled\ Ele.Power_{CHP\_x}\ [p.u]}{\sum Scheduled\ Elec.Power_{CHP\_x}\ [p.u]}$$

Eq. 61

Then the participation of the each unit's generation is computed with:

$$Generation\ participation_{cont\_unit} = Generation\ correction * pf_{cont\_unit}$$

Eq. 62

Finally the desired controllable unit's generation dispatch is obtained with:

$$Desired\ Generation_{cont\_unit} = Generation\ participation_{cont\_unit} + Scheduled\ Ele.Power_{cont\_unit}$$

Eq. 63

The base of per unit value is the combined nominal electrical power of the controllable units. The same additional provisions taken for the participation factors in the heat system are taken here for the electrical system with relation to the electricity storage participation.

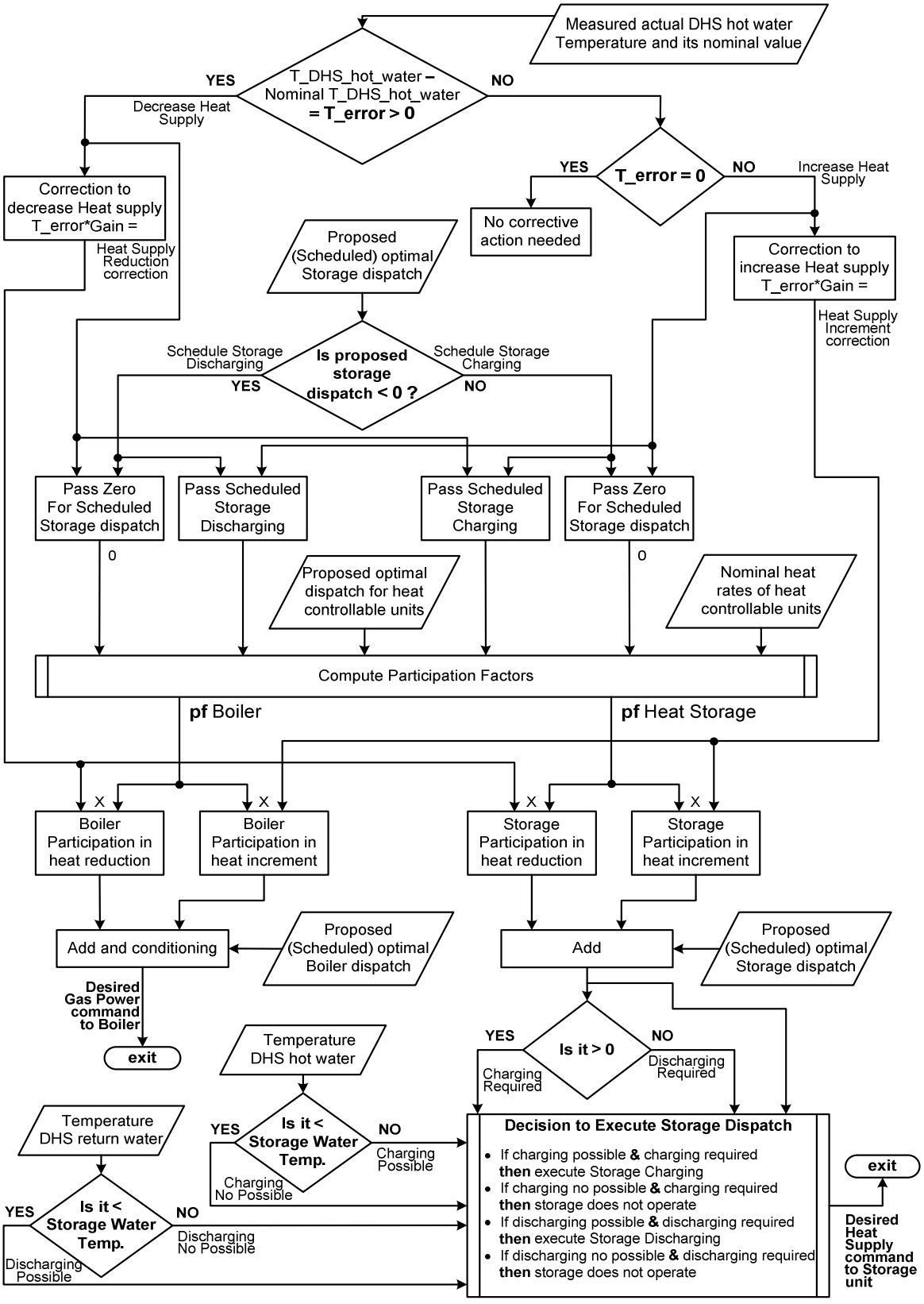

Figure 43 Flow charge indicating the main control operation logic for the heat system

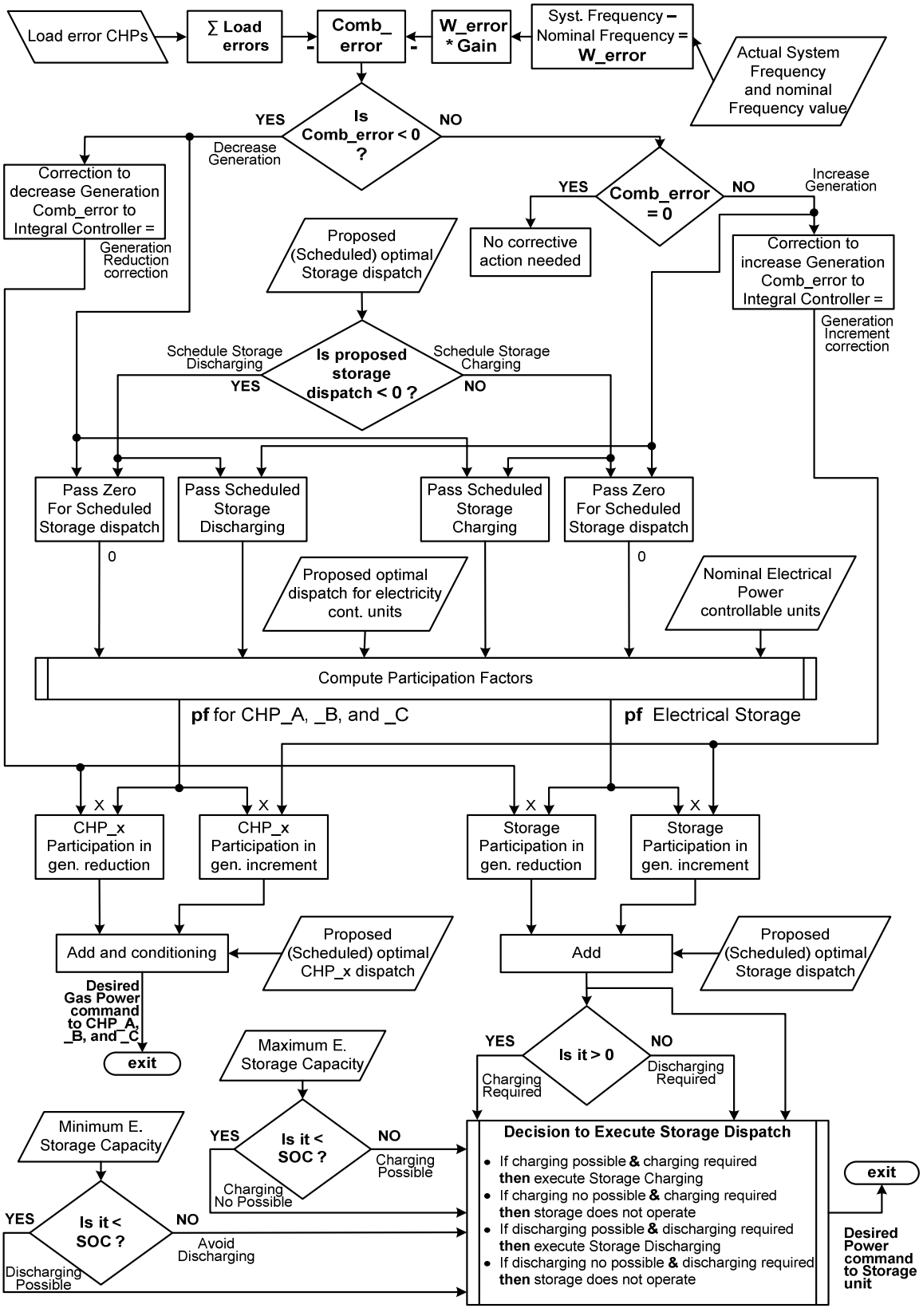

Figure 44 Flow charge indicating the main control operation logic for the electrical system

Data used and Specific values for the Studied DGS

The sizing of DGS components was done for the electrical and heat load obtained from the software program developed by the University of Amsterdam and specified in Chapter 4. The Heat and Electrical load patterns are shown in Figure 45. The electrical system was designed for a maximum demand of 300kW$_e$ and the heat system designed for a maximum demand of 1590kW$_{th}$. Regarding this, the parameters for the operation of the DG components are listed in Table 5. The pattern for wind speed was given from a forecasting software and shown in Figure 46.

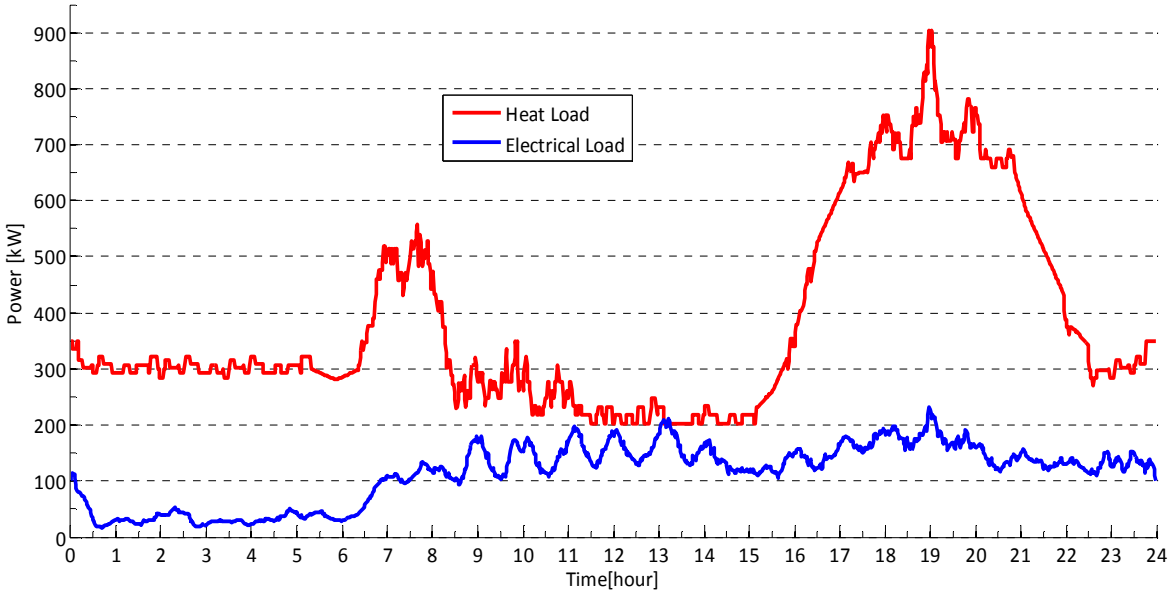

Figure 45 Electricity and Heat winter demand pattern of a residential district of 200 dwellings

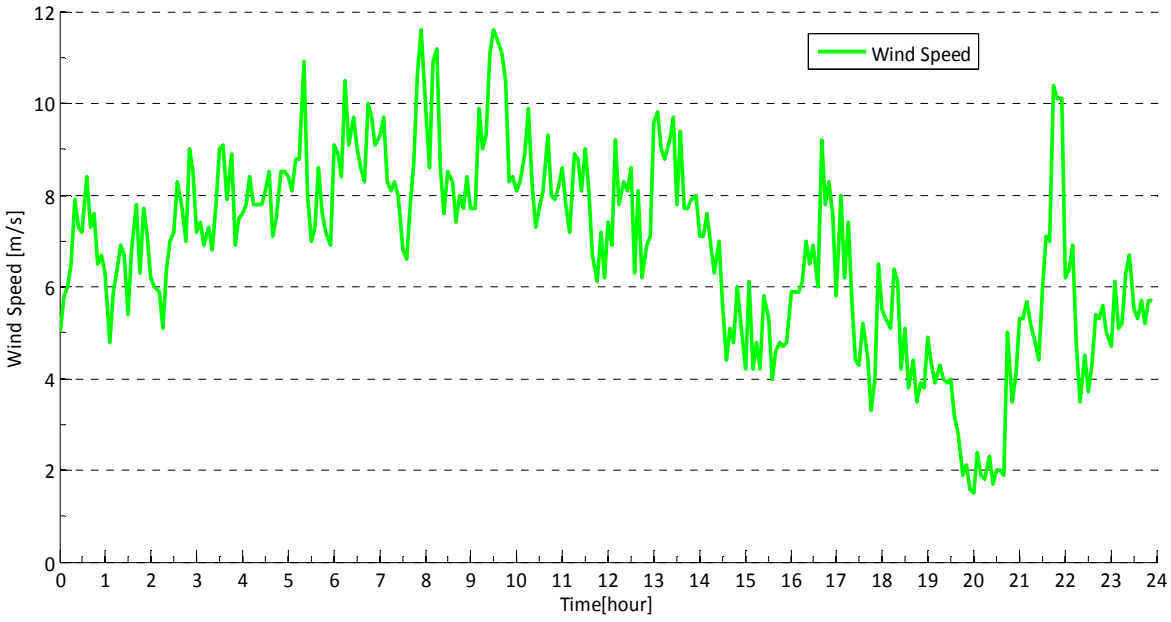

Figure 46 Wind speed pattern

CHP_A and C

Name	*Abbrev.*	*Value*	*unit*
Minimum Gas Power setpoint	$P_{gas\ min}$	89	kW
Nominal Gas Power	$P_{gas\ rated\ (nominal)}$	333	kW
CHP Nominal Electrical Power	T_{rated}	100	kW
Heat Rate	HR	11988	kJ/kWh
Rated Exhaust Recuperator Temperature	T_{ER}	270	C
Generator Nominal Apparent Power	S_{base}	133	kVA
CHP Nominal Thermal Power	$P_{h,rate}$	155	kW
Exhaust Gases Mass Flow Reference	$\phi_{m,gases}$	0.86	kg/s
Water Mass Flow cold-side	$\phi_{m,DH}$	11	kg/s
Overall Heat Transfer Coefficient -Shell-Tubes HEx	$U_{HEx,CHP}$	70	W/ m^2K
Area of Heat Exchanger	$A_{HEx,CHP}$	29	m^2

CHP_B

Name	*Abbrev.*	*Value*	*unit*
Minimum Gas Power setpoint	$P_{gas\ min}$	83	kW
Nominal Gas Power	$P_{gas\ rated\ (nominal)}$	308	kW
CHP Nominal Electrical Power	T_{rated}	80	kW
Heat Rate	HR	13860	kJ/kWh
Rated Exhaust Recuperator Temperature	T_{ER}	278	C
Generator Nominal Apparent Power	S_{base}	104	kVA
CHP Nominal Thermal Power	$P_{h,rate}$	150	kW
Exhaust Gases Mass Flow Reference	$\phi_{m,gases}$	0.83	kg/s
Water Mass Flow cold-side	$\phi_{m,DH}$	11	kg/s
Overall Heat Transfer Coefficient -Shell-Tubes HEx	$U_{HEx,CHP}$	70	W/ m^2K
Area of Heat Exchanger	$A_{HEx,CHP}$	25	m^2

Wind Turbine

Name	*Abbrev.*	*Value*	*unit*
Wind Turbine Nominal Power	P_{nom}	120	kW
Nominal Rotor Speed	$\omega_{r,nom}$	4.94	rad/s
Wind Turbine Total Inertia	H	1.2	s

Electricity Storage

Name	*Abbrev.*	*Value*	*unit*
Nominal Battery Stack Capacity	Q	1250	Ah
Maximum Power Rate for Charging/Discharging	$P_{e\_st\_cmd}$	100	kW
Initial state of charge	SOC	50	%
Standby losses, based on 5% losses per year	$P_{e\_st\_loss}$	3.61e-4	W

District Heating System

Name	*Abbrev.*	*Value*	*unit*
Maximum Designed District Heating Load	ϕ_{q,DH_max}	1590	kW
Designed District Heating Water Mass Flow	$\phi_{m,DH}$	11	kg/s
Service Water Heating Load			
Maximum Designed Service Water Heating Load	ϕ_{q,sw_max}	200	kW
Space Heating Load			
Desired Temperature Indoor	T_{indoor}	20	°C
Maximum Designed Space Heating Load	ϕ_{q,sh_max}	1390	kW
Mass of Air inside District Properties	M_{air}	126930	kg
Area of Walls all District Properties	A_{walls}	23067	m^2

Area of Windows all District Properties	A_{wnds}	2133	m^2
Area of Roof all District Properties	A_{roof}	19600	m^2
Radiator			
Maximum Designed Radiator Water Mass Flow	ϕ_{m,rad_max}	13.3	kg/s
Area of Radiator all District Properties	A_{rad}	2592	m^2
Mass of Water flowing in Radiator at time unit	$M_{w,rad}$	13.3	kg
Proportional Gain Radiator Controller	$K_{P,rad}$	50000	
Space Heating Heat Exchanger			
Maximum Designed SH HEx Water Mass Flow	ϕ_{m,DH_sh_max}	9.5	kg/s
Area of SH HEx all District Properties	A_{HEx_sh}	191	m^2
Mass of Water flowing in SH HEx Cold Side at time unit	$M_{S1,sh}$	13.3	kg
Mass of Water flowing in SH HEx Hot Side at time unit	M_{DH_sh}	10	kg
Proportional Gain SH HEx Controller	$K_{P,sh}$	1200	
Service Water Heating Heat Exchanger			
Maximum Designed SW HEx Water Mass Flow	ϕ_{m,DH_sw_max}	1.5	kg/s
Area of SW HEx all District Properties	A_{HEx_sw}	41	m^2
Mass of Water flowing in SW HEx at time unit	M_{DH_sw}	1	kg
Proportional Gain SH HEx Controller	$K_{P,sw}$	16	
Heat Storage			
Maximum Designed Capacity		190	kW-h
Maximum Designed Charging and Discharging	ϕ_{q,st_max}	380	kW
Mass of storage medium -Water	M_{st}	6545	kg
Surface Area of Tank	A_{st}	44.5	m^2
Thickness Insulator	$d_{insulator}$	0.2	m
Thickness soil	d_{soil}	1	m
Area of Heat Storage Heat Exchanger	A_{HEx_st}	38	m^2
Designed Storage HEx Water Mass Flow	$\phi_{m,st}$	3.6	kg/s
Hot Water Heating Boiler			
Boiler Nominal Power	ϕ_{q,fur_max}	550	kW
Nominal Gas Power	P_{gas}	757	kW
Dimensionless Temperature	Θ_{fl}	0.25	
Area of Heat Exchange to Waterwalls	A_{HEx_boiler}	9	m^2
Average Boiler Efficiency @ mean $T_{air,outside}$	η_{boiler}	72	%
Pre-Insulated Pipelines			
Surface Area of Pipeline	A_{DH_pipe}	306	m^2
Internal diameter of Pipeline		65	mm
Thickness Insulator	$d_{insulator}$	33	mm
Thickness soil	d_{soil}	0.5	m
Mass of Water flowing in DH pipe at time unit	M_{DH_w}	11	kg

Table 5 Specific parameters used in the modeling of the DGS components

Simulations and Results

This section first presents the results of simulations performed over the DGS model when operating under a demonstrative load. This is done in order to clearly visualize the control actions taken by the designed control strategy. Later the results for the operation of the DGS following the proposed dispatch from the optimization module under the electrical and heat load obtained for a real district are shown.

Heat system operation under demonstrative load

The combined operation of the DGS's components that make up the heat system is shown and explained in the following figures and paragraphs. The simulation was carried out with a demonstrative load to visualize and verify the different features of the heat system and its controllers. The heat supplied by CHP_B and CHP_C was kept constant during the simulation, while CHP_A heat supply participation changed along it. The scheduled optimal dispatch for the boiler and heat storage was set to zero, therefore the minimum participation factors, one for boiler and one tenth for heat storage, were used to distribute the remaining heat load.

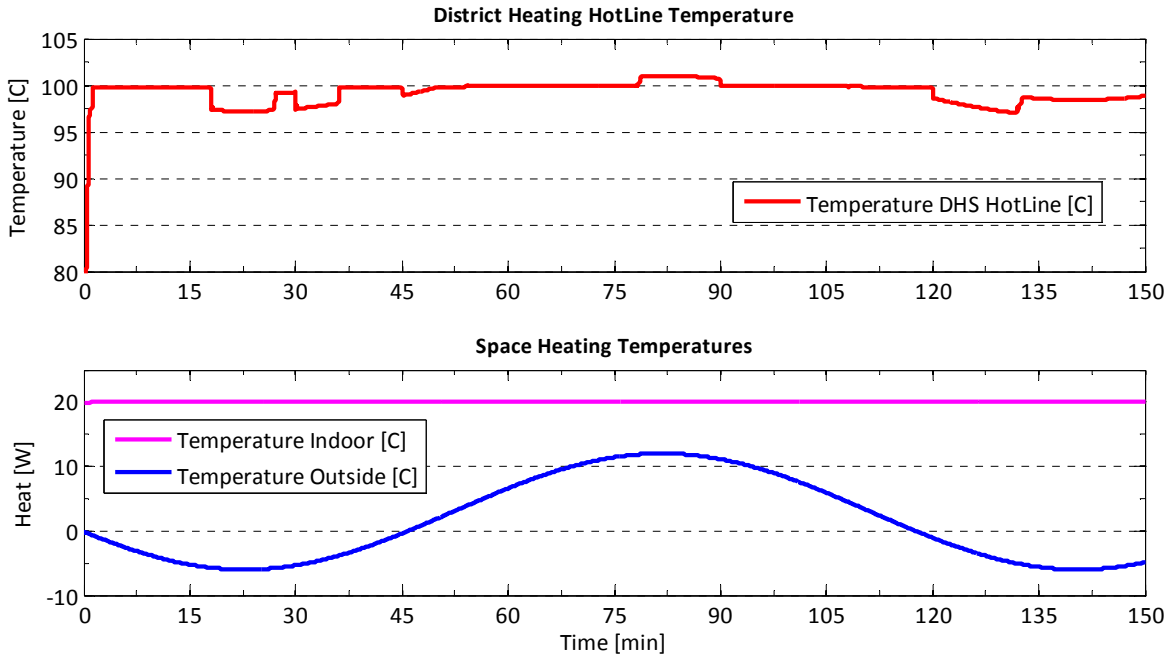

Figure 47 District Heating System main temperatures to control and air temperature outdoor

The main objective of the DGS main controller regarding its heat system is fulfilled. Figure 47 shows the DHS Hot line temperature kept close to its 100 degrees Celsius reference when the heat demand is within design. In minute 20, the DHS Hot line temperature drops below 98 °C due to the temperature outside is lower than the -4°C design and the service water heating load is 100kW higher than design (see Figure 48). Despite this extreme operation condition, the indoor temperature is maintained at 20 °C and just a marginal variation happened, although not possible to visualize in the graph.

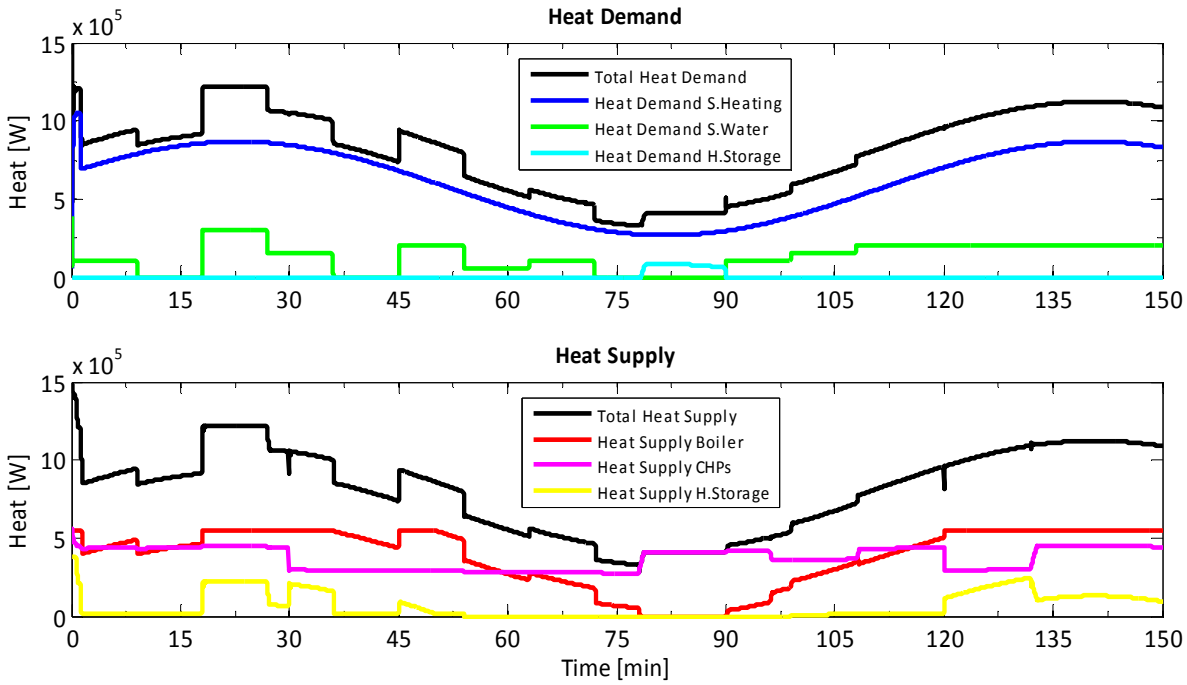

Figure 48 Heat Demand and Supply of the DGS

The service water load's discrete fluctuation shows in Figure 48 at minute 20 that boiler heat supply goes to maximum and the heat storage is commanded to discharge in order correct the error in the DHS Hot line temperature. At minute 30 the CHP_A has been turned off and the main control again controlled storage to compensate imbalance, given that the boiler is at full throttle. At minute 80 the main control has turn off the boiler and makes the storage to charge in order to balance the heat system due to the low demand and high heat supply from the CHPs.

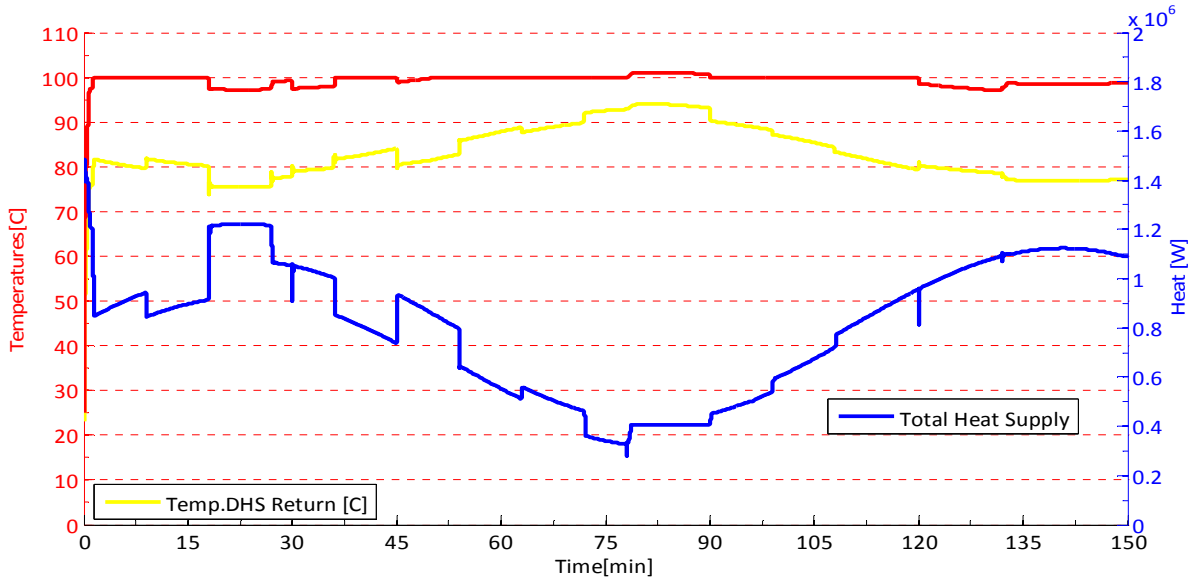

Figure 49 Heat Supply, DHS Hot Line Temperature (in red) and DHS Return Line Temperature

Figure 49 shows how the amount of heat supply is related with the temperature level that the DHS return water has. The main control is in charge of raising the return water temperature to the reference.

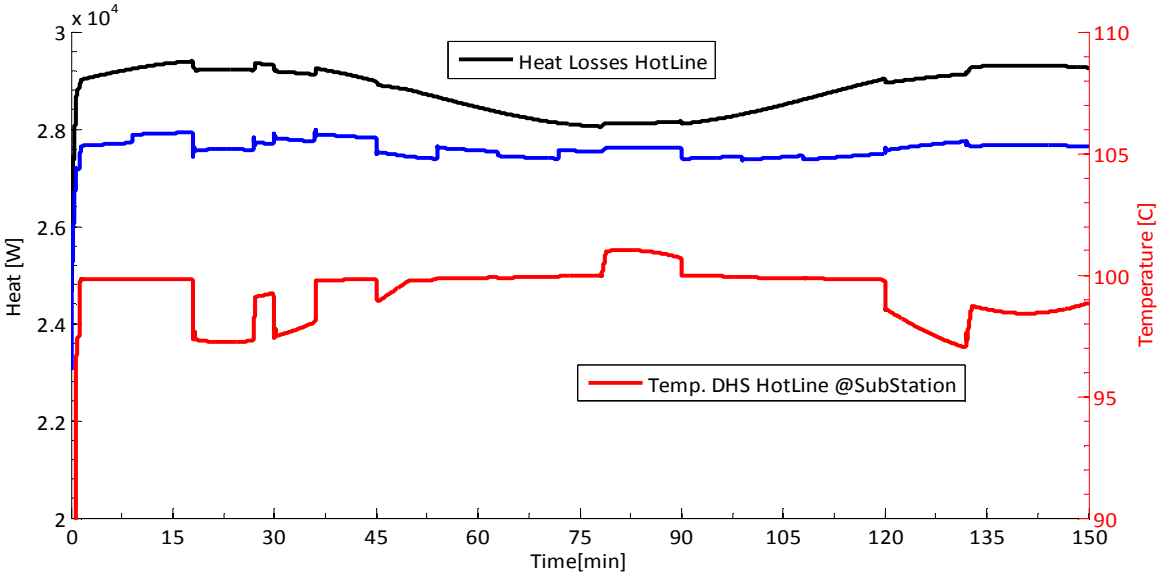

Figure 50 Heat Losses in the pipelines, in blue Heat losses at Return Line

The DHS model also includes the heat losses that the pipelines have due to outside temperature. In Figure 50 it is clear how the DHS Hot Line losses follow the pattern of the outside temperature but they also depend on the hot line water's temperature. The effect of these losses is shown in the fall of DHS Hot Line temperature at the entrance of the sub-station. It is in the order of 1 degree Celsius.

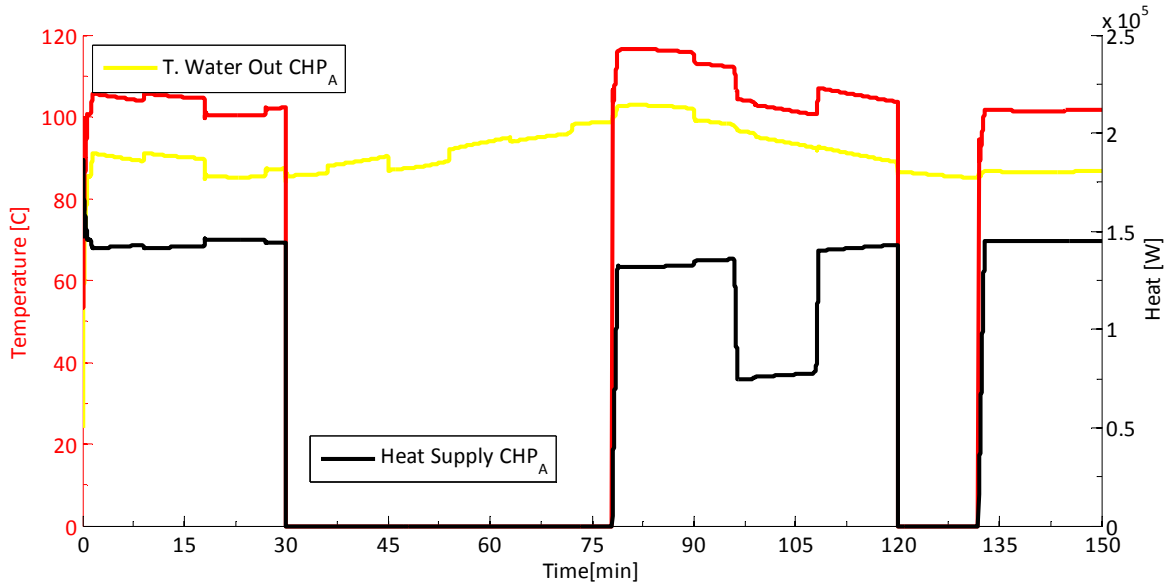

Figure 51 Operation of the CHP_A, in red Temperature of flue gases out of CHP

The CHP_A exchanges as much heat to the DHS water flow depending it the input temperature of its flue gases and the input temperature of the water. When the CHP is switch off, the water temperature corresponds to the output of the previous CHP in the daisy chain.

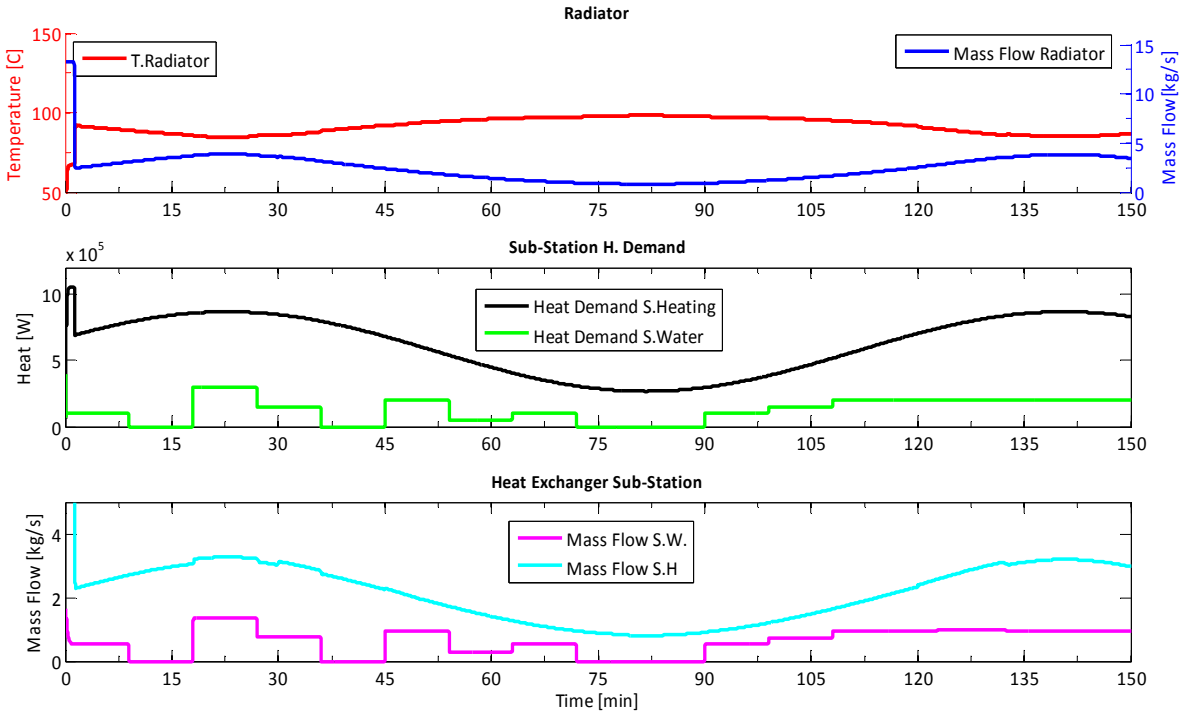

Figure 52 Sub-Station operation

Regarding the primary control operating in the DHS Sub-Station, the temperature control performed by varying the mass flow is depicted Figure 52. In the top graph, the radiator input temperature supplies the heat to keep the desired indoor temperature. The mass flow circulating in the radiator network changes to maintain the exact amount of heat needed, thus it is shown that when the space heating demand is low, at minute 80, the mass flow is the lowest.

The controller in the heat exchangers also operates to satisfy their requested heat demand. Middle and bottom graph in Figure 52 show how the mass flow varies in accordance with the heat demanded respectively.

Figure 53 shows the change in heat storage temperature due to its commanded charging and discharging. During the period between 60 and 75 minutes the storage is not operating and the effect of the heat losses towards outside can be seen in the slight falling of the storage temperature. More over the pattern of these losses is depicted in Figure 54 top graph. The main control also determines the availability of storage operation. In the middle and bottom graphs of Figure 54, for example the availability for discharging between minute 53 and 98 is suppressed because the temperature of the storage water is lower than the return's, as shown in Figure 53.

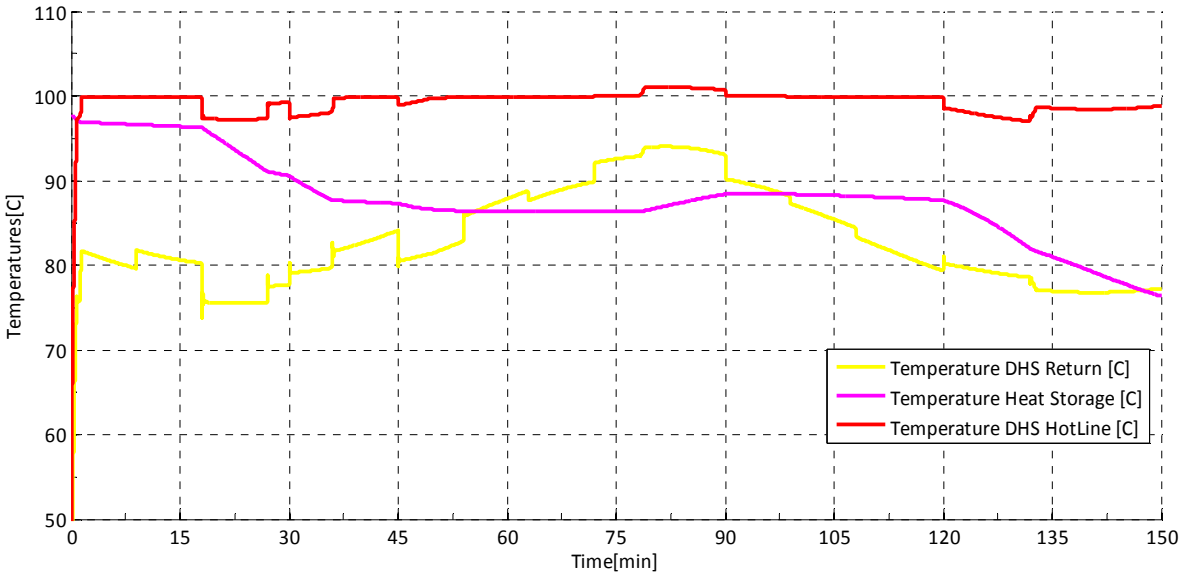

Figure 53 Temperature of Heat Storage Water

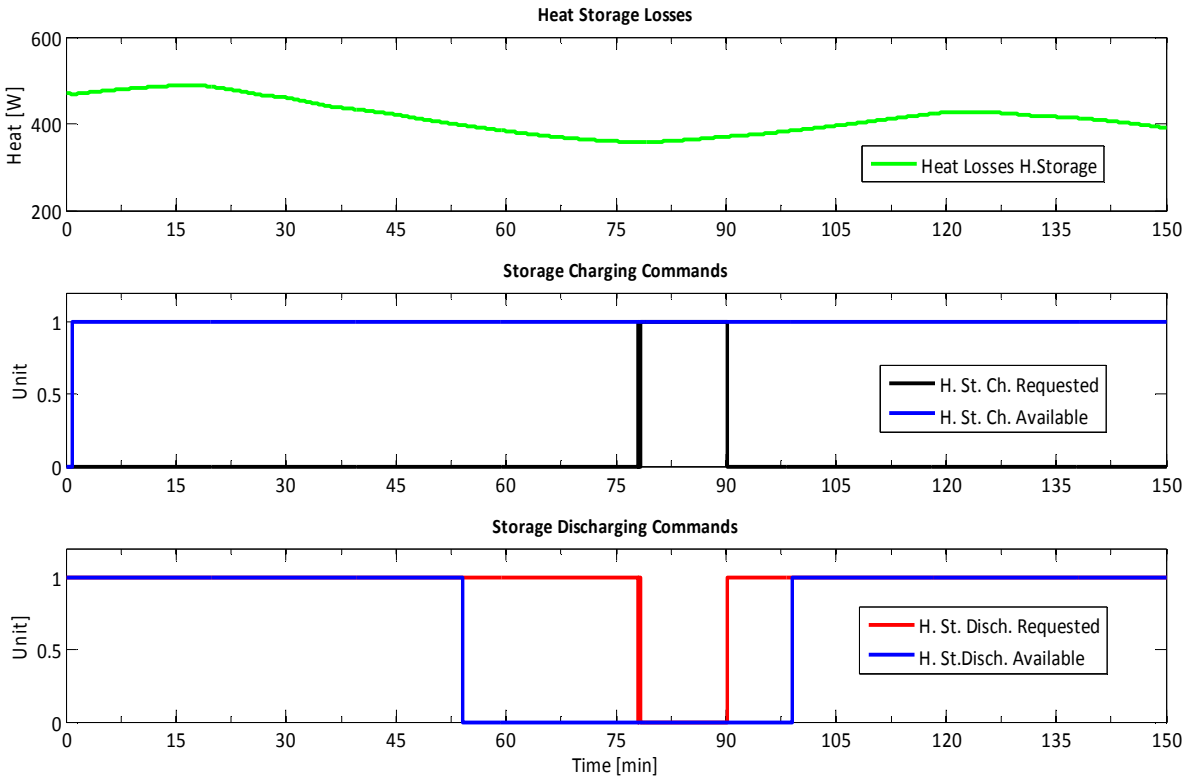

Figure 54 Heat Storage control signals and losses

Finally, the request for charging and discharging is shown in Figure 54 as well. For example, the main control does not execute the requested discharging operation at minute 60 because it identified that the heat storage is not available for discharging, but commands storage charging at minute 80 without problem.

Electrical System operation under demonstrative Load

The operation of the DGS's components that comprise the electrical system and their controllers was simulated using a demonstrative load. This electrical load and a wind speed pattern were selected to permit a clear visualization of the DGS's electrical system components attributes and performance. The participation factors for CHPs and electricity storage where kept constant, being the participation factor among CHPs even and the electricity storage's participation factor half the value of the CHP's.

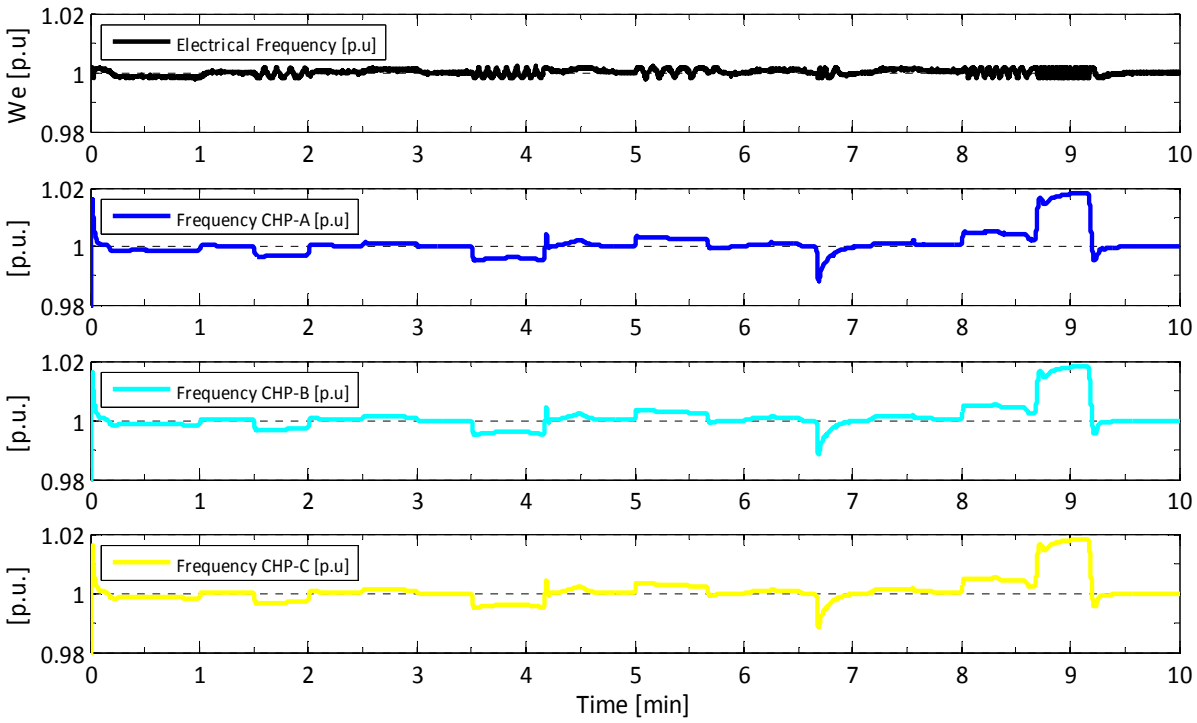

Figure 55 System Frequency and Rotor Speed of each CHP

The aim of the main and primary controllers (maintaining nominal frequency of operation) is achieved properly. Figure 55 shows how the system electrical frequency and the CHP's generators frequency is corrected and maintained near to its nominal value during the 10 minutes simulation. Although the large load increment (above CHP's capacity) from minute 3.5 to 4 (see Figure 56), the main and primary controllers keep the frequency helped by the electricity storage (see Figure 60). Right after minute 4 the wind turbine starts generating, helping the system to reestablish frequency to nominal. A large load reduction starts at minute 5 and the controllers are able to deal with it just allowing a slight increment in frequency. At minute 6.7 the CHP_A is commanded to shutdown, this operation generates a large frequency fall which is stopped by the primary control and corrected with help of the main controller. Starting at minute 8 load decreases steadily while the wind power increases steadily, thus the main controller reduces the natural gas dispatch command to CHP_B and C (see Figure 58 and Figure 59), producing the shutdown of the CHPs at ca. minute 8.7. Operating at this condition, the resulting frequency is only corrected by the action of the electricity storage. The electricity storage has been commanded to charge since there was a surplus of wind power and increases its charging rate after the CHPs turned off (see Figure 60). Given its fix participation factor (in this simulation) the electricity storage charging rate cannot be corrected fast enough to follow properly the sharp load reduction slop. However, an even larger frequency excursion is avoided and

frequency is maintained with an error that is corrected slowly. At minute 9.2 the fast load falling rate decreases and the controller makes the frequency to its nominal value.

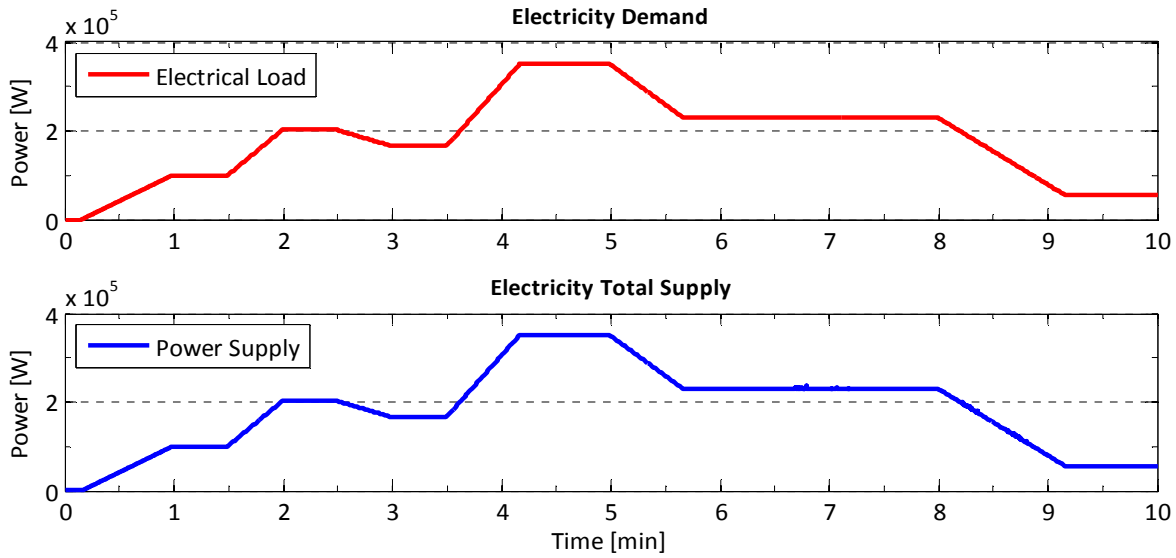

Figure 56 Balance between generation and demand of electricity

The DGS's control strategy is quite suitable for following the load pattern as Figure 56 displays.

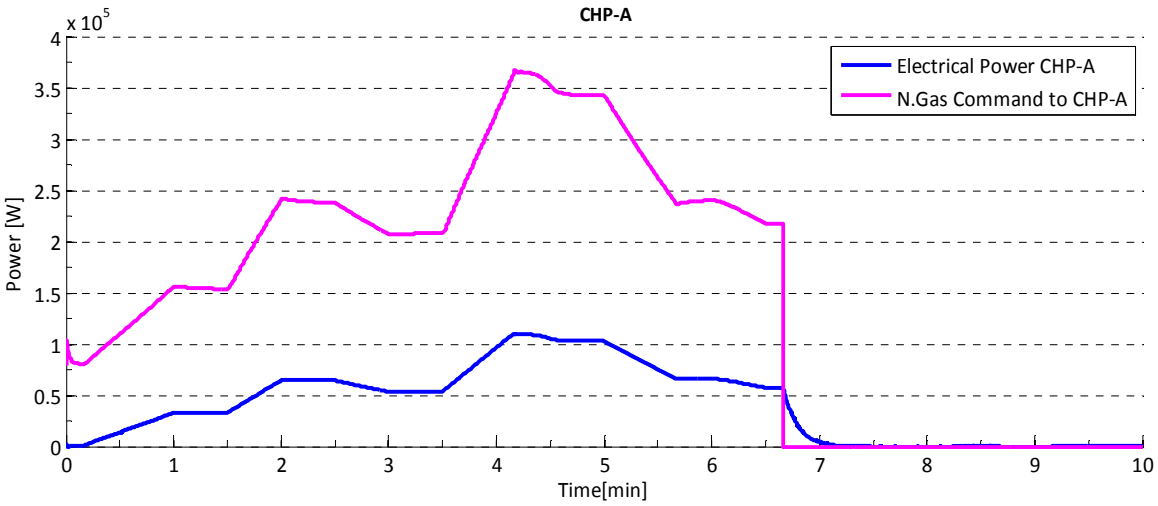

Figure 57 Natural gas power command to CHP_A and its corresponding electricity generation

The CHP_A receives from the main controller the command of natural gas power amount in order to generate the desired electrical power. The CHP model incorporates a feature regarding CHP's turn off command (N.Gas Command to zero). In Figure 57, at minute 6.7 the CHP is commanded to turn off, this action is carried out through a fast but smooth electrical power shutdown.

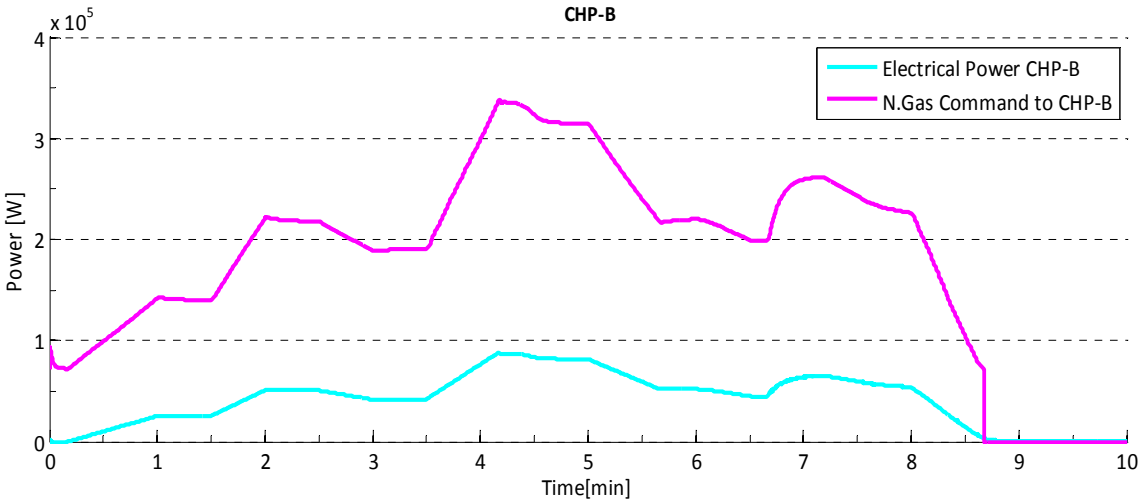

Figure 58 Natural gas power command to CHP_B and its corresponding electricity generation

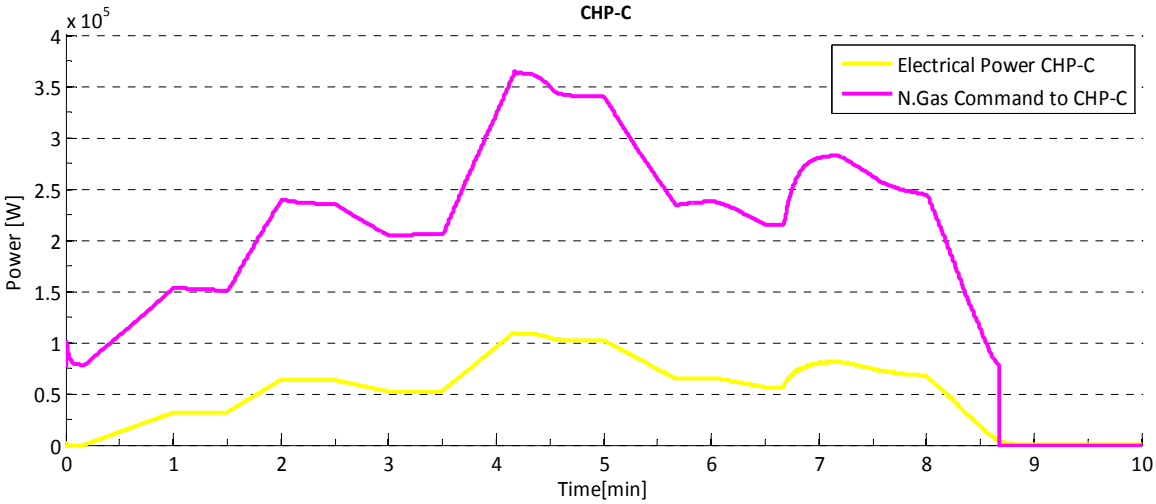

Figure 59 Natural gas power command to CHP_C and its corresponding electricity generation

Figure 58 and Figure 59 show the CHPs electricity generation and its corresponding natural gas power amount command. Two things regarding these figures are: owing to the CHP_A shutdown at minute 6.7, its electricity generation is assumed by CHP_B and C with a smooth transition, which is performed by the main control. The second thing is that although both CHP have the same participation factor, its generation is not the equal. This is because the main control reckons the CHPs' desired generation according to the nominal capacity of each CHP. Therefore, the generation transferred from CHP_A to the others two gives more load to the CHP_C than to CHP_B.

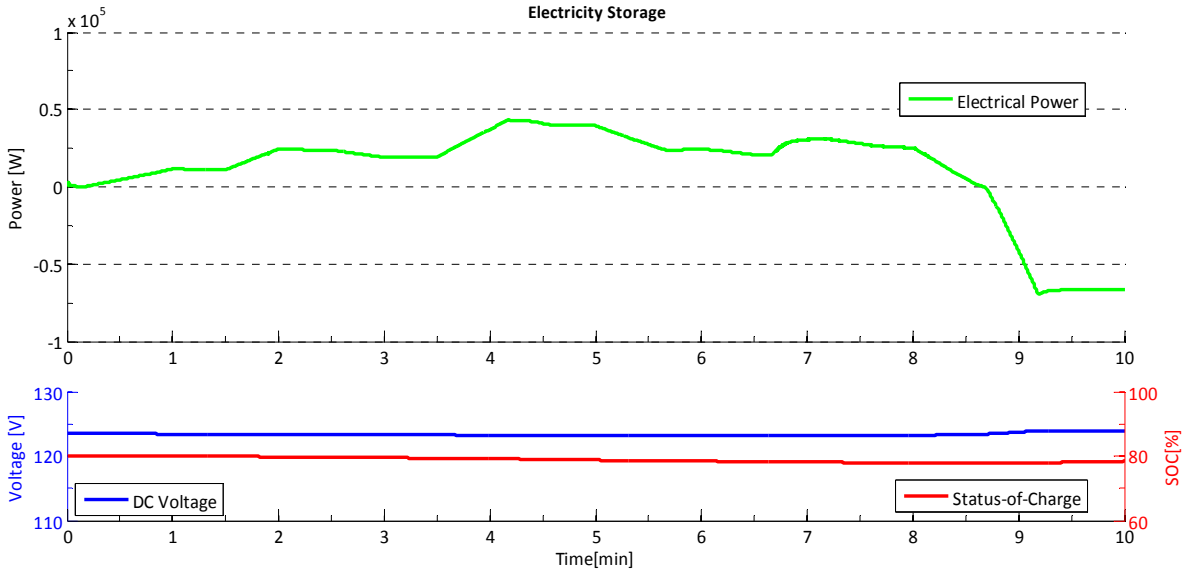

Figure 60 Power supplied (+) or taken (-) by battery stack and its DC Voltage and Status of Charge

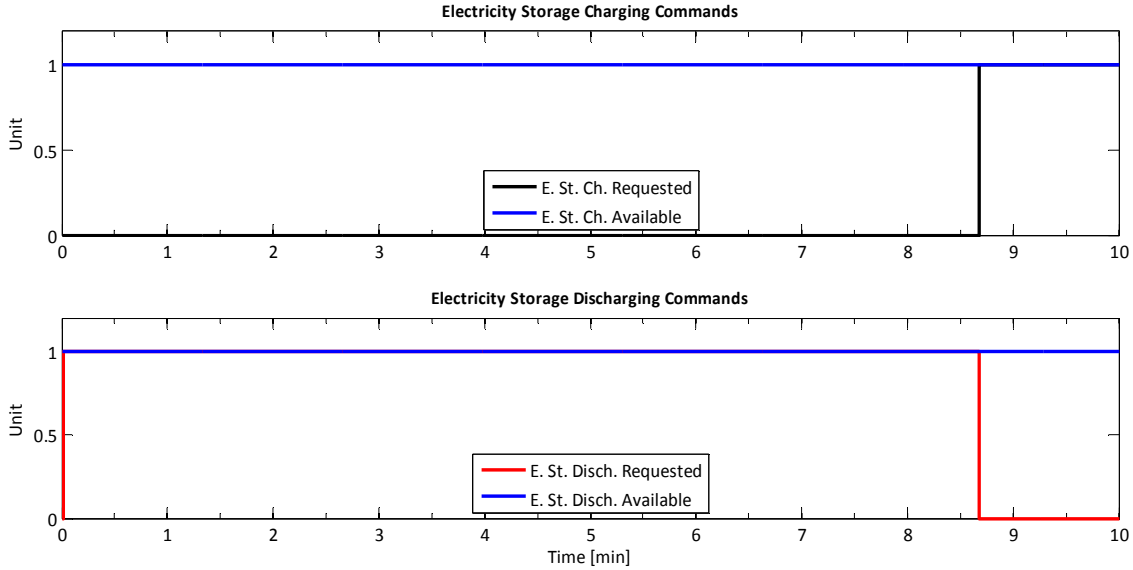

Figure 61 Status for Electricity storage operation

Electricity Storage operates only under command of the main control. Figure 60 shows the charging (negative region) and discharging (positive region) operation of the battery stack. The status of charge is within its allowed region during the entire simulation; therefore storage operation is available as shown in Figure 61. This figure also shows the required operation status.

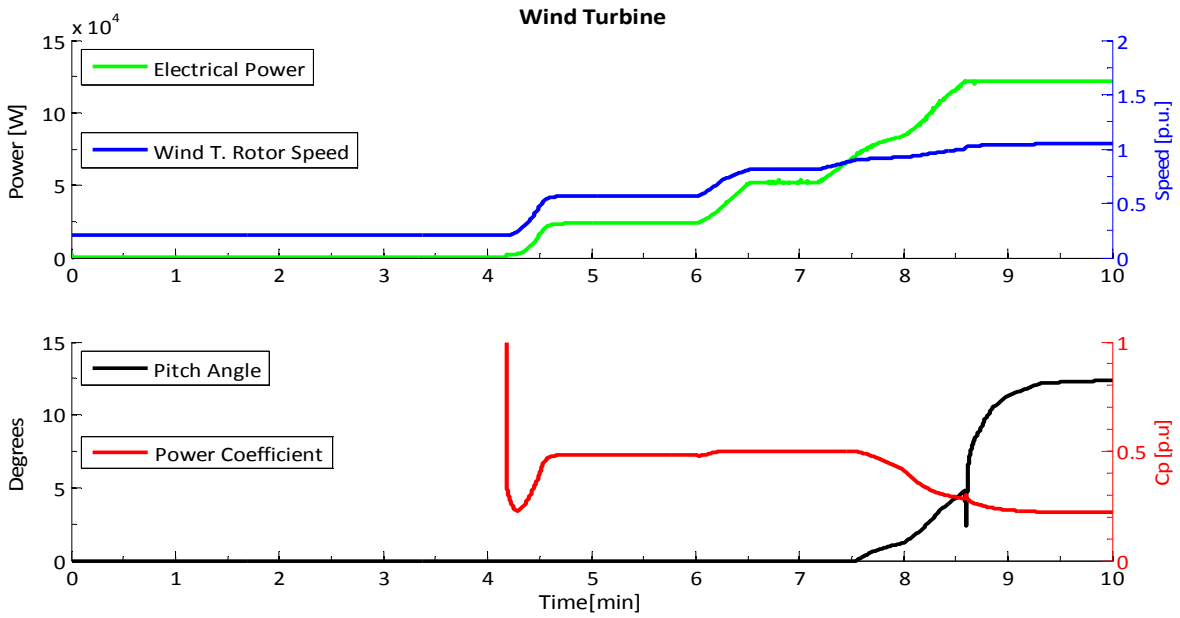

Figure 62 Wind Turbine operation data

The operation of the wind turbine is depicted in Figure 62. The turbine rotor speed increases following the increment of wind speed in order to obtain the optimal power generation. The power coefficient reaches its maximum at minute 4.5 and keeps it until later to fall after the wind turbine enters in its Zone 1C and later Zone 2 of operation (power limitation). Starting at minute 7.5 the wind turbine operates in Zone 1C, so the pitch angle increases smoothly. Roughly at minute 8.6 the nominal power of the turbine is reached and the pitch angle changes rapidly to maintain the nominal power.

Figure 63 shows the electrical system three phase voltage and currents. This example of DGS's electrical system operation shown that the designed controllers successfully managed the operation of each of the modeled DGS's components under large load changes.

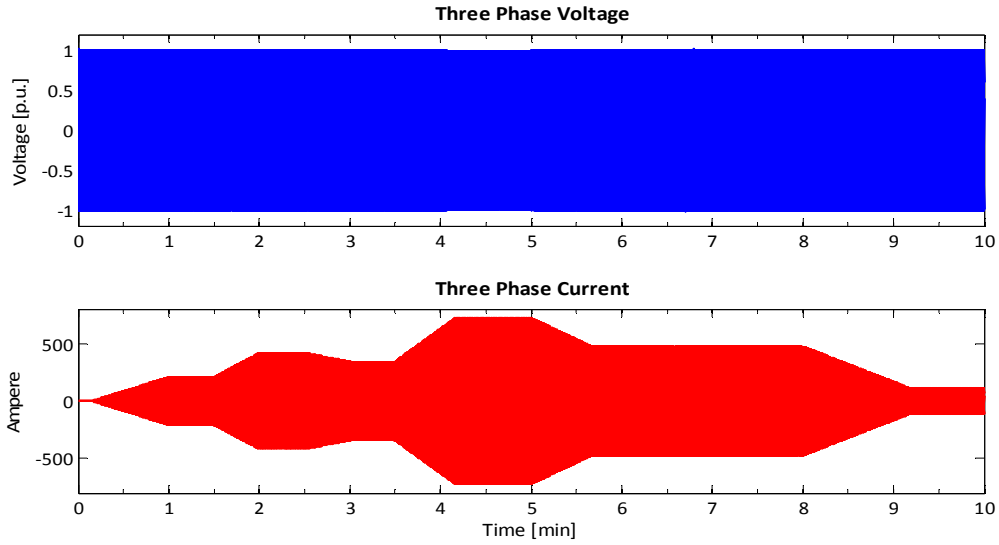

Figure 63 Electrical System, three phase voltage and current, and combined error for main control operation

Operation of DGS with a residential heat and electricity load pattern

In this simulation, the operation of the DGS resulted from using each unit's optimal dispatch and the load and wind speed patterns specified in Figure 45 and Figure 46 respectively.

Results of optimization problem for optimal dispatch of DGS's components

Using a one-day forecast for heat and electricity demand (based on Figure 45) and one-day wind power forecast (based on wind speed) the optimal dispatch of each dispatchable unit was computed applying the technique explained in Chapter 3 at intervals of 15 minutes. The solution of the minimization problem was obtained using the parameters listed in Table 6 and in earlier tables. The CHP's efficiencies for conversion of natural gas into electricity and heat are function of the amount of natural gas power as per equations Eq. 64 and Eq. 65 respectively.

$$\eta_{g-e}^{CHP-x} = A_{CHP-x} - B_{CHP-x} * P_{g\_CHP-x} \quad \textbf{Eq. 64}$$

$$\eta_{g-h}^{CHP-x} = C_{CHP-x} + D_{CHP-x} * P_{g\_CHP-x} \quad \textbf{Eq. 65}$$

Name	*Abbrev.*	*Value*	*unit*
Economic Objective Function, Coefficient a	a	0.0171	€/kW-h/15min
Economic Objective Function, Coefficient b	b	0.0001	€/kW-h^2/15min
Electrical Efficiency CHP_A & C, Coefficient A	$A_{CHP-A\&C}$	0.39	
Electrical Efficiency CHP_A & C, Coefficient B	$B_{CHP-A\&C}$	29.87	
Thermal Efficiency CHP_A & C, Coefficient C	$C_{CHP-A\&C}$	0.41	
Thermal Efficiency CHP_A & C, Coefficient D	$D_{CHP-A\&C}$	20.2	
Electrical Efficiency CHP_B, Coefficient A	A_{CHP-B}	0.337	
Electrical Efficiency CHP_B, Coefficient B	B_{CHP-B}	23.796	
Thermal Efficiency CHP_B, Coefficient C	C_{CHP-B}	0.426	
Thermal Efficiency CHP_B, Coefficient D	D_{CHP-B}	21.85	
Cost of Turn On Boiler		1	€
Cost of Turn On CHP_A		1.3	€
Cost of Turn On CHP_B		1.5	€
Cost of Turn On CHP_C		1.2	€
Minimum Time On Boiler		15	minutes
Minimum Time On CHP_A		60	minutes
Minimum Time On CHP_B		45	minutes
Minimum Time On CHP_C		60	minutes
Minimum Time Off Boiler		0	minutes
Minimum Time Off CHP_A		30	minutes
Minimum Time Off CHP_B		30	minutes
Minimum Time Off CHP_C		30	minutes

Table 6 Parameters used in the Optimization module

The reckoned optimal DGS's one-day operation cost is 5255 monetary units. If neither heat nor electricity storage would be part of the DGS, the optimized operation cost would have been 5510 monetary units. Meaning roughly 5% savings in operation costs when storage is included. The proposed optimal dispatch for the DGS's units is shown in Figure 64, Figure 65 and Figure 66.

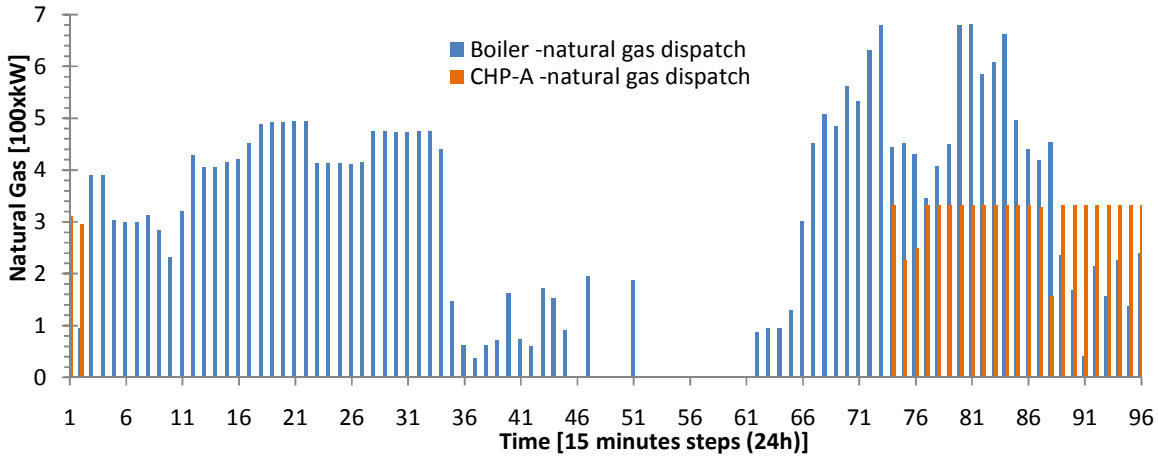

Figure 64 Scheduled optimal dispatch for Boiler and CHP-A

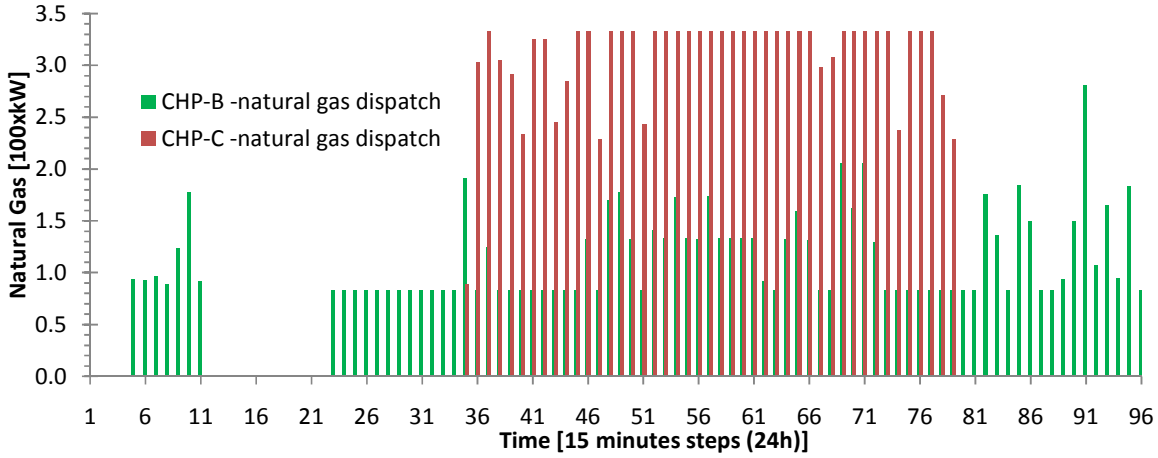

Figure 65 Scheduled optimal dispatch for CHP-B and CHP-C

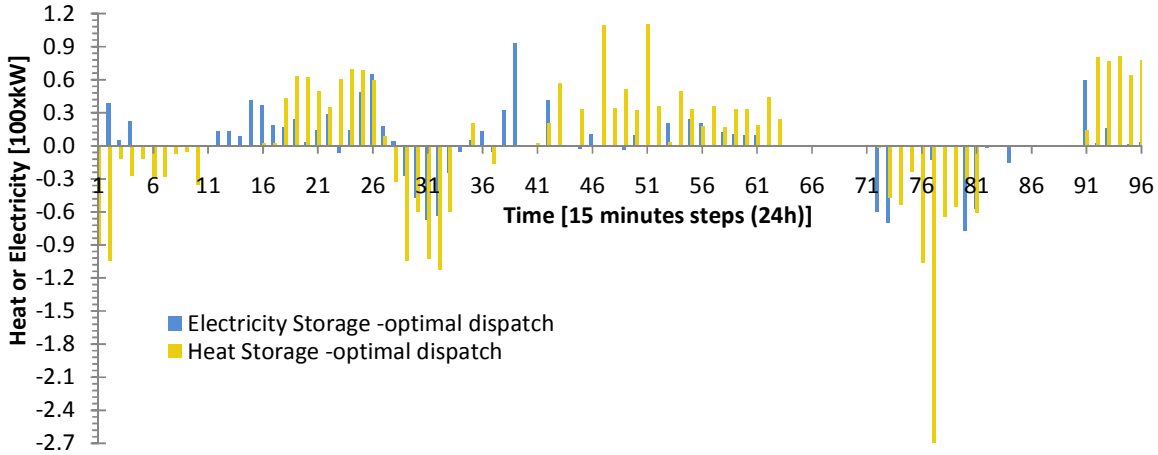

Figure 66 Scheduled optimal dispatch for Electricity Storage and Heat Storage

Results of simulating the DGS's operation with residential load patterns

The final test of the modeled DGS and its designed control strategy was performed using a residential load of heat and electricity. The model used the reckoned optimal dispatch values and the simulation was run for a 24 hours period. The participation factors of the CHPs and electricity storage now are not fixed and vary according to equations Eq. 61 and Eq. 62, with a minimum electricity storage pf of one tenth. Boiler and heat storage's participation factors follow equation Eq. 57.

Figure 67 and Figure 68 do show that the DGS's control strategy carries out properly its desired objectives. Frequency, indoor temperature and DHS hot line temperature are all kept within their desired values. It means that the demanded heat and electrical loads were satisfied successfully as they are depicted in Figure 69 and Figure 70. The large frequency excursions shown in Figure 67 and occurring at around hour 8 and around hour 6 are due to the fact that the main control decided to shutdown the only CHP working at those periods (CHP-B). Therefore, the frequency control is executed for the electricity storage along, which has a low participation factor, at that moment. This fact results in a longer time to restore the frequency to nominal.

The temperature at the DHS return line, shown in Figure 71, reaches a minimum value of 85 degrees Celsius when delivering the largest heat demand, which is within the design ranges. Figure 72 shows the heat losses at the pipelines, both in total account for 56kW, which were not considered when solving the optimal dispatch. Representing an extra economical burden.

The operation of CHP_A following its given optimal dispatch is shown in Figure 73 and Figure 74. This figure also shows that the actual natural gas consumption differs from the commanded one, this owing to the primary control, which performs through the CHP's governor. Figure 75 and Figure 76 show the operation of CHP_B, which has some differences with the reckoned optimal dispatch. An example is that it is commanded to turn off at some point in hour 8, although the optimal dispatch says to be on. It means that the main controller found that it was optimum to turn it off in order to satisfy the demand at that specific operation period.

The operation of the electricity storage and heat storage is depicted throughout Figure 80, Figure 81, Figure 82 and Figure 83. The power peak in the electricity storage at hours 6, 7 and 8 belong to internal simulation anomalies. The storages work within their limits, having the heat storage reaching close to its upper limit and being no able to discharge in some points e.g. between hours 8 and 9.

Figure 85 and Figure 86 show the participations factors for each of the controllable DGS's components. The participation factor of each DGS's component is designed to be reckoned according to its given optimal dispatch for each period of time. For example between hour 9 and 18 the participation factor for CHP-C is larger than for CHP-A because CHP-C's optimal dispatch values are larger. Thus, the on-line operation of the DGS attempts to follow the given optimal economic dispatch.

Finally, all the results shown in this simulation strongly support the achievement of a suitable control strategy for the operation of the modeled DGS's components.

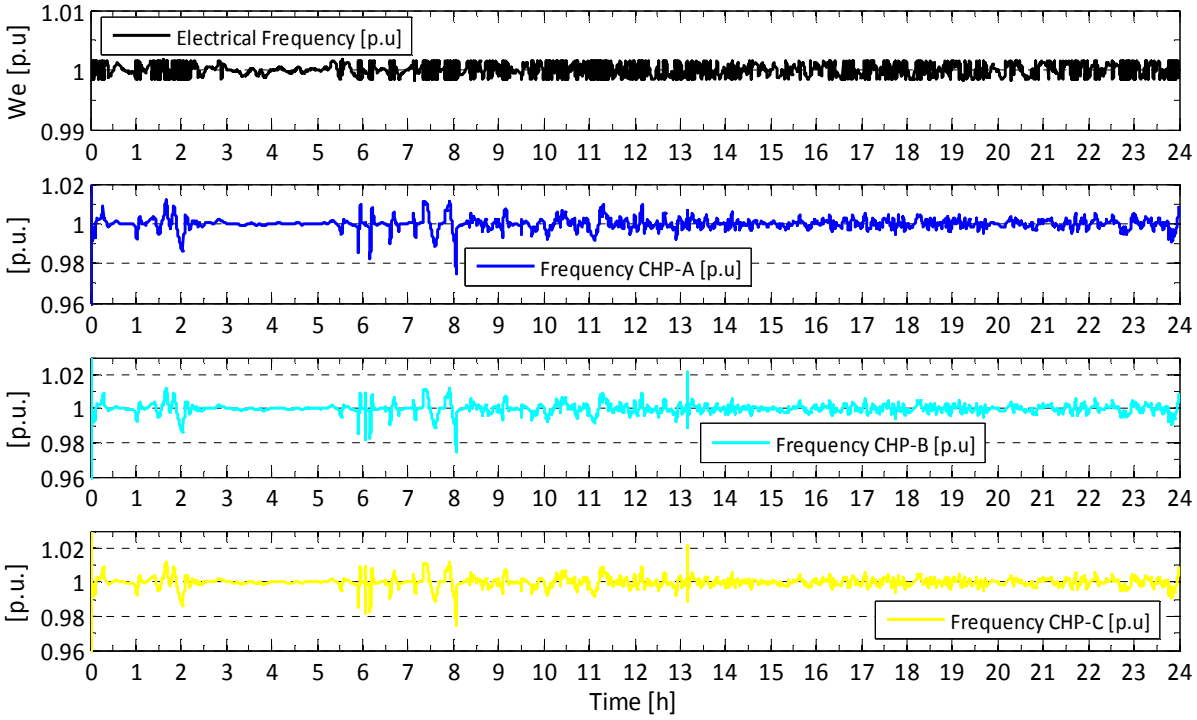

Figure 67 Frequency of the electrical system and rotor speed of CHPs

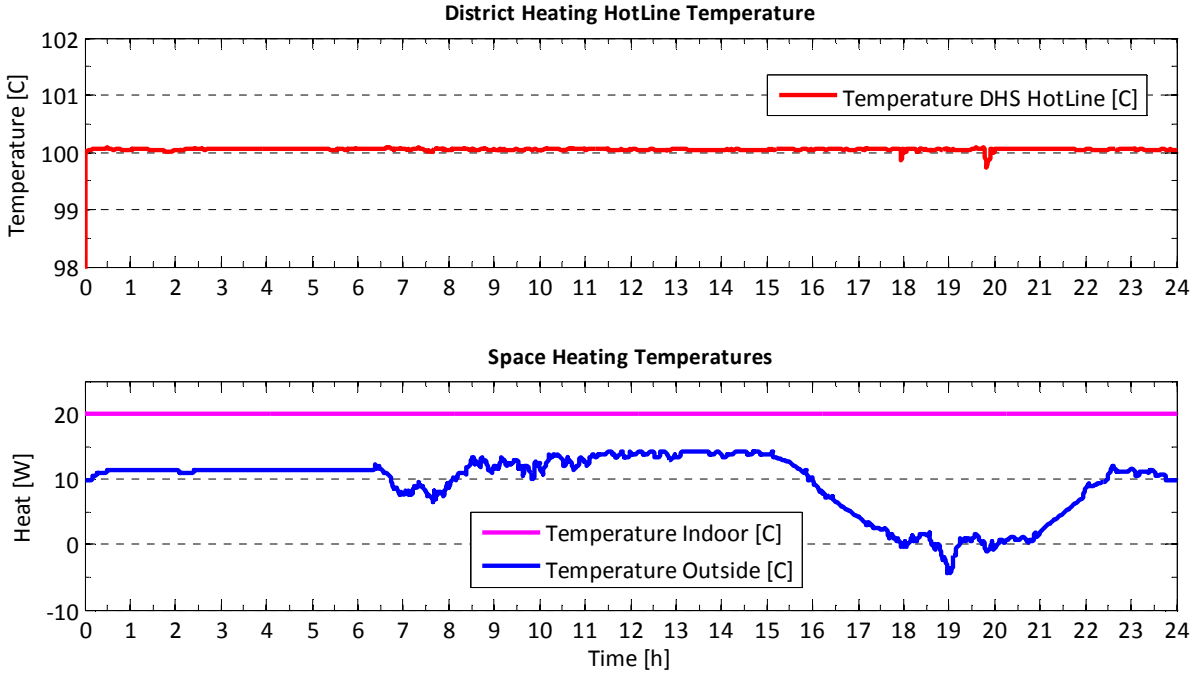

Figure 68 Main temperatures of the DGS for operation of the DHS and outdoor temperature

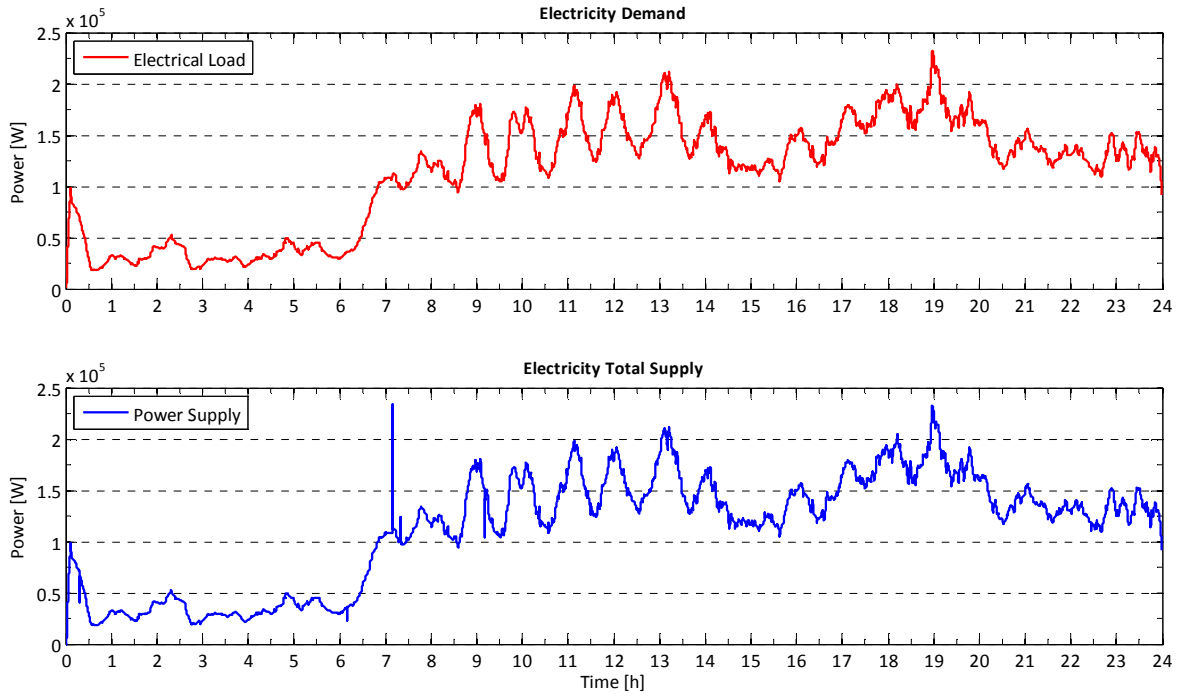

Figure 69 Electricity balance of the DGS

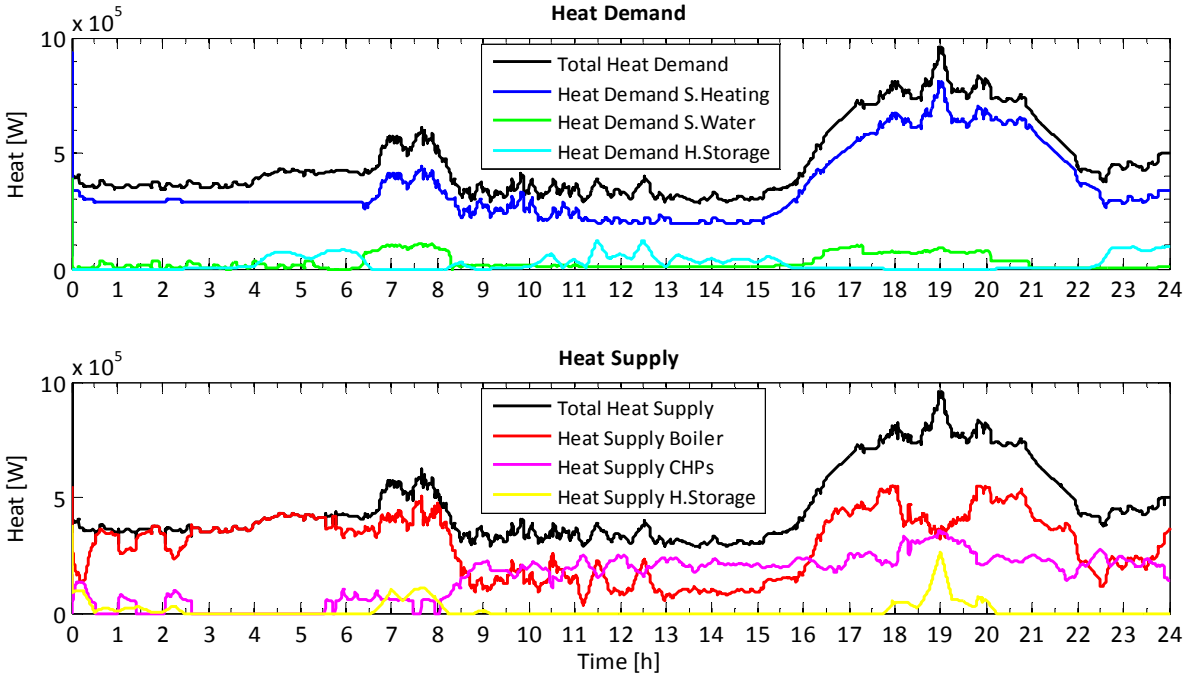

Figure 70 Heat Balance of the DGS with specific contribution of each actor

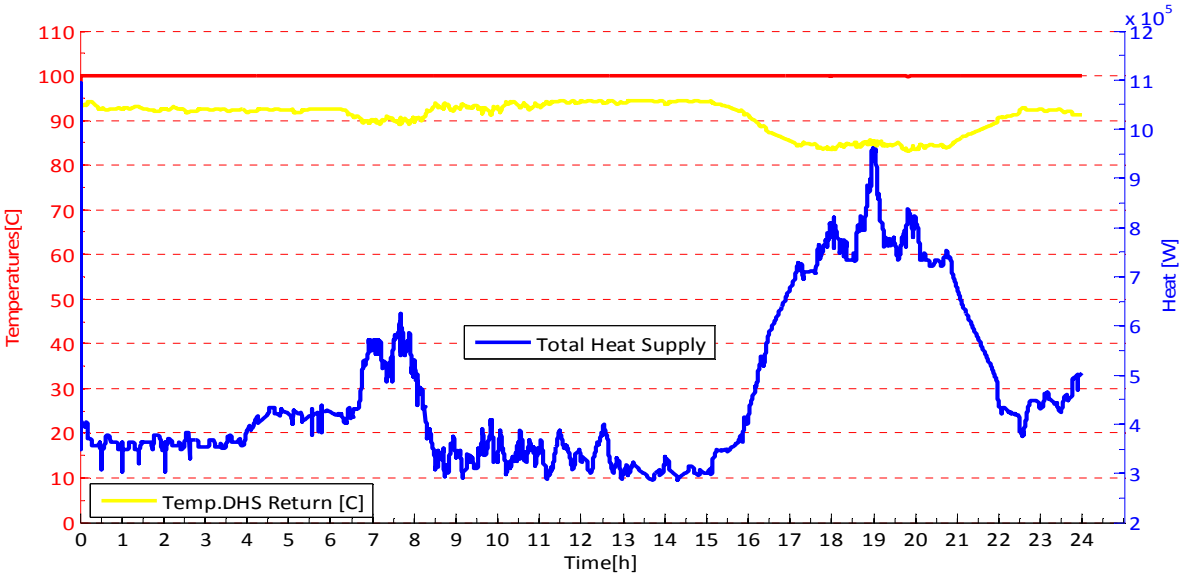

Figure 71 Temperatures of the water in DHS pipe lines, in red DHS Hot pipeline

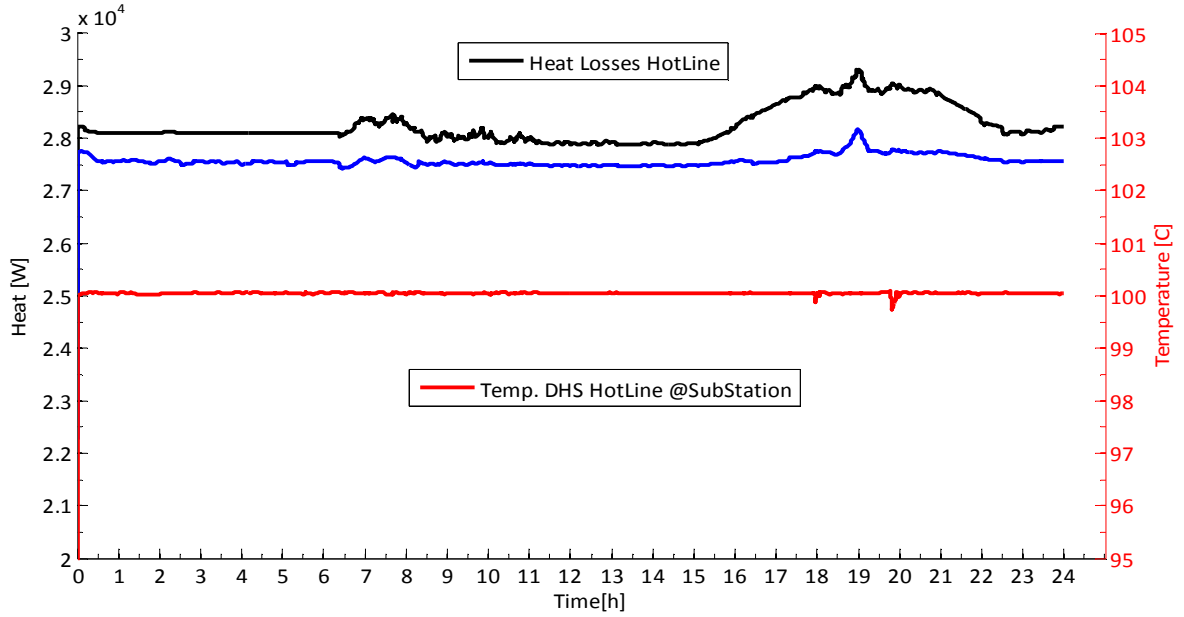

Figure 72 Pipeline heat losses, in blue losses in the return line

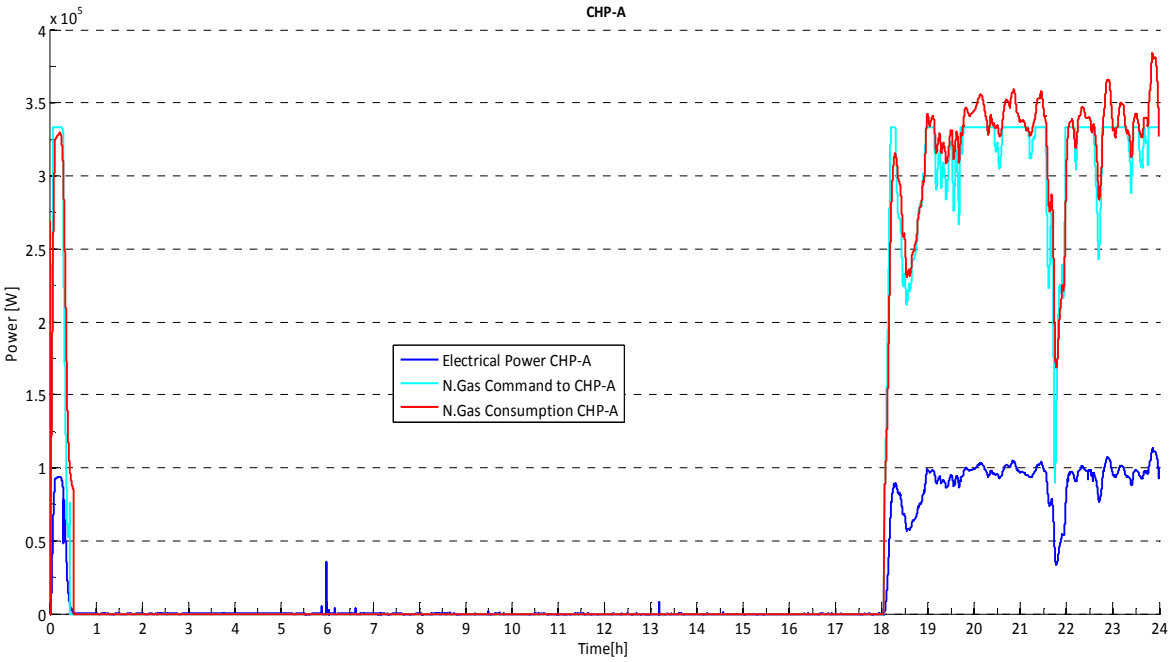

Figure 73 CHP_A natural gas consumption and its electricity production

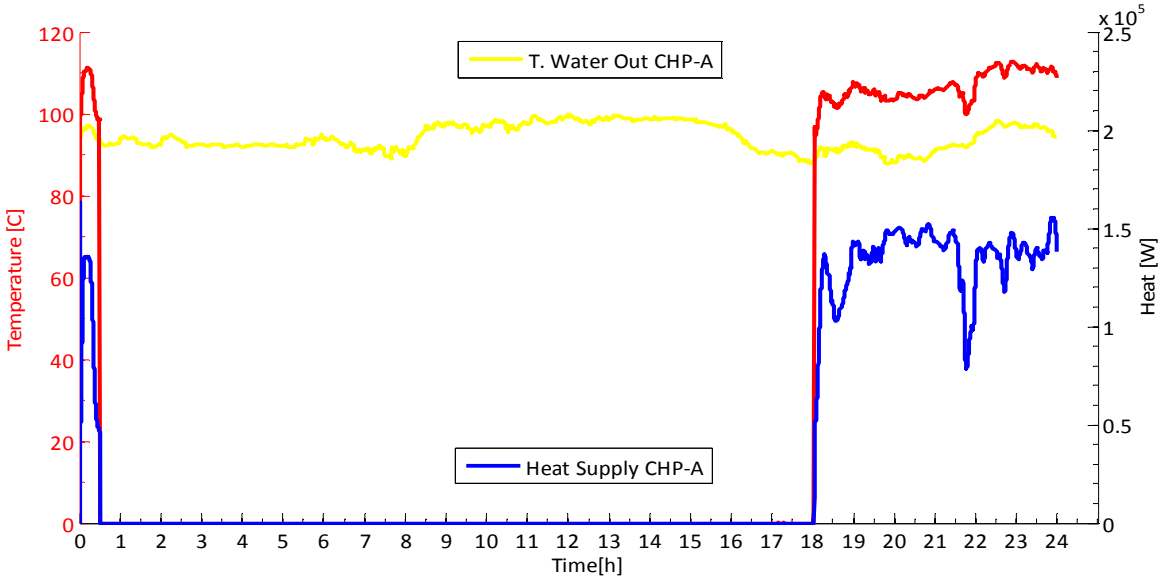

Figure 74 CHP_A heat supplied and water and exhaust gases (in red) temperatures leaving its HEx

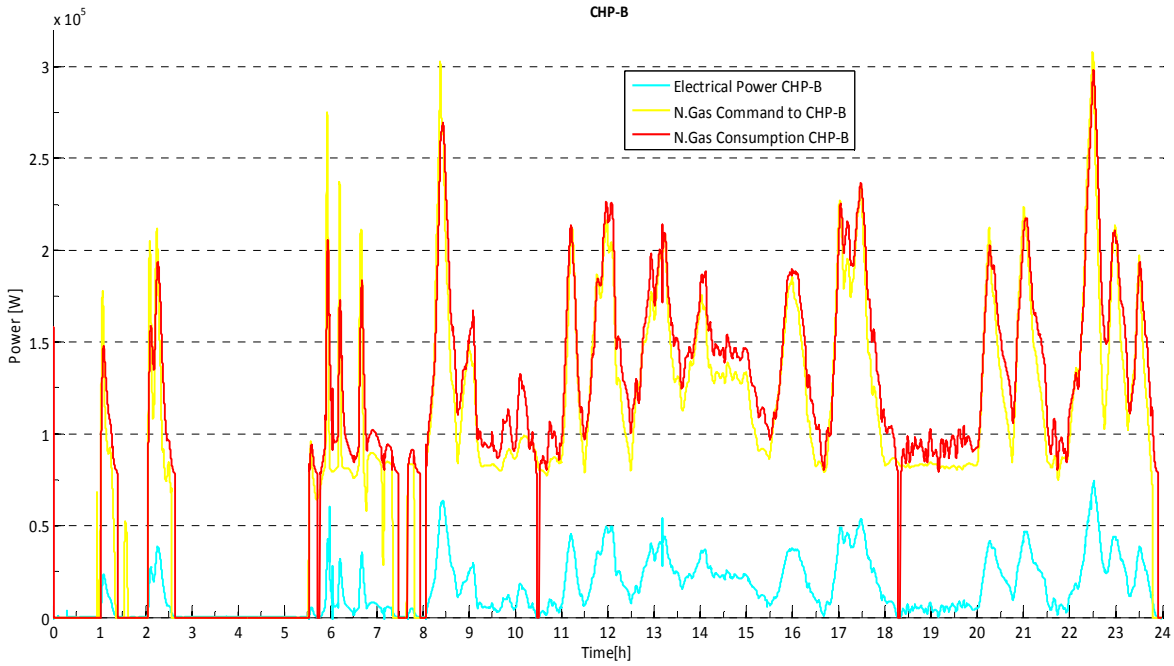

Figure 75 CHP_B natural gas consumption and its electricity production

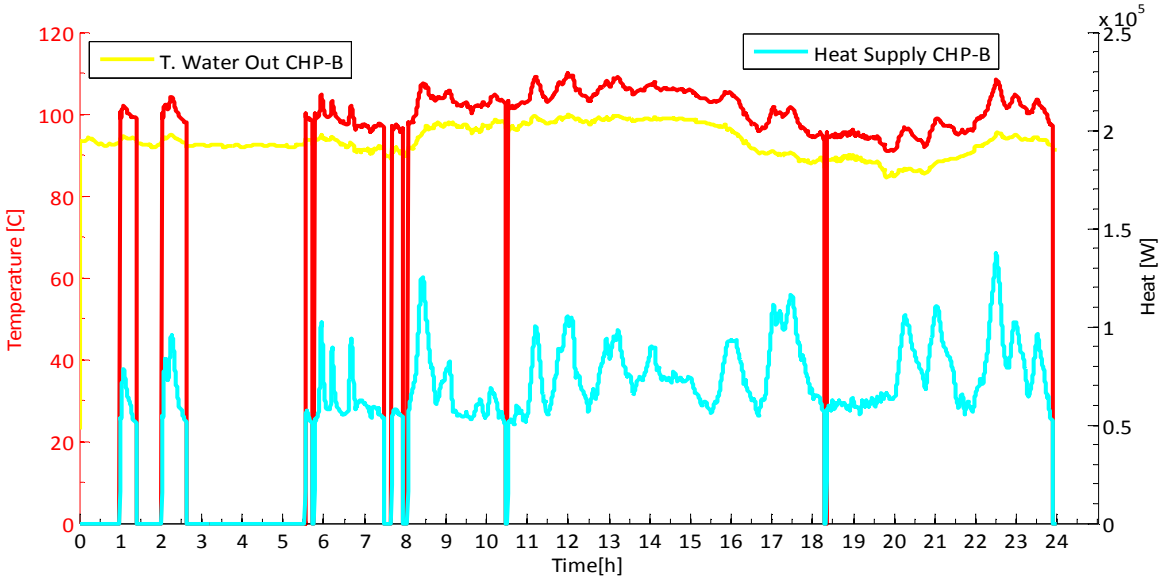

Figure 76 CHP_B heat supplied and water and exhaust gases (in red) temperatures leaving its HEx

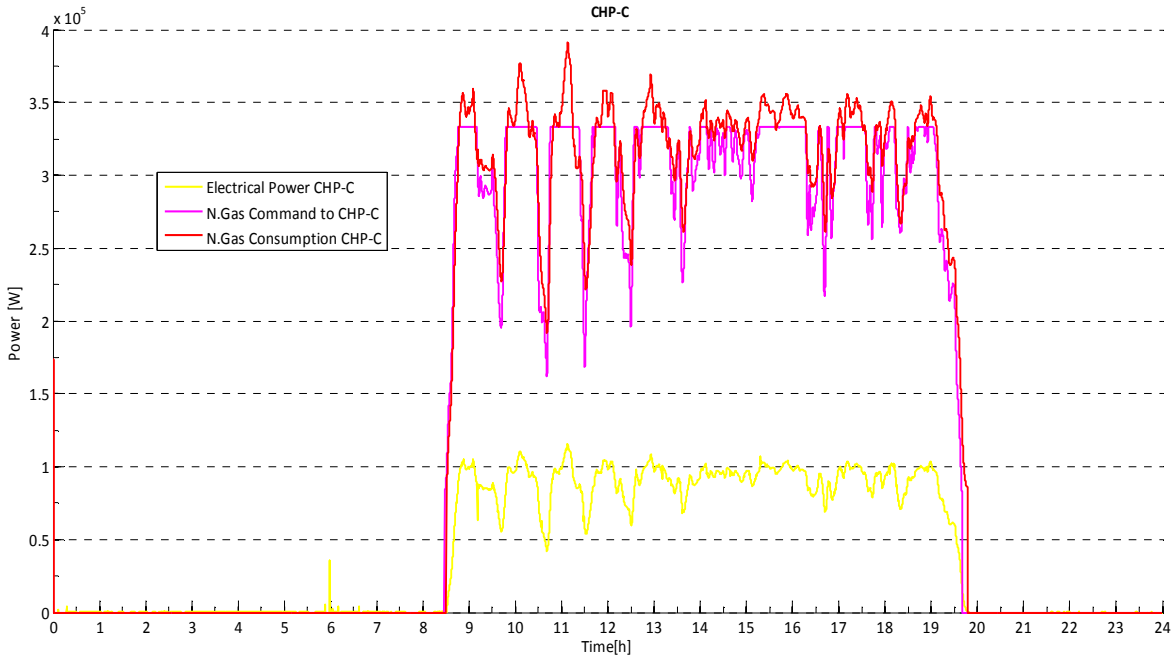

Figure 77 CHP_B natural gas consumption and its electricity production

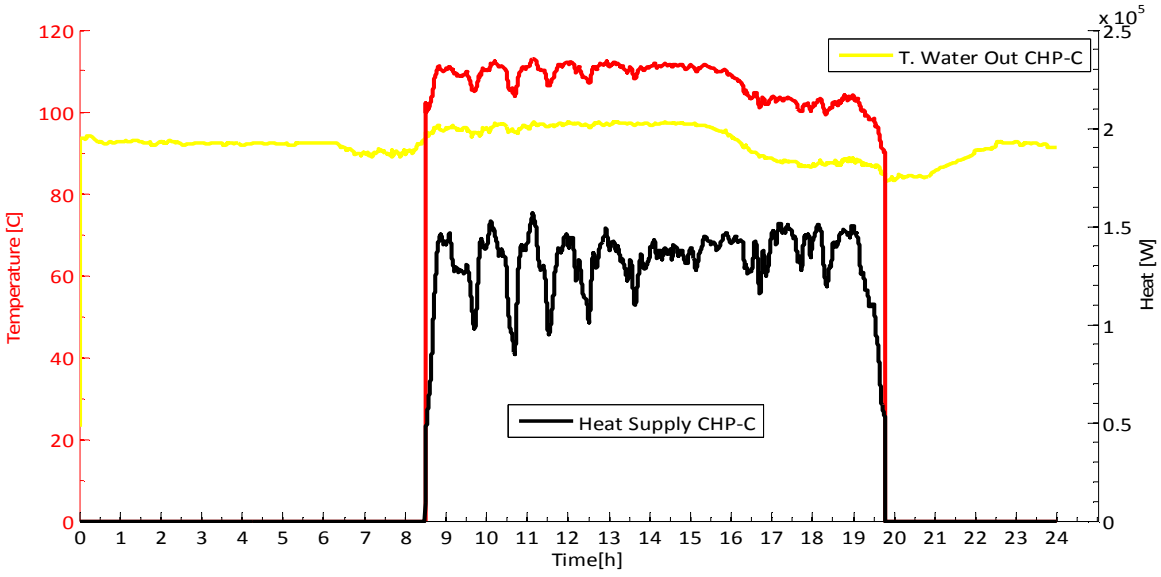

Figure 78 CHP_C heat supplied and water and exhaust gases (in red) temperatures leaving its HEx

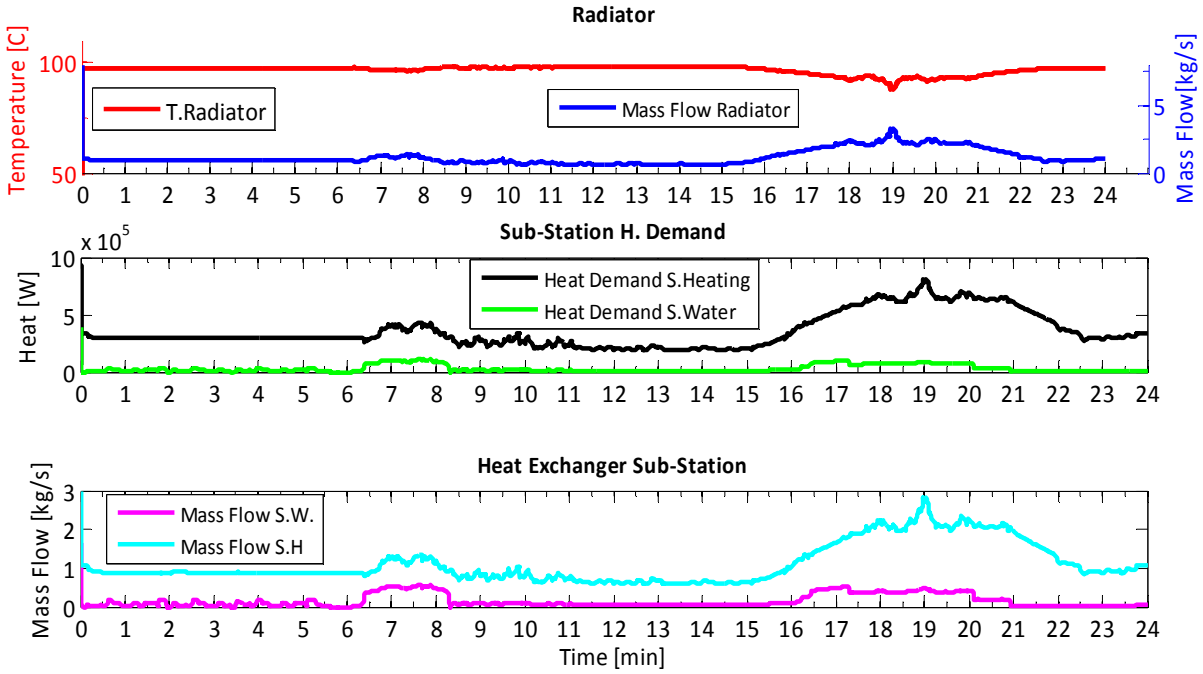

Figure 79 Sub-Station values

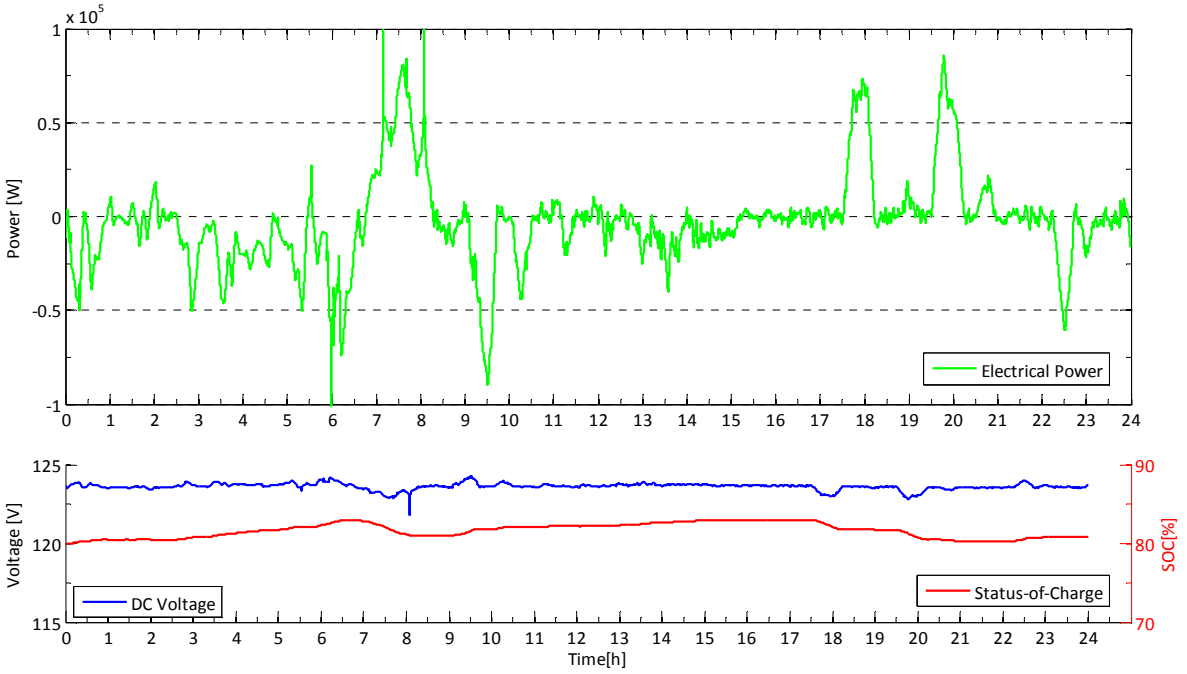

Figure 80 Electricity Storage Supplying (+) or Charging (-), its status of charge and terminal voltage

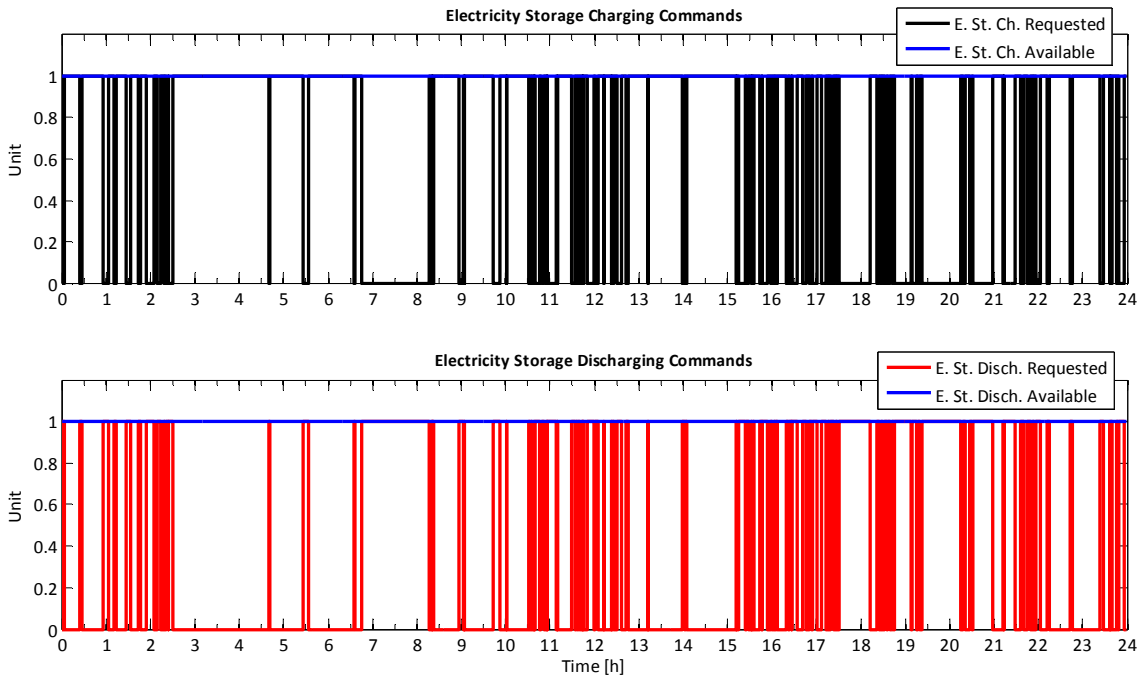

Figure 81 Electricity Storage request and availability status

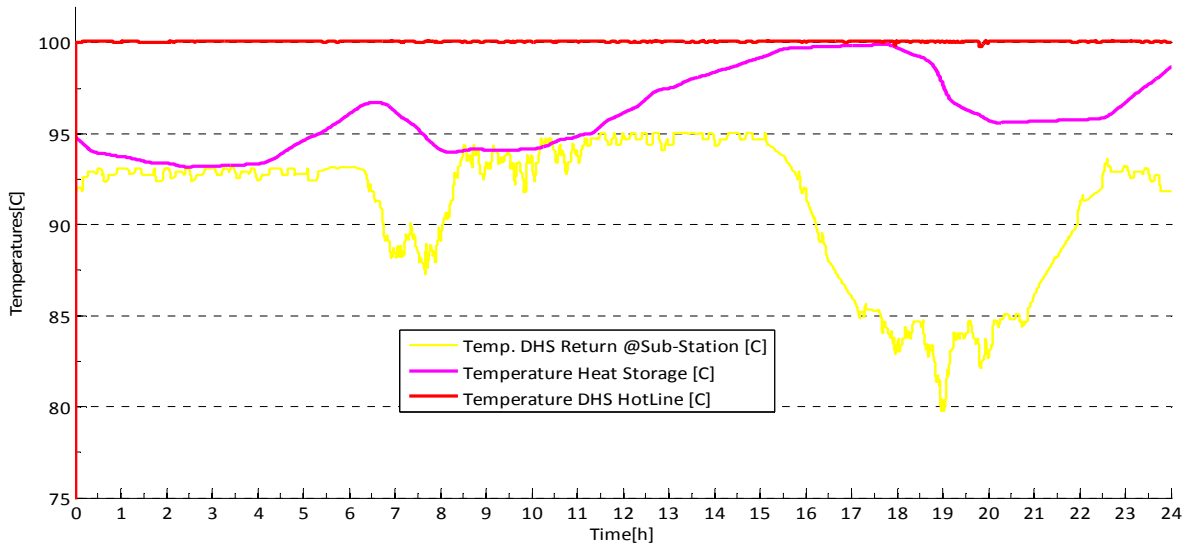

Figure 82 Heat Storage temperature of water and its operation limits

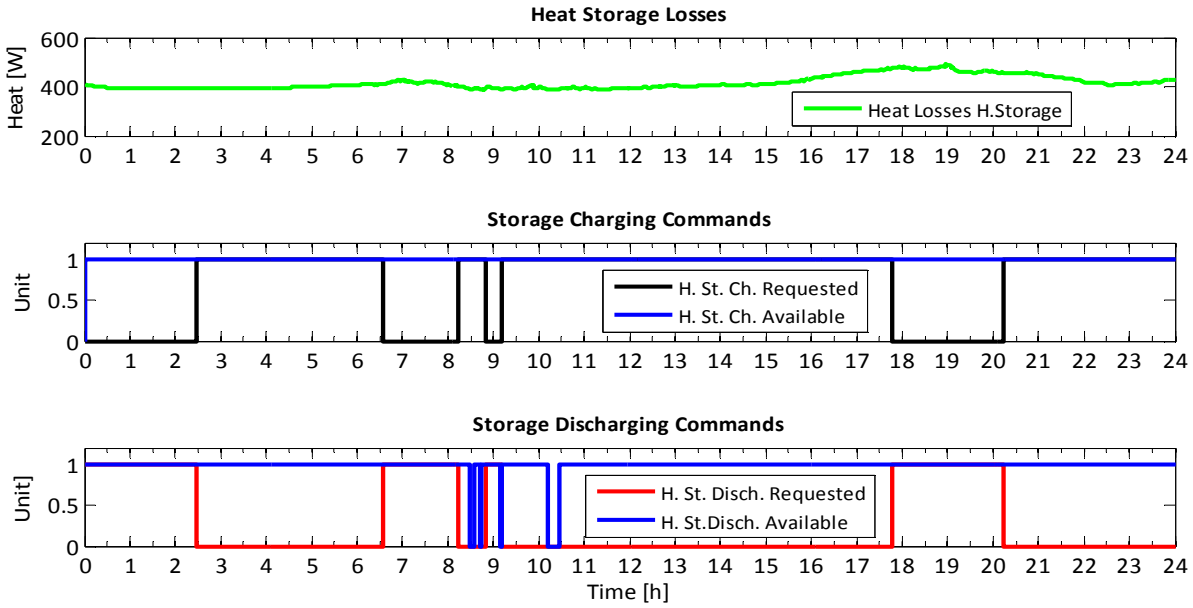

Figure 83 Heat Storage losses, availability and request

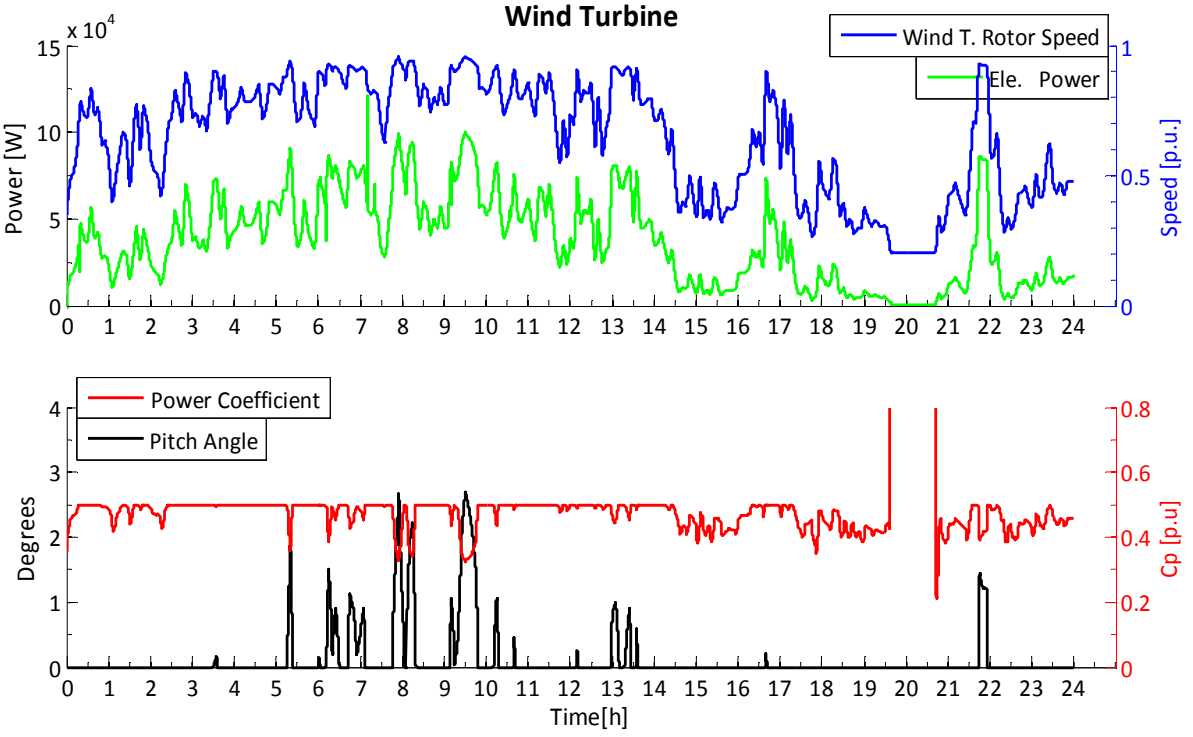

Figure 84 Wind Turbine electricity generation and operation variables

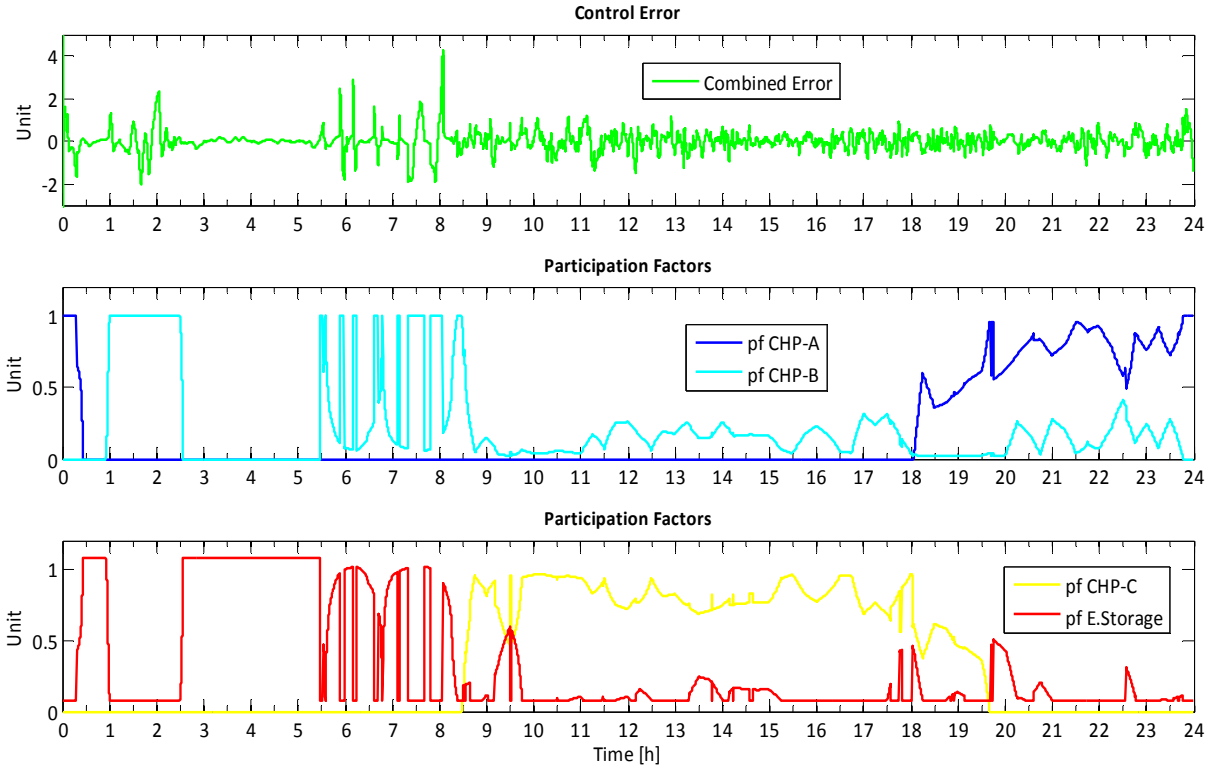

Figure 85 Combined error for the operation of main control-Electrical system and participation factors

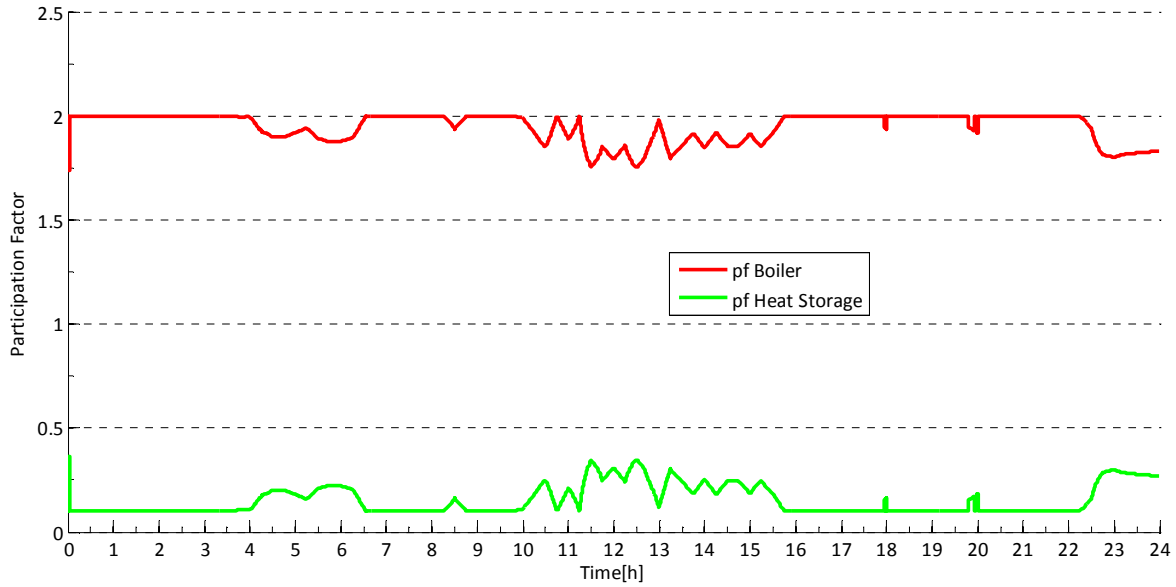

Figure 86 Participation factors of heat suppliers

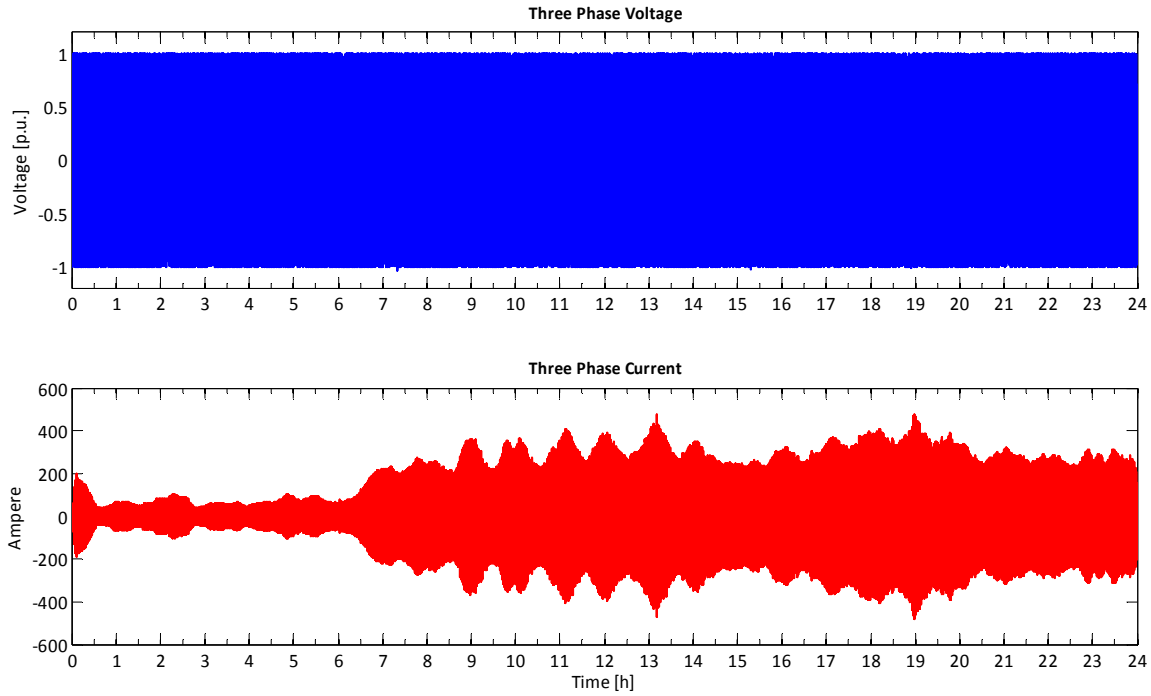

Figure 87 Three phase voltage and current of the DGS

CONCLUSIONS AND RECOMMENDATIONS

- The stated objective of this MSc thesis project was achieved. A suitable control strategy that satisfies the requirements of the distributed energy management system has been designed and tested. It shows proper performance when tested with its planned residential district level application. It also demonstrates sufficient control command when tested on large load variation patterns. Hence a stable, robust and appropriately simple control strategy was obtained.

- The joint-collaboration optimization technique for unit commitment of multi-energy carrier systems with storage, developed as part of this thesis project, presents an innovative approach to solve optimization problems when commitment of storage devices is analyzed. It shows good performance and keeps repeatability of the results.

- The implemented models of components of the distributed generation system properly characterize their intended level of modelling. Slow dynamics behaviour of the components is well represented with them. Frequency excursions due to load changes or new load dispatch are properly visualized. Temperature changes in the heat system are well described by the developed models for heat exchangers and heat losses.

- The operation of the studied autonomous distributed generation system under distributed energy management system control is according to what was expected for an islanded system. Frequency variations are larger than the corresponding to a grid connected system. And large overloads are a threat that only can be overcome with load shedding. Nevertheless, the design control strategy is quite applicable for normal operation of the system and for example load shedding can be implemented without altering the modular structure of the designed main controller.

- The developed simulation platform with CHP, wind turbine and battery stack models in the electrical system, and hot water heating boiler and hot water storage tank in the heat system can be used to simulate the behaviour of multi-energy systems with other configurations, given its modular structure. Additionally, the control logic can be modified to incorporate different trends, for example controlling of the dispatch of wind energy when it is bought from a third party.

- In order to create a more detailed simulation platform for electrical and district heating systems, the developed DGS model should be extended to operate also regarding reactive power and pipelines pressures. Therefore additional control techniques and monitoring have to be incorporated into the main controller.

- Regarding the current models for boiler and heat storage, a better characterization of them can be achieved by including the modelling of their heat exchangers. It can be done by adapting the developed heat exchanger for CHP or for DHS sub-station. Nevertheless, the complexity of the model will increase and its suitable implementation at model level and at the control level should be analyzed thoroughly.

- An interesting work to follow is to analyze the behaviour of the DGS when a multi-objective energy dispatch is aimed. The optimization technique should be adapted to cope with multi-objective functions and the main control logic as well.

- The developed simulation platform as part of this thesis project is quite adaptable and other components can be added without too much effort. For example the analysis of operation of a DGS that includes a fuel cell can be obtained having this simulation platform as base.

REFERENCES

[1] M. Geidl, *et al.*, "Energy hubs for the future," *Power and Energy Magazine, IEEE,* vol. 5, pp. 24-30, 2007.

[2] M. Geidl, *et al.*, "A greenfield approach for future power systems," presented at the Cigre, Paris, 2006.

[3] M. Geidl, "Integrated Modeling and Optimization of Multi-Carrier Energy Systems," PhD dissertation, ETH Zurich, Zurich, 2007.

[4] M. Geidl and G. Andersson, "Optimal Power Flow of Multiple Energy Carriers," *Power Systems, IEEE Transactions on,* vol. 22, pp. 145-155, 2007.

[5] M. Geidl and G. Andersson, "Optimal Coupling of Energy Infrastructures," in *Power Tech, 2007 IEEE Lausanne*, 2007, pp. 1398-1403.

[6] A. J. Wood and B. F. Wollenberg, *Power generation, operation, and control*, 2nd ed. New York: J. Wiley & Sons, 1996.

[7] L. Ramirez-Elizondo and G. Paap, "Unit Commitment in Multiple Energy Carrier Systems," in *41st North American Power Symposium*, Starkville, Mississippi, 2009.

[8] R. a. A.-C. E. I. American Society of Heating, *ASHRAE Handbook - Heating, ventilating, and Air-conditioning systems and Equipment*. Atlanta, 2008.

[9] I. Dincer and A. Hepbasli, "District Energy Systems," in *Encyclopedia of Energy Engineering and Technology - 3 Volume Set (Print Version)*, ed: CRC Press, 2007, pp. 316-331.

[10] M. D. Ilic and J. Zaborszky, *Dynamics and control of large electric power systems*. New York: Wiley, 2000.

[11] B. Avramovic and L. H. Fink, "Energy management systems and control of FACTS," *International Journal of Electrical Power & Energy Systems,* vol. 17, pp. 195-198, 1995.

[12] Z. Yingyuan, *et al.*, "Study of energy management system for distributed generation systems," in *Electric Utility Deregulation and Restructuring and Power Technologies, 2008. DRPT 2008. Third International Conference on*, 2008, pp. 2465-2469.

[13] M. Hable, *et al.*, "An integral energy management for decentralized power systems," presented at the 17th International Conference on Electricity Distribution, CIRED, Barcelona, 2003.

[14] W. Schellong, "Integrated energy management in distributed systems," in *Power Electronics, Electrical Drives, Automation and Motion, 2006. SPEEDAM 2006. International Symposium on*, 2006, pp. 492-496.

[15] A. Dowrueng, *et al.*, "Decentralised Energy Management System with comprehension of fluctuated renewable energy resources," in *Clean Electrical Power, 2009 International Conference on*, 2009, pp. 316-319.

[16] H. Muller, *et al.*, "Studies of distributed energy supply systems using an innovative energy management system," in *Power Industry Computer Applications, 2001. PICA 2001. Innovative*

Computing for Power - Electric Energy Meets the Market. 22nd IEEE Power Engineering Society International Conference on, 2001, pp. 87-90.

[17] M. Arnold*, et al.*, "Model-based predictive control applied to multi-carrier energy systems," in *Power & Energy Society General Meeting, 2009. PES '09. IEEE*, 2009, pp. 1-8.

[18] S. Brini*, et al.*, "Economic Dispatch for Power System Included Wind and Solar Thermal Energy," *Leonardo Journal of Sciences (LJS),* vol. 8, pp. 204-220, 2009.

[19] C. Changsong*, et al.*, "Research of energy management system of distributed generation based on power forecasting," in *Electrical Machines and Systems, 2008. ICEMS 2008. International Conference on*, 2008, pp. 2734-2737.

[20] A. Engler and N. Soultanis, "Droop control in LV-grids," in *Future Power Systems, 2005 International Conference on*, 2005, pp. 6 pp.-6.

[21] N. D. Hatziargyriou*, et al.*, "Management of microgrids in market environment," in *Future Power Systems, 2005 International Conference on*, 2005, pp. 7 pp.-7.

[22] J. Hetzer*, et al.*, "An Economic Dispatch Model Incorporating Wind Power," *Energy Conversion, IEEE Transactions on,* vol. 23, pp. 603-611, 2008.

[23] T. Hiyama and K. Kitabayashi, "Neural network based estimation of maximum power generation from PV module using environmental information," *Energy Conversion, IEEE Transactions on,* vol. 12, pp. 241-247, 1997.

[24] F. Katiraei and M. R. Iravani, "Power Management Strategies for a Microgrid With Multiple Distributed Generation Units," *Power Systems, IEEE Transactions on,* vol. 21, pp. 1821-1831, 2006.

[25] J. A. P. Lopes*, et al.*, "Defining control strategies for MicroGrids islanded operation," *Power Systems, IEEE Transactions on,* vol. 21, pp. 916-924, 2006.

[26] V. Miranda*, et al.*, "Better prediction models for renewables by training with entropy concepts," in *Power Engineering Society General Meeting, 2006. IEEE*, 2006, p. 2 pp.

[27] E. Ortjohann*, et al.*, "A hierarchy control strategy of distributed generation systems," in *Clean Electrical Power, 2009 International Conference on*, 2009, pp. 310-315.

[28] Warsono*, et al.*, "Economic Load Dispatch for a power system with renewable energy using Direct Search Method," in *Universities Power Engineering Conference, 2007. UPEC 2007. 42nd International*, 2007, pp. 1228-1233.

[29] Warsono*, et al.*, "Economic Load Dispatch Optimization of Renewable Energy in Power System Using Genetic Algorithm," in *Power Tech, 2007 IEEE Lausanne*, 2007, pp. 2174-2179.

[30] R. L. Welch*, et al.*, "Comparison of feedforward and feedback neural network architectures for short term wind speed prediction," in *Neural Networks, 2009. IJCNN 2009. International Joint Conference on*, 2009, pp. 3335-3340.

[31] Y. Zilong*, et al.*, "Design of energy management system in distributed power station," in *Sustainable Power Generation and Supply, 2009. SUPERGEN '09. International Conference on*, 2009, pp. 1-5.

[32] L. Ramirez-Elizondo*, et al.*, "A technique for unit commitment in multiple energy carrier systems with storage," in *Environment and Electrical Engineering (EEEIC), 2010 9th International Conference on*, 2010, pp. 106-109.

[33] P. Breeze, *Power Generation Technologies*, First ed. Great Britain: Elsevier, 2005.

[34] P. A. Pilavachi, "Mini- and micro-gas turbines for combined heat and power," *Applied Thermal Engineering,* vol. 22, pp. 2003-2014, 2002.

[35] CBS, "Increased application of CHP systems," S. Netherlands, Ed., ed. The Hague: CBS, 2009.

[36] G. W. Massey, *Essentials of distributed generation systems*, First ed. Sudbury, Massachusetts: Jones and Bartlett, 2010.

[37] Y. Zhu and K. Tomsovic, "Development of models for analyzing the load-following performance of microturbines and fuel cells," *Electric Power Systems Research,* vol. 62, pp. 1-11, 2002.

[38] P. Kiameh, *Power generation handbook*. New York: McGraw-Hill, 2003.

[39] D. Lane, "Brayton Cycle: The Ideal Cycle for Gas-Turbine Engines in Relation to Power Plants," ed. Reno: University of Nevada, 2001.
[40] A. M. Y. Razak, "Gas turbine combustion," in *Industrial Gas Turbines*, ed Cambridge, England: CRC Press, 2007.
[41] W. I. Rowen, "Simplified Mathematical Representations of Heavy-Duty Gas Turbines," *Journal of Engineering for Power,* vol. 105, pp. 865-869, 1983.
[42] L. N. Hannett*, et al.*, "A governor/turbine model for a twin-shaft combustion turbine," *Power Systems, IEEE Transactions on,* vol. 10, pp. 133-140, 1995.
[43] L. N. Hannett and A. H. Khan, "Combustion turbine dynamic model validation from tests," *Power Systems, IEEE Transactions on,* vol. 8, pp. 152-158, 1993.
[44] L. M. Hajagos and G. R. Berube, "Utility experience with gas turbine testing and modeling," in *Power Engineering Society Winter Meeting, 2001. IEEE*, 2001, pp. 671-677 vol.2.
[45] A. K. Saha*, et al.*, "Study of microturbine models in islanded and grid-connected mode," in *Universities Power Engineering Conference, 2008. UPEC 2008. 43rd International*, 2008, pp. 1-5.
[46] S. R. Guda*, et al.*, "A Simulink-based microturbine model for distributed generation studies," in *Power Symposium, 2005. Proceedings of the 37th Annual North American*, 2005, pp. 269-274.
[47] R. C. Dorf*, et al.*, *Modern Control Systems*: Addison-Wesley Longman Publishing Co., Inc., 1997.
[48] L. McLeister, "PID Control," ed. Fort Collins, USA: Woodward, 1992.
[49] G. Ellis, *Control System Design Guide: Using Your Computer to Understand and Diagnose Feedback Controllers*: Elsevier Science Inc., 2003.
[50] P. Krause*, et al.*, *Analysis of electric machinery and drive systems*, 2nd ed. New York: Wiley-Interscience, 2002.
[51] MathWorks™, "MatLab®/Simulink®," R2008b ed. USA, 2008.
[52] WWEA, "World Wind Energy Report 2009," World Wind Energy Association, Bonn Germany 2010.
[53] J. F. Manwell, *Wind Energy Explained*, 1st ed. Great Britain: John Wiley & Sons Ltd, 2002.
[54] A. Hansen*, et al.*, "Overall control strategy of variable speed doubly-fed induction generator wind turbine," in *Nordic Wind Power Conference*, Gothenburg, Sweden, 2004.
[55] J. G. Slootweg*, et al.*, "General model for representing variable speed wind turbines in power system dynamics simulations," *Power Systems, IEEE Transactions on,* vol. 18, pp. 144-151, 2003.
[56] Enercon. (2010, Jun 1st). *Enercon Wind Turbines Product Overview Booklet*. Available: http://www.enercon.de/en/_home.htm
[57] S. Heier and R. Waddington, *Grid integration of wind energy conversion systems*. Chichester: Wiley, 2006.
[58] A. G. Abo-Khalil and L. Dong-Choon, "Dynamic Modeling and Control of Wind Turbines for Grid-Connected Wind Generation System," in *Power Electronics Specialists Conference, 2006. PESC '06. 37th IEEE*, 2006, pp. 1-6.
[59] Sunnyway. (2010, June 20th). *Datasheet SWE122000 battery*. Available: http://www.sunnyway-battery.com/Pro_Img/20097291061137455.pdf
[60] W. J. Beek and K. M. K. Muttzall, *Transport Phenomena*, second ed. Chichester, England: John Wiley & Sons Ltd, 1999.
[61] L. Haiyan and P. Valdimarsson, "District heating modelling and simulation," in *Thirty-Fourth Workshop on Geothermal Reservoir Engineering*, Stanford, USA, 2009.
[62] T. Persson and J. Wollerstrand, "Dynamic modelling of a domestic hot water system using Simulink," in *45th Conference on Simulation and Modelling, SIMS*, Copenhagen, Denmark, 2004.

[63] L. Li and M. Zaheeruddin, "A control strategy for energy optimal operation of a direct district heating system," *International Journal of Energy Research,* vol. 28, pp. 597-612, 2004.
[64] I. Dincer*, et al.*, "Performance analyses of sensible heat storage systems for thermal applications," *International Journal of Energy Research,* vol. 21, pp. 1157-1171, 1997.
[65] M. E. Flynn and M. J. O'Malley, "A drum boiler model for long term power system dynamic simulation," *Power Systems, IEEE Transactions on,* vol. 14, pp. 209-217, 1999.
[66] V. Ganapathy, *Industrial Boilers and Heat Recovery Steam Generators*. New York, USA: Marcel Dekker, Inc., 2003.
[67] A. G. Blockh, *Heat Transfer in Steam Boiler Furnaces*. Leningrad, USSR: Hemisphere Publishing Corporation, 1988.
[68] The_Engineering_ToolBox. (2010, April 2nd). *Tools and Basic Information for Design, Engineering and Construction of Technical Applications.* Available: http://www.engineeringtoolbox.com/thermodynamics-t_36.html
[69] Colonial. (2010, June 15th). *Pumbling and Heating supply*. Available: http://www.colonialsupply.com/resources/radiator.htm
[70] APV-SPX, "APV Heat Transfer Handbook," in *A History of Excellence*, ed. Getzville, USA: SPX Corporation, 2008.
[71] PPSL_District_Energy, "Datasheets and Guide Specification for Logstor Ror pre-insulated pipe system," ed. Herfordshire, UK: PPSL, 2008.

APPENDIX

MatLab/SIMULINK block diagrams of some models and main control

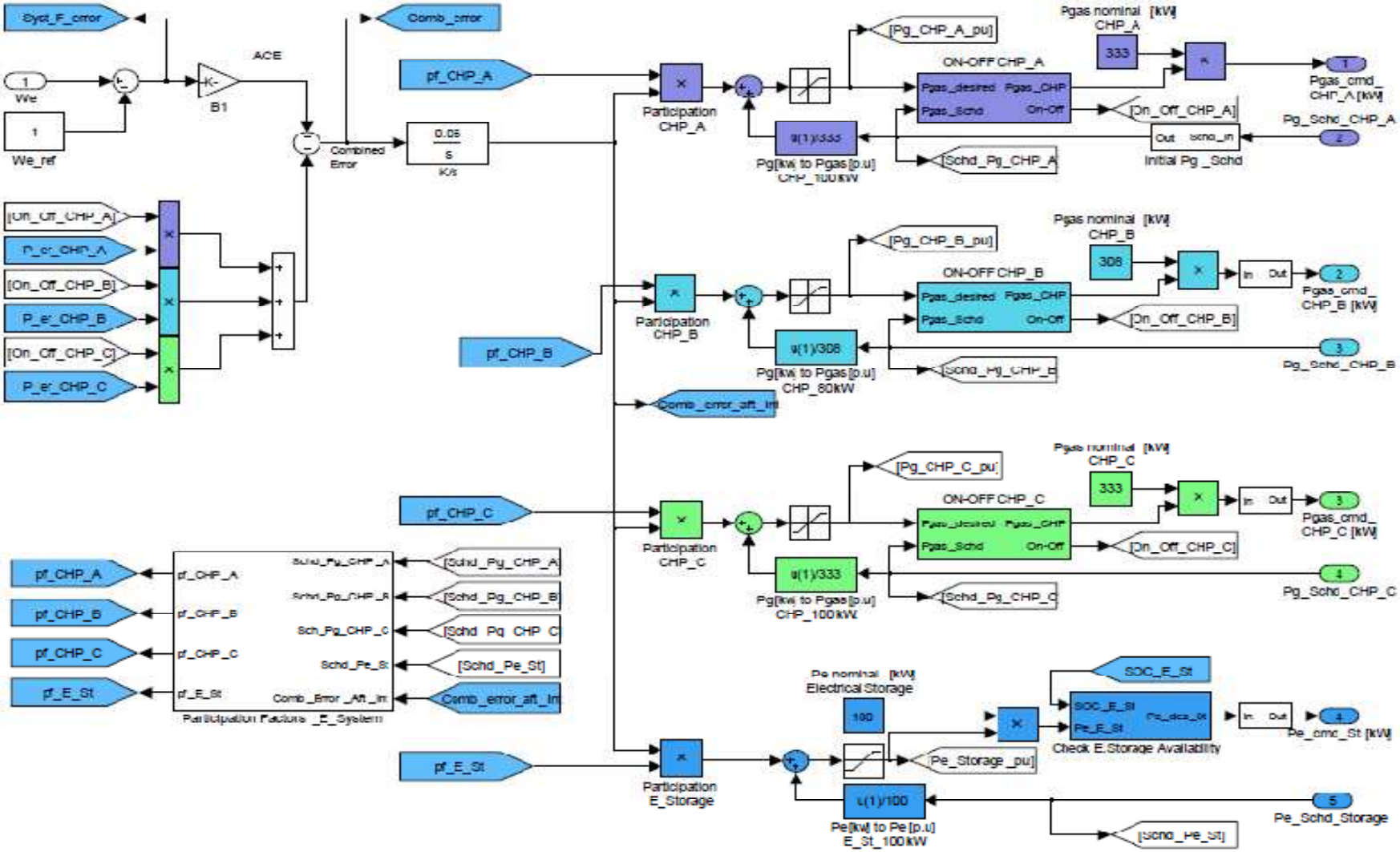

Block diagram of main control –Electrical system

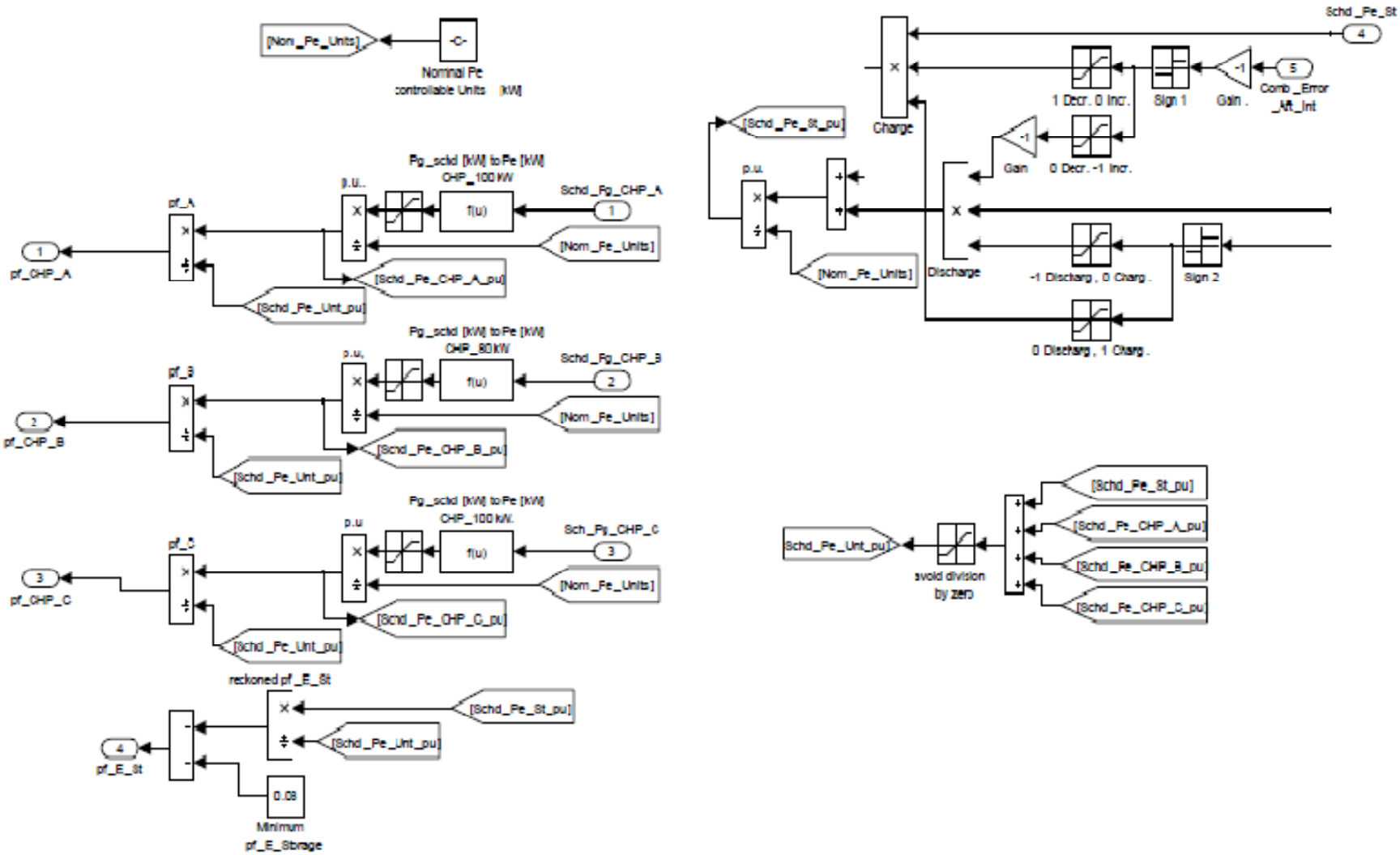

Block diagram of participation factors –Electrical system

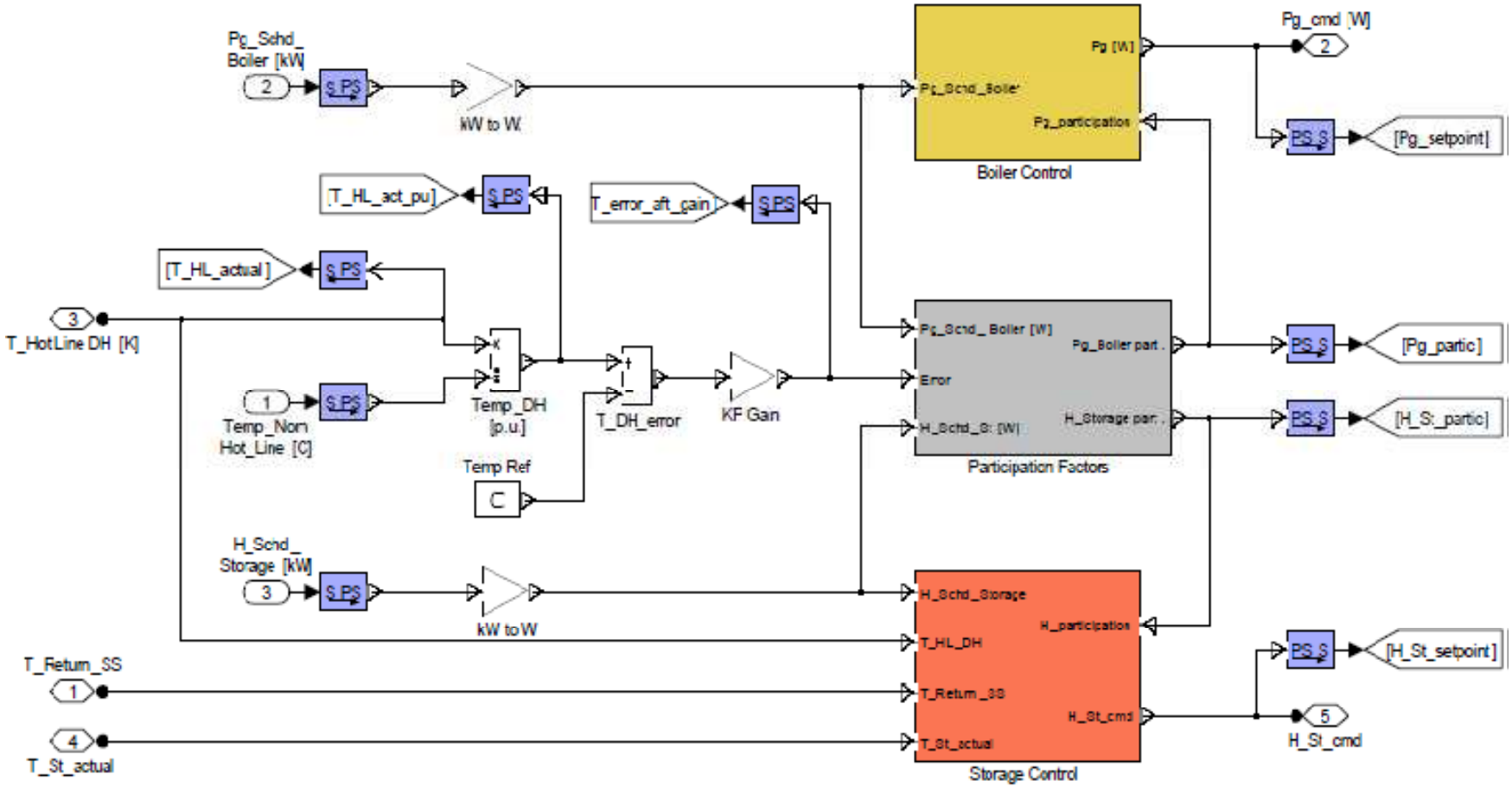

Block diagram of main control –Heat system

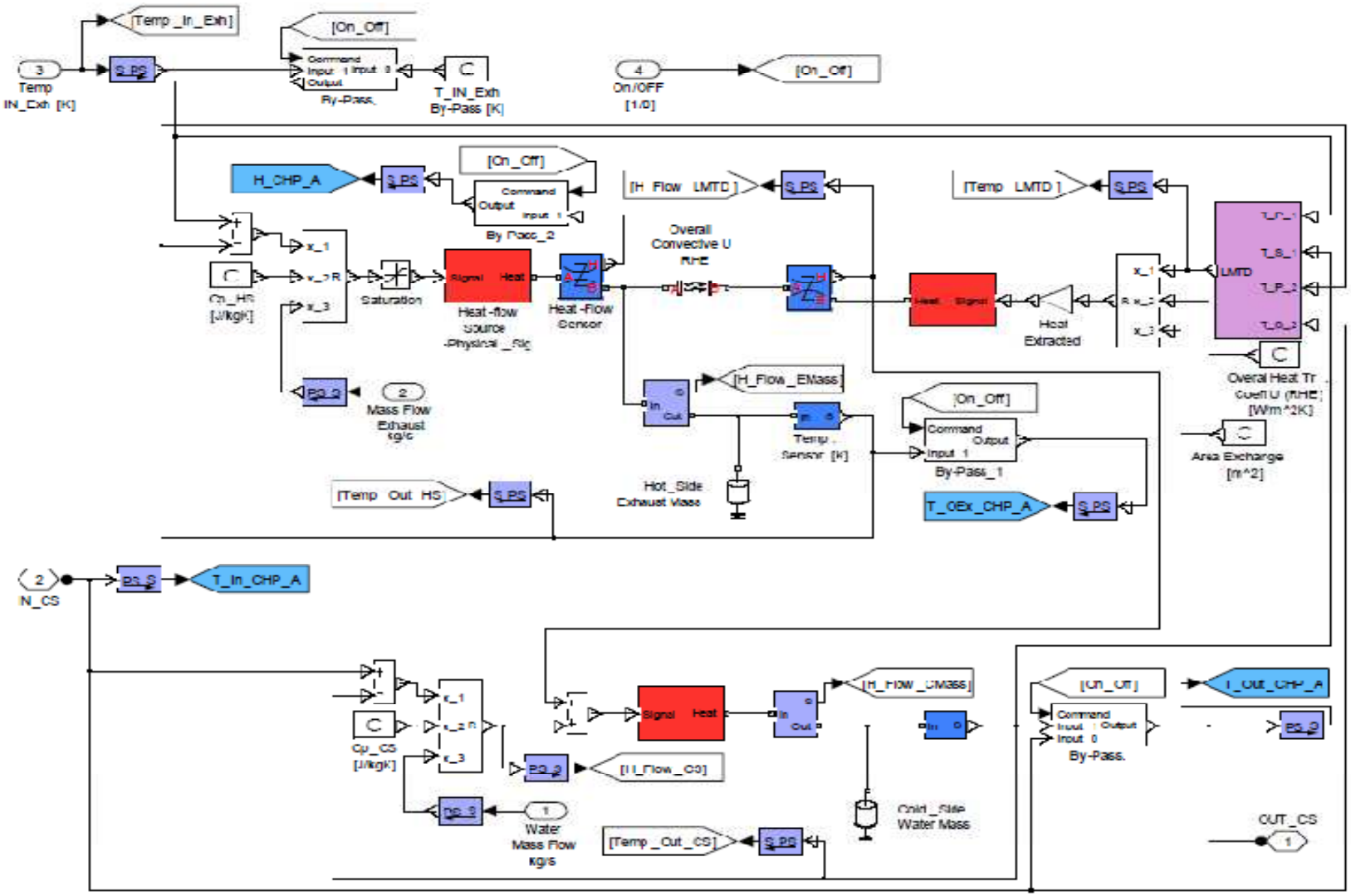

Block diagram of Heat exchanger

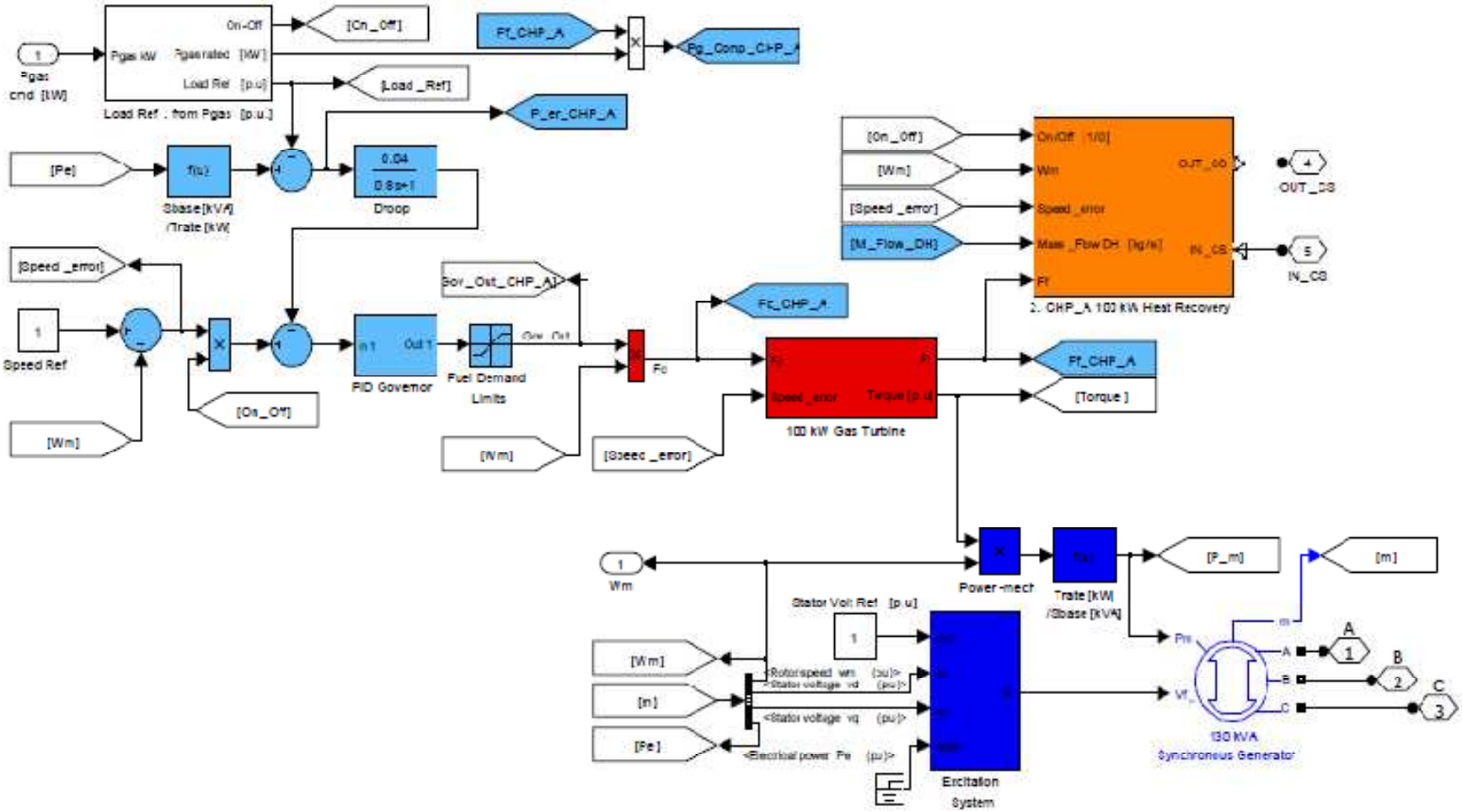

Block diagram of CHP

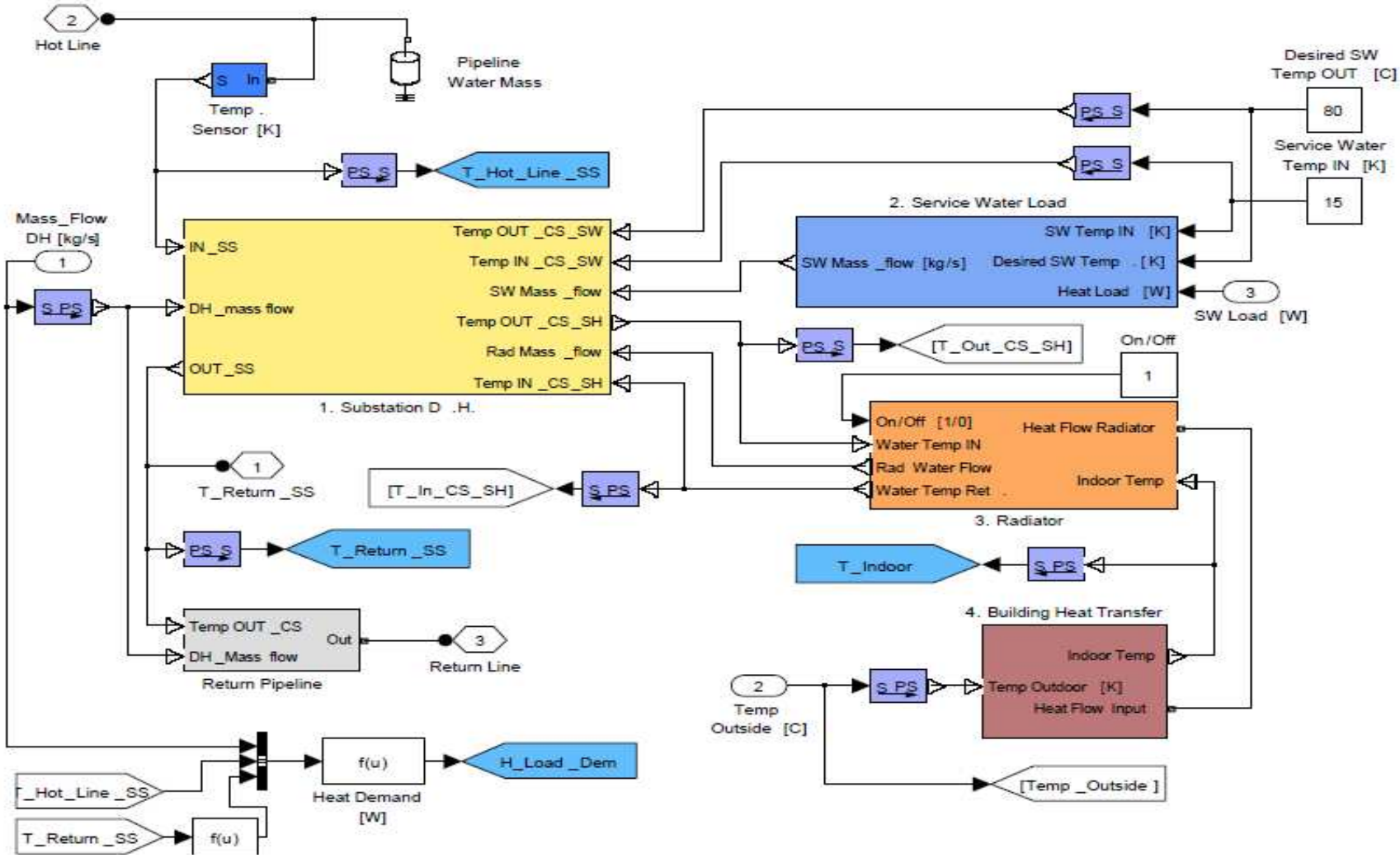

Block diagram of Sub-Station